PRODUCTION AND CHARACTERIZATION OF ACTIVATED CARBON FROM SULPHONATED STYRENE DIVINYLBENZENE COPOLYMER

A THESIS SUBMITTED TO
THE GRADUATE SCHOOL OF NATURAL AND APPLIED SCIENCES
OF
THE MIDDLE EAST TECHNICAL UNIVERSITY

BY

Wisam ABDALLAH

IN PARTIAL FULFILLMENT OF THE REQUIREMENTS
FOR
THE DEGREE OF MASTER OF SCIENCE
IN
CHEMICAL ENGINEERING

AUGUST 2004

Approval of the Graduate School of Natural and Applied Sciences

Prof. Dr. Canan ÖZGEN
Director

I certify that this thesis satisfies all the requirements as a thesis for the degree of Master of Science.

Prof. Dr. Timur DOĞU
Head of Department

This is to certify that we have read this thesis and that in our opinion it is fully adequate, in scope and quality, as a thesis and for the degree of Master of Science.

Dr. Cevdet ÖZTİN
Co-Supervisor

Prof. Dr. Hayrettin YÜCEL
Supervisor

Examining Committee Members

Prof. Dr. Nurcan BAÇ (METU- CHE)

Prof. Dr. Suzan KINCAL (METU- CHE)

Prof. Dr. Suna BALCI (GAZI- CHE)

Dr. Cevdet ÖZTİN (METU- CHE)

Prof. Dr. Hayrettin YÜCEL (METU- CHE)

I hereby declare that all information in this document has been obtained and presented in accordance with academic rules and ethical conduct. I also declare that, as required by these rules and conduct, I have fully cited and referenced all material and results that are not original to this work.

Wisam ABDALLAH

ABSTRACT

PRODUCTION AND CHARACTERIZATION OF ACTIVATED CARBON FROM SULPHONATED STYRENE DIVINYLBENZENE COPOLYMER

ABDALLAH, Wisam
M.S., Department of Chemical Engineering
Supervisor: Prof. Dr. Hayrettin YÜCEL
Co-Supervisor : Dr. Cevdet ÖZTİN
August 2004, 134 pages

Activated carbon was produced from strong cation-exchange resins, sulphonated styrene divinylbenzene copolymers originally in H^+ form, by means of carbonization and steam activation in an electrical furnace. One macroporous resin produced by BAYER Chemicals Inc., Lewatit MonoPlus SP 112 H, was used in the research. Products of carbonization and activation were characterized by using BET, Mercury Porosimetry, Helium Pycnometry and SEM techniques. The effect of carbonization time and temperature on the BET surface areas of the resins were also investigated.

Two sets of carbonization experiments (Set 1 and 2) were performed in which time and temperature were varied in order to study their effects on the BET surface areas of the products. In activation experiments (Set 3), carbonized ion-exchangers (600 ^{o}C, 1 hr) were activated with steam at 900°C, changing the time of activation and the steam flow rate. The temperatures of the water bath used for steam generation were selected as 60°C, 80°C and 90°C.

The pore structures of activated carbons were determined by proper techniques. The volume and area of macropores in the pore diameter range of 8180-50 nm were determined by mercury intrusion porosimetry. Mesopore (in the range of 50-2 nm) areas and volumes were determined by N_2 gas adsorption technique at -195.6^oC, BET surface areas of the samples were also determined, in the relative pressure range of 0.05 to 0.02, by the same technique. The pore volume and the area of the micropores with diameters less than 2 nm were determined by CO_2 adsorption measurements at 0^oC by the application of Dubinin Radushkevich equation.

In the experiments of Sets 1 and 2, the BET surface area results of the six different carbonization times ranging from 0.5 to 3 hours gave almost the same value with a maximum deviation of 5% from the average showing almost no effect on the areas of the products. In the experiments of Set 3 , the sample activated at 800°C for 6 hrs had the highest BET area, 2130 m^2/g, and the one activated at 800°C for 1 hr had the lowest BET area 636 m^2/g. N_2 adsorption/ desorption isotherms showed no distinct hysteresis indicating a cylindrical geometry of the pores. Adsorption isotherms further indicated that the pores are both highly microporous and mesoporous. N_2 (BET) and CO_2 (D-R) surface areas of the samples were in the range of 636-2130m^2/g and 853-1858 m^2/g, respectively. Surface areas of the samples consisted of about 8-53% mesopores and 47-92% micropores.

Keywords: Activated carbon, Ion-exchangers, Sulphonated styrene-divinylbenzene copolymer, Carbonization, Pore structure, Steam activation

ÖZ

SÜLFONLANMIŞ STİREN DİVİNİL BENZEN KOPOLİMERİNDEN AKTİF KARBON ÜRETİMİ VE KARAKTERİZASYONU

ABDALLAH, Wisam
Yüksek Lisans, Kimya Mühendisliği Bölümü
Tez Danışmanı: Prof. Dr. Hayrettin YÜCEL
Yardımcı Tez Danışmanı: Dr. Cevdet ÖZTİN
Ağustos 2004, 134 sayfa

Sülfonlanmış stiren divinil benzen kopolimeri yapısına sahip H^+ formundaki kuvvetli katyon değiştirici reçineler üzerinde elektrikli fırında karbonizasyon ve aktivasyon deneyleri yapılarak aktif karbon üretilmiştir. Bu araştırmada, BAYER Chemicals Inc. tarafından üretilen makro gözenekli bir reçine olan Lewatit MonoPlus SP 112 H kullanılmıştır. Karbonizasyon ve aktivasyon ürünlerinin karakterizasyonunda BET ve cıva porozimetresi teknikleri kullanılmıştır. Karbonizasyon ve aktivasyon ürünleri, BET, Civa Porozimetresi, Helyum Piknometresi, and SEM teknikleriyle incelenmiştir. Karbonizasyon zamanı ve sıcaklığın reçinelerin BET yüzeyi üzerindeki etkisi de araştırılmıştır.

Karbonizasyon deneylerinde zaman ve sıcaklığın değiştirildiği iki set halinde (Set 1 ve 2) deney yapılmıştır. Aktivasyon deneylerinde (Set 3), karbonize iyon değiştiricileri (600 ^oC, 1 saat) 900^oC'lik buharla aktivasyon zamanı ve buhar debisi değişitirilerek aktive edilmiştir. Buhar üretimi için kullanılan su banyosunun sıcaklıkları 60°C, 80°C ve 90°C olarak seçilmiştir.

Aktif karbonların gözenek yapıları uygun tekniklerle belirlenmiştir. Gözenek çapları 8180-50 nm arasında olan makrogözeneklerin hacmi ve yüzey alanı civa (intruzyon) porozimetresi ile ölçülmüştür. Mezogözenek (50-2nm arasında) yüzey alanları ve hacimleri -195.6^{o}C de N_2 gaz adsorbsiyon tekniği ile, BET yüzey alanları da 0.05-0.02 bağıl basınç aralığında yine aynı teknikle belirlenmiştir. Yarıçapları 2 nm den küçük olan mikrogözeneklerin gözenek hacmi ve yüzey alanı 0^{o}C de CO_2 adsorpsiyon ölçümleri ve Dubinin-Raduskhevic denkleminin kullanılmasıyla elde edilmiştir.

Set 1 ve 2 deneylerinde, 0,5 ile 3 saat arasında değişen karbonizasyon zamanlarından ölçülen BET yüzey alanları ortalamadan en fazla 5% sapmalı değerler vermiş ve karbonizasyon zamanının ürünlerin yüzeyine hemen hemen hiç etkisi olmadığı gözlenmiştir. Set 3 deneylerinde, 6 saat boyunca 800°C'de aktive edilen örnek 2130m^2/g ile en yüksek BET yüzeyine ulaşırken, 1 saat boyunca 800°C'de aktive edilen örnekte ise 636m^2/g olan en düşük BET yüzeyi kaydeldilmiştir. Gözenek geometrisinin silindirik yapıda olduğunun bir ifadesi olarak azot adsorpsiyon/desorpsiyon izotermlerinde belirgin bir histeresis gözlenmemiştir. Adsorpsiyon izotermleri gözeneklerin çoğunlukla mikro ve mezo gözenek türünde olduğunu göstermektedir. Ürünlerin N_2 (BET) ve CO_2 (D-R) yüzey alanları sırasıyla 636-2130m^2/g ve 853-1858m^2/g değerleri aralığında saptanmıştır. Aktif karbonların gözenek yapıları yüzde 8-53 civarında mezogözenekler ve yüzde 47-92 mikrogözeneklerden oluşmaktadır.

Anahtar Kelimeler: Aktif karbon, İyon değiştiriciler, Sülfonlanmış stiren divinil benzen kopolimeri, Karbonizasyon, Gözenek yapısı, Buhar aktivasyonu

To My Dearest Father…

ACKNOWLEDGEMENTS

I believe that this part is much more difficult than writing the thesis itself, because here one stands at acknowledging the people with whom he spent most of his days during his work, and finds it really a kind of an impossible mission to thank individually all the people who contributed in the preparation of his thesis, either directly or indirectly.

It is a great honor for me to express my sincere appreciation to my thesis supervisors, Prof. Dr. Hayrettin YÜCEL and Dr. Cevdet ÖZTİN for their continuous support, guidance and helpful suggestions during my study and for their interest in its progress. I can just say that I felt I am a part of their family and never as a stranger away from his home country.

I wish to express my sincere appreciation to all the members my family for their infinite encouragement, support and help during my study. I especially would like to express my deepest gratitude to my brother Dr. Nazih ABDALLAH for his continuous encouragement and patience. Never forgot my dear fiancé for her nice existence in my life and for her infinite moral support and care.

I would also like to deeply thank my laboratory mate Nezih Ural YAĞŞİ for his infinite help and suggestions. I also thank my house-mates Hasan ALAMEDDINE and Maher DERNAIKA. Not forgetting my dear brothers Mohamad ALKHATIB, Husein ELHATTO, Faris ABUHASAN, Ayman ELWALI and Ismail ELHADI for their support during my study. I should also mention İsmail DOĞAN, Anıl ERDOĞDU, Gaye YÜCEL, Onur DİRİ, Volkan GENÇ, Bora ATALIK, Volkan

DEĞİRMENCİ, Ali Emrah KEYFOĞLU, Gülsüm ÖZDEN, Pelin TOPRAK, Serdar ERKAN, Ayşe BAYRAKÇEKEN, Mustafa Esen MARTI, Sinan OK, Özgür AVŞAR and many others, who gave me helpful suggestions for the improvement of the document and moral support.

I would also like to thank Prof. Dr. Suna BALCI, Dr. Funda Turgut for their help in the physical analysis of the products. Finally, I would like to thank Mrs. Gülten ORAKÇI, Ms. Mihrican AÇIKGÖZ, Ms. Kerime GÜNEY, Mr. Turgut AKSAKALl, and Mr. Selahattin UYSAL for their help in the chemical and physical analyses. Besides I would like to thank all the members of the workshop for their help. Also, I thank Ms. Şebnem ŞENER (from Öktek Company) for supplying the material used throughout my study.

TABLE OF CONTENTS

LIST OF TABLES

LIST OF FIGURES

LIST OF SYMBOLS

A_m : Cross-sectional area of the adsorbate, m^2

C : A constant in equation 4.2.2

CSA_{N2} : Cross sectional area of nitrogen molecule, m^2

D_p : Pore diameter, μm

E_i : Adsorption potential, KJ/mole

ΔG : Gibbs free energy change of the reaction, KJ/mole

I : Intercept of the BET plot

K : A constant in equation C.1

M : Adsorbate molecular weight, g/mol

n : Amount adsorbed, moles

N_A : Avagadro's constant, $6.023*10^{23}$ molecules/mol

P_i : Partial pressure of the gas, i

P : Pressure, atm, Pa, psia, mmHg

P_0 : Saturation pressure, mmHg

q_1 : Heat of adsorption of the first layer

q_2 : Heat of adsorption of the second and subsequent layers

R : The gas constant, $8.314x10^7$erg/mole-K, $8.314x10^{-3}$ KJ/mole-K

r_p : Actual pore radius, mean radius of the liquid meniscus, nm or μm

r_K : Kelvin radius

r_{KAVE} : Average Kelvin radius

r_{PAVE} : Average pore radius

S : Slope of the BET plot

S_{BET} : BET surface area, m^2/g

S_{cum} : Cumulative pore surface area, m^2/g

S_{macro} : Macropore surface area, m^2/g

S_{meso} : Mesopore surface area, m^2/g

t : Thickness of the adsorbate layer

t_m : Thickness of the monolayer

T : Temperature, °C

T_c : Critical temperature of the adsorption, °C

V : Volume adsorbed, cm^3/g

V_p : Volume of the penetrometer, cm^3

V_{pore} : Pore volume, cm^3

V_s : Volume of the sample, cm^3

V_0 : Micropore Volume, cm^3/g

V_{cum} : Cumulative volume, cm^3/g

V_{Hg} : Volume of the mercury, cm^3

V_m : Monolayer volume, cm^3/g

V_{macro} : Macropore volume, cm^3/g

V_{meso} : Mesopore volume, cm^3/g

V_{mol} : Molar volume of the nitrogen, $34.6x10^{24}$ A^3/mol at -195.6°C

ΔV_{gas} : Incremental molar adsorbed gas volume, cm^3/g

ΔV_{Liq} : Incremental molar adsorbed liquid volume, cm^3/g

W_0 : Limiting adsorption space volume value

W_a : The quantity of adsorbed at a particular relative pressure

W_{Hg} : Weight of the mercury, g

W_m : The quantity of adsorbed at correspond to BET monolayer

W_p : Weight of the penetrometer, g

W_s : Weight of the sample, g or mg

Greek Letters

μm : Micrometer (10^{-6} meter)

°A : Angstrom (10^{-10} meter)

ρ : Liquid density, g/cm^3

ρ_{He} : Helium (True Density), g/cm^3

ρ_{Hg} : Mercury (Apparent Density), g/cm^3

θ : Contact angle of mercury, 130° and Fraction of surface occupied by adsorbate

σ : Cross sectional area of a CO_2 molecule, m^2/g

γ : Surface tension

CHAPTER I

INTRODUCTION

It is not always recognized how much important carbon materials are in our industrialized world. Although carbon exists in two main crystallographic forms, graphite and diamond, most carbons are polycrystalline and their properties are determined by their crystallite size, degree of alignment, extent of defects and content of impurities (Rodriguez- Reinoso, 1991).

Carbon materials can be prepared from a very large number of organic precursors which may contain heteroatoms and inorganic constituents in addition to carbon. A high temperature carbonization process will produce the removal of volatile components, yielding a solid residue higher in carbon content.

Activated carbon is a microcrystalline form of carbon with very high porosity and surface area. Its chemical structure allows it to preferentially adsorb organic materials and other nonpolar compounds from gas or liquid streams. It has become one of the technically most important and most widely used adsorbents due to its high adsorptive capacity. Present technology demands very large production of activated carbons with appropriate characteristics for each particular application. In general, an activated carbon, which is used in any of the most common applications, must have adequate adsorptive capacity,

mechanical strength, and chemical purity. Furthermore, all these specifications should be accompanied by low production cost.

Activated carbon is obtained from a carefully controlled process of dehydration, carbonization and oxidation of organic substances. It can be prepared for research in the laboratory from a large number of materials. However, the most commonly used ones in commercial practice are peat, coal, lignite, wood and agricultural by-products such as coconut shell (Balcı, 1992). It can also be manufactured from various synthetic resins such as; styrene-divinylbenzene and acrylonitrile– divinylbenzene copolymers .The main steps in the production of activated carbon are carbonization and activation. The carbonization step is usually performed in an inert atmosphere to remove volatile matter. The activation step is a mild oxidation with such oxidizing gases as steam, carbon dioxide, or air to develop an efficient pore structure (Hashimoto et al., 1979).

The product of simple carbonization, that is the pyrolysis of starting material with the exclusion of air and without the addition of chemical agents, is usually an inactive material with a specific surface area of order of several m^2/g and has low adsorption capacity. A carbon with a large adsorption capacity can be prepared by activating the carbonized products with a reactive gas. The majority of activated carbon used throughout the world is produced by steam activation (physical activation). In this process, the carbonized product is reacted with steam over 900^0C.

Another procedure used in the production of activated carbon involves the use of chemical activating agents before the carbonization step. The most commonly used activating agents are phosphoric acid, zinc chloride and salts of

sodium and magnesium. Chemical agents act as dehydration agents and they may restrict the formation of tar during carbonization. Chemical activation is usually carried out at lower temperatures than the simple pyrolysis and the activation process with steam or carbon dioxide. The production at lower temperatures promotes the development of a porous structure, because under these conditions elementary crystallites of smaller dimensions are formed (Smisek and Cerny, 1970).

Most of the available surface area of activated carbon is nonpolar in nature. However, during production the interaction of surface with oxygen produces specific active sites giving the surface of slightly polar in nature. As a result, carbon adsorbents tend to be hydrophobic and organophilic (Ruthven, 1984).

A proper activated carbon has a number of unique characteristics: a large internal surface area, dedicated (surface) chemical properties and good accessibility of internal pores. Conventional classification of pores according to their diameters, originally proposed by Dubinin (1947) and now officially adopted by the International Union of Pure and Applied Chemistry, (IUPAC) is mostly used. According to IUPAC definitions three groups of pores are distinguished with respect to their dimensions:

Macropores: Pores with diameters larger than 50 nm (0.05μm)

Mesopores: Pores with diameters between 2nm and 50 nm (0.002μm - 0.05μm)

Micropores: Pores with diameters less then 2 nm (0.002μm)

Submicropores: Pores with diameters between 0.8 nm and 2 nm (0.0008μm - 0.002μm)

There are three commercial types of activated carbon with respect to product dimensions:

- Pellet Activated Carbon with particle sizes in the range of 0.8-5mm

- Granular Activated Carbon (GAC) with particle sizes in the range of 0.2-5mm

- Powdered Activated Carbon (PAC) with particle sizes smaller than 0.18mm (Yağşi, 2004).

Most activated carbons contain pores of different sizes; micropores, transitional mesopores and macropores. Therefore they are considered as adsorbents with a wide variety of applications. Micropores generally contribute to the major part of the internal surface area. Macro- and mesopores can be regarded as the highways into the carbon particle, and are crucial for kinetics. Macropores can be visualized using Scanning Electron Microscopy (SEM). The pore size distribution is highly important for the practical application; the best fit depends on the compounds of interest, the matrix (gas, liquid) and treatment conditions.

The quality (surface area, pore size distribution and hence adsorptive properties) of activated carbons are directly related to the nature of starting material, the type of the production method and the temperature of production. In other words, the desired pore structure of an activated carbon product is attained by combining the right raw material and activation conditions (Balcı, 1992).

Activated carbon adsorbs molecules from both liquid and gaseous phases depending upon the pore size distribution of the adsorbent (and also upon the

geometry and size of the adsorbate molecule). In adsorption from the gas phase, mainly microporous carbon is used whereas mesoporous carbon is applied in liquid phase processes. Application of mesoporous activated carbons include; drinking water purification, waste-water treatment, sweetener decolorization, food and chemical processing. On the other hand, microporous carbons are used for solvent recovery, gasoline emission control, cigarette filters and industrial emission gas treatment (Benaddi, 2000).

With its high surface area, activated carbon is a widely used adsorbent but it is also an oxidation catalyst, which can trigger spontaneous combustion of collected organics. To improve safety and reduce the possibility of fire, synthetic materials can be used as adsorbents.

An interesting example to synthetic materials is styrene-divinylbenzene copolymer, which is widely used commercially as ion-exchange resin in different ionic forms. Styrene-divinylbenzene copolymers have rather well-defined physical and chemical properties, such as spherical shape, resistance to attrition, and chemical structure, which offer distinct advantages over traditional precursors for activated carbon. The natural disadvantage of high cost for the copolymers when used as raw material for activated carbon may be compensated with better characterized products (Shelly, 1994).

Styrene-divinylbenzene copolymers to which sulfonic acid groups have been added make up the basic structure of strong cation exchangers in various exchangeable ionic forms. These resins possess favorable properties in regard to pyrolysis leading to activated carbons.

A synthetic adsorbent was made by a patented process, which pyrolyses a sulfonated styrene-divinylbenzene copolymer, to produce a carbon replica of the original copolymer structure. Unlike activated carbon, this synthetic material was reported to have highly reproducible properties, including greater hydrophobicity and pore size distribution both of which impact adsorptive capacity. The synthetic material is 3 to 4 times more hydrophobic than activated carbon, so its adsorptive capacity is undaunted by exhaust streams with relative humidity as high as 90%. Since carbon adsorption tends to fall off as relative humidity approaches 70%, added measures to reduce relative humidity increase the overall cost of a carbon-based system. Carbon's operating life is also limited, since for this application the material typically loses about 10% of its activity each time it is regenerated. For continuous operation of activated carbon beds, this requires periodic removal and replacement of the spent carbon but this synthetic adsorbent is reported to be regenerable hundreds of times with no significant loss of adsorptivity (Shelley, 1994).

The main aim of this study was to investigate the production and characterization of activated carbon produced from sulfonated styrene-divinylbenzene copolymers which are normally used as cation exchangers using steam for the activation of the carbonized products. The results of this study may also be related to spent ion-exchangers which, after serving their useful life as ion exchangers, must be disposed of. This study may, in this respect, be regarded as a preliminary step for the probable beneficiation of spent ion exchangers in the manufacture of activated carbons.

CHAPTER II

LITERATURE SURVEY

Ion exchangers are spherical solid materials of rather well-defined chemical structure and composition. They contain essentially only carbon and hydrogen, and elements from the active groups attached to the matrix. Furthermore they retain the original spherical shape during pyrolysis. These facts have attracted interest in the research and production of activated carbon using ion exchangers.

The main steps in the production of activated carbon are again carbonization and activation. The carbonization step is usually performed in an inert atmosphere to remove volatile matter. The activation step is a mild oxidation with such oxidizing gases as steam, carbon dioxide, or air to develop an efficient pore structure.

Cation exchangers are more often used than anion exchangers as precursors of activated carbon. Residual elemental analysis and off-gas analysis show that the decomposition ratio of cationic resins (50 wt% even at 600°C) is less than that of anionic resins (about 90 wt% above 400°C). (Matsuda et al., 1986) Therefore, the main interest of this study was based on cation exchangers.

Sulfonated styrene-divinylbenzene cation exchangers decompose into various pyrolysis products when they are heated in an inert atmosphere. These products can be grouped into two classes: char and gases, according to their volatility. Char is a carbon-rich non-volatile solid residue, usually constituting approximately 30-50 % of the original material (the so-called "yield"). Gases contain such products as SO_2, H_2S, styrene, toluene, etc.

The production of activated carbon is a typical gas-solid reaction. The adsorptive capacities of activated carbon are mainly associated with its internal pore properties such as pore surface area, pore volume and pore size distribution, which develop during the activation of chars. Therefore a detailed search on the mechanism which explains the changes in the pore properties during carbonization and activation is necessary.

2.1 CARBONIZATION AND PHYSICAL ACTIVATION STUDIES

A few studies have been carried out on activated carbon produced from ion-exchangers. Production steps, initially carbonization and then activation in various oxidizing atmospheres have been found to lead to favorable pore development.

Winslow et al. (1956) studied on pyrolysis of crosslinked styrene polymers. They pyrolyzed a series of styrene-divinylbenzene copolymers under nitrogen at 365°C and atmospheric pressure. Increases in divinylbenzene content caused reduction in degradation rates and led to larger residues having higher thermal stability indicating the competition between condensation processes and chain seissions. All weight losses from volatilization began almost immediately and bore no apparent relation to polymer softening. On the

contrary, samples containing more then 10% divinylbenzene shrank but retained their original shape throughout decomposition. The close resemblance between pyrolysis patterns of linear and crosslinked (2% divinylbenzene) polystyrene agrees with similar behavior in other low density polymer networks. If breakdown really follows a depolymerization course, the decoupling process would free styrene units and leave behind pendant styryl groups still attached to adjacent chains.

Wolff (1959) set up a model in which the char was considered to be formed from small cubes which are stacks of graphitic crystalline planes (crystallite). Upon the activation of the char in such a structure, the activating agent randomly attacks the planes and removes large segments of the individual planes to form micropores of only a few angstroms width. He adopted the probability concept to analyze the random removal of the individual planes and developed an analytical relationship between the pore surface area and the density of the activated carbon.

Bothe et al. (1979) studied the stability behavior of sulfonated styrene-divinylbenzene resins by differential thermal analysis. The first endothermic transformation is at temperatures between 90°C and 180°C interpreted as the dehydration of the resin. The second transformation is caused by the desulfonation of the polymeric acid beyond 300°C. Decomposition of the polymer matrix takes place after 400°C. The unsulfonated polymer changes color and becomes liquid while the sulfonated cation exchanger retains its spherical form. The decomposition of the resin in the acid form is more complex since there is no sharp peak at temperatures beyond 400°C. This is probably due to the formation of sulphones.

Neely et al. (1981) studied on the carbonization of polymer carbons derived from porous sulfonated polystyrene. He noticed that when macroreticular sulfonated styrene/divinylbenzene (S-DVB) is heated in an inert atmosphere, a series of endothermic reactions occur beginning with the loss between 100 and 200°C of the last water of hydration from each sulfonate group followed by desulfonation and finally carbonization. When the temperature is raised from room temperature up to 300°C, 83% of the total sulfur in the starting material is volatilized. It is concluded that the volatile sulfur produced up to 300°C is exclusively SO_2. As the temperature is raised from 300 to 500°C, 70% of the remaining sulfur is volatilized predominantly as SO_2. However, smaller quantities of H_2S and elemental sulfur are also present in the off-gases. Of the carbon in the original polymer 28.8% is lost as volatile hydrocarbons, predominantly as styrene and toluene. At temperatures above 500°C the aromatization reactions can proceed thermally by the direct loss of hydrogen to produce new carbon-carbon bonds. The majority of the weight loss above 500°C is hydrogen. By 1000-1200°C the densities are nearly those of graphite (2.25 g/cc). As the degree of polynuclear aromatic character increases both density and the C/H atomic ratios increase.

The pore structure of polymer carbons derived from porous sulfonated polystyrene was also studied. The pore size has shrunk somewhat from an average pore size of 243 A° in the sulfonated material to 223 A° in the pyrolyzed product. A loss in macropore void fraction (macroporosity) occurs between 300 and 400°C. The 300°C-material has porosity very similar to that of the copolymer and the 400°C-material has porosity in line with that of all the higher temperature products. Above 400°C the nearly constant macroporosity is consistent with a uniformly shrinking macropore structure. In a similar way

between 400 and 1200°C the macropores shrink proportionately as the microspheres shrink.

Unlike the macropores, the void fraction due to micropores increases as the heat treatment temperature rises. As the skeleton shrinks in volume, the porosity of the microspheres increases markedly. One half of the volume created as the skeleton becomes denser at higher temperatures creates micropores and the other half appears as shrinkage of the microspheres. The volume of 4.3-6.0A° pores reaches a maximum between 700 and 800°C. By 1200°C, the micropores are nearly all in the range of 4.3-2.5 A° and are sufficiently small to exclude N_2. In spite of the increasing micropore volume and decreasing pore size which should result in increasing surface area, the surface area measured by nitrogen adsorption at liquid nitrogen temperatures decreases at higher heat treatment temperatures, consistent with lack of access of the nitrogen to a large fraction of the micropore volume.

Miura et al. (1984) classified the carbonized materials into two groups: graphitizing carbon and nongraphitizing carbon. The schematic representation of the structure of both carbons was shown in Figure 2.1. In the figure straight lines represent graphitic layers, the stacks of which are called crystallite, and the curved lines at the periphery of the individual crystallites indicate the nonorganized carbon. Carbons prepared by pyrolysis of organic substances at 1000°C are said to consist of groups of from two to four parallel graphitic layers of less than 20A° in diameter and be comprised of 15 to 45% of nonorganized carbon. The crystallite and the nonorganized carbon react with the active agents at different rates. The nonorganized carbon includes hydrogen, hydrocarbon radicals, or other functional groups, and is more reactive than the crystallite carbon. However, the models which take into account the difference in the

reactivity between the crystallite and the nonorganized carbon has not been presented.

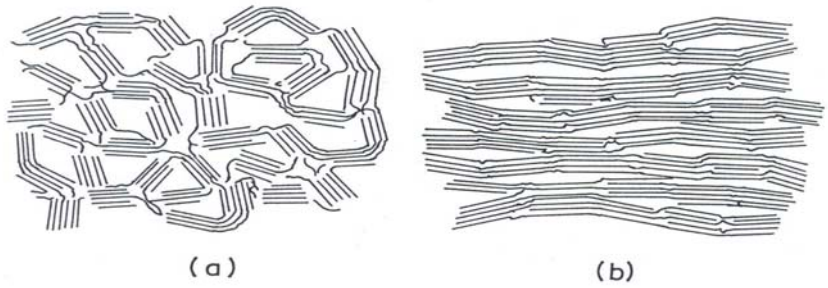

Figure 2.1 Schematic Representation of (a) Non-graphitizing and (b) Graphitizing Structure of Activated Carbon (Smisek and Cerny, 1970)

Matsuda et al. (1986) studied the decomposition of ion exchange resins by pyrolysis. Both anion and cation exchange resins consist of base polymer and functional groups. The former is a copolymer of styrene and divinylbenzene, and the latter is sulfonic acid (cation resin) or quaternary ammonium (anion resin). Figure 2.2 compares the changes in resin weight as a function of pyrolysis temperature for anionic and cationic resins. The anionic resin decomposes in two steps and the residual ratio is about 10 wt% above 400°C, indicating that decomposition ratio is 90 wt%. Pyrolysis products, residue elemental ratios and off-gas compositions are shown in Figure 2.3 for anionic resins. Its functional group is quaternary ammonium, and nitrogen is contained in it only as indicated in Figure 2.2. At 200°C, methylamine gas is generated and nitrogen content in the residue decreases. These results indicate that the functional group decomposes in this temperature range. Subsequently, hydrocarbon gases are generated and carbon content in the residue decreases above 400°C, corresponding to the base polymer pyrolysis. Therefore, the functional group and base polymer decompose at 200 and 400°C, respectively, for the anionic resin. On the other hand, the cationic resin has been pyrolyzed in the temperature range from 200 to 300°C, and the decomposition ratio being only 50 wt% even at 600°C. Figure 2.4 shows the pyrolysis products for cationic resins with the

functional sulfonic acid group (-SO_3H). In this case, the functional group decomposes at 300°C, because SO_2 and H_2O gases are generated and sulfur and oxygen contents in the residue decrease at this temperature. Only a small amount of hydrocarbon gases are generated above 400°C, and most of the carbon, which forms the base polymer, remain in the residue. These facts indicate that only a small amount of the base polymer is pyrolyzed in the cationic resin.

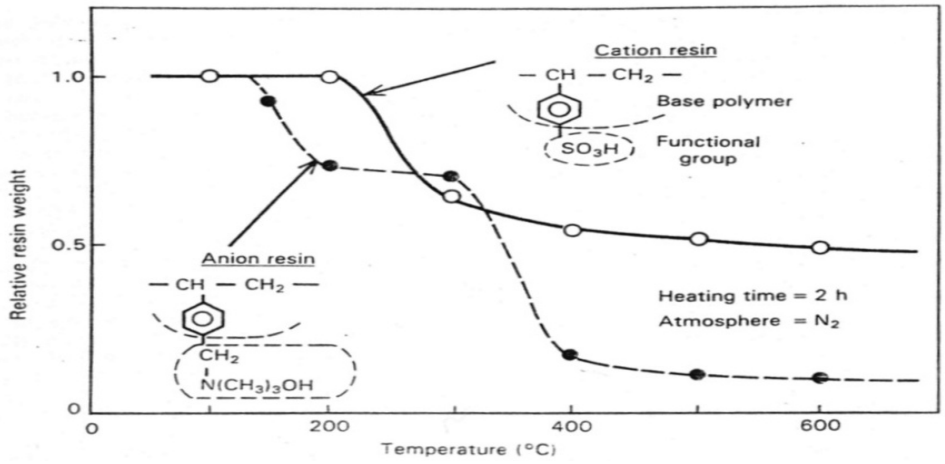

Figure 2.2 Weight Changes of Anion and Cation Exchange Resins During Pyrolysis. (Matsuda, 1986)

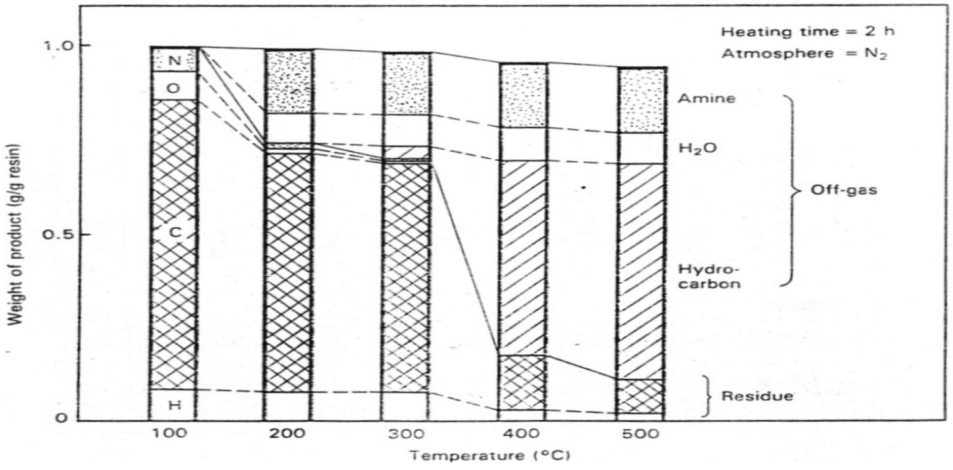

Figure 2.3 Pyrolysis Products for Anion Exchange Resins (Matsuda, 1986)

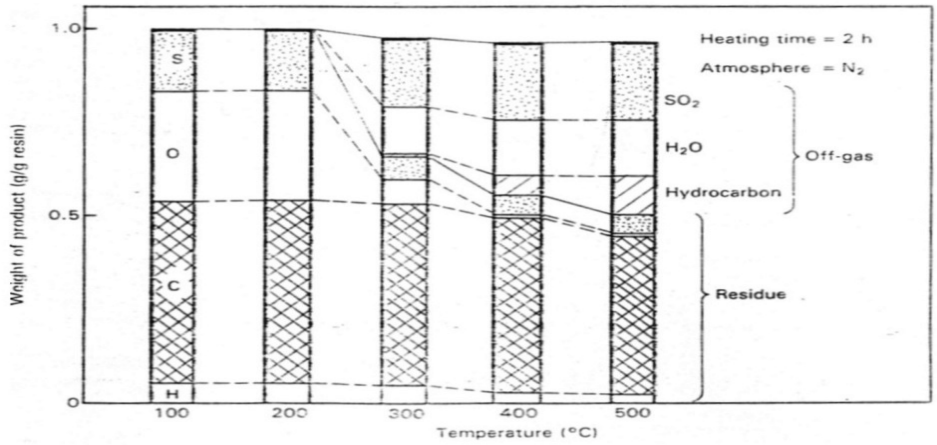

Figure 2.4 Pyrolysis Products for Cation Exchange Resins (Matsuda, 1986)

Sulfur in the functional group is a key factor to understanding the low decomposition ratio or high heat resistance of the cationic resin. Most of the sulfur changes into SO_2 gas at 300°C; however, about 35% of the sulfur still remains in the residue above 400°C. Matsuda and coworkers presumed that this sulfur made the base polymer thermally stable. About 35 % of the functional groups form sulfonyl bridges (- SO_2 -) between base polymers. It is generally known that such bridges make polymers thermally stable and most of the carbon in the polymer remains in the residue after pyrolysis without gasification. Therefore, the low decomposition ratio (50 wt % at 600°C) of the cation resin can reasonably be attributed to the formation of sulfonyl bridges during pyrolysis.

Sastri et al. (1993) studied the high-temperature carbonization of ion exchange resins. As the heat treatment is progressively increased, a carbonaceous mass is produced with a high char yield. The solid density increases as the pyrolysis temperature is raised to 700°C, and remains at a fairly constant value upto 1200°C. Further heat treatment to 2700°C results in a reduction in the density.

Kolarz et al. (1994) studied on the influence of heat treatment conditions on the porosity changes of sulfonated S-DVB copolymers. They obtained the cation exchangers in H^+ and Ca^{2+} forms with two ion-exchange group concentrations (0.5 and 2.4 mmol/g in samples A and B, respectively). Strong thermal decomposition of the surface sulfonated S-DVB copolymer A in argon starts at 400°C and is accompanied by a significant decrease of its mesopore volume. The chars obtained at this temperature have no sulfonic groups.

Pyrolysis at 900°C of the sulfonated copolymers A and B leads to high-temperature chars with the yields close to 16% and 30%. Greater concentration of sulfonic groups in copolymer B than in copolymer A not only increases the yield of the chars, but also gives a char with a greater volume of very fine micropores. On the other hand, pyrolysis of the cation exchanger B, in its H^+ and Ca^{2+} forms, was carried out at 900°C. At temperatures below 400°C, the thermal resistance of the ion-exchanger in the hydrogen form is higher than that of the calcium doped sample. But starting from about 500°C, the loss of weight of both samples becomes similar and changes little with further increase of temperature. At 900°C the final loss of weight of both pyrolyzed copolymers is close to 70%, which means a not very high yield of about 30%. The addition of calcium increased the reactivity of the char.

Kolarz observed that the high temperature char from the strongly sulfonated copolymer, after steam activation at 800°C to a 50% burn-off, renders a sorbent with a well-developed microporous structure and a high effective surface area (1180 m^2/g). This sorbent, with good sorptive properties towards gases and vapors, is also characterized by a narrow distribution of micropore sizes. It is the calcium-doped sulfonated copolymer, after its high-temperature pyrolysis and steam activation, which leads to a sorbent with a

well-developed mesoporosity and particularly wide micropores. The activated char from the calcium-doped ion exchanger has a surface area of 580 m^2/g.

Kocırık et al. (2001) studied on the carbonization of bead-shaped polymers for application in adsorption and in composite membranes. Biopolymers such as bead cellulose, macroporous polymers in bead form such as methacrylate copolymers (GMA–EDMA), acrylonitrile terpolymers (GMA–AN–EDMA), styrene divinylbenzene (St–DVB) and acrylonitrile divinylbenzene (AN–DVB) copolymers, as well as strong acid ion exchangers were tested to obtain products in bead form with a high specific surface area and good sorption and mechanical properties. To improve the resistance to block formation in polymers during the carbonization period, solutions of some salts are soaked into the polymer. A mixture of salts (NH_4Cl, $FeCl_3$ and $ZnCl_2$), was used in the treatment of polymers to stabilize the porous structure at 300, 700 and 1000°C. Pre-treating was performed at 275°C in the presence of air to oxidize the polymer.

The presence of the salts of transition metals also has a catalytic effect on oxidation reactions, which proceed in the presence of oxygen at this temperature. In nitrogen, depolymerization of methacrylate and divinylbenzene copolymers occurs at 250 and 350°C, respectively; this is less pronounced in highly crosslinked polymers impregnated with salts. The mass loss during the carbonization of bead cellulose was very high, especially when wet bead cellulose was being treated. Bead cellulose was carbonized in nitrogen atmosphere. Carbon dioxide is not suitable because it gave very small surface area. In nitrogen atmosphere a product with a specific surface area 480 m^2/g is formed. Also the highest pore volume and thus the lowest mean pore radius were reached in this case. The pretreated product was brown, after carbonization it was metallic black, but the spherical shape of the particles was not preserved.

Carbonization of methacrylate macroporous bead shaped copolymers in the presence of carbon dioxide was also not very successful. The specific surface area and pore volume values were low. Even with a low carbonization temperature (700°C) used with methacrylate copolymers and even with acrylonitrile terpolymers, the bead form was not preserved. Brownish-black and black products with bad mechanical properties or brittle agglomerates were obtained in this case.

The best results were obtained starting from styrene–divinylbenzene copolymers and even from acrylonitrile–divinylbenzene copolymers. Carbonization of styrene–divinylbenzene copolymers generates regular spherical particles. An adsorbent with microporous structure, with a specific surface area of 1140 m^2/g and mean pore radius of 2.5 nm was obtained. Starting from styrene–divinylbenzene ion-exchangers, microporous products with mean pore radius from 1 to 1.9 nm were prepared. At higher carbonization temperatures, materials with values of specific surface area (549 m^2/g) similar to carbon were obtained. By prolonging reaction times from 1.5 to 10 h, products with higher values of specific surface area were obtained. The yield of the reaction changed from 20 to 40 wt. %. Longer carbonization time results in lower reaction effectiveness and also in lower specific surface area due to polymer scorching. By carbonization of styrene–divinylbenzene ion exchangers with sulfogroups, microporous adsorbents with a narrow pore diameter distribution, in the form of regular spherical particles having metallic lustre could be prepared. Styrene–divinylbenzene cation-exchangers are better starting materials than acrylonitrile–divinylbenzene copolymers, because they yield products with higher specific surface areas. Differential scanning measurement indicates that in comparison with non-substituted copolymers, degradation of cation exchanger proceeds at higher temperature and depolymerization is minimized. All these

factors contribute to the better results reached in transforming styrene–divinylbenzene cation exchangers. During carbonization the amount of sulfur decreases from 15.7% S in the starting ion exchanger to 0.49% S and after 10 h of carbonization the sulfur in the product was not detected. (Kocırık, 2001)

From the efficiency point of view, carbonization of styrene–divinylbenzene ion-exchangers appears as the best solution of the given problem. The styrene–divinylbenzene matrix bearing the sulfo-groups provides higher thermal stability, thus diminishing parallel depolymerization and increasing product yield. The yield of the carbonized product increased with the degree of polymer cross-linking, owing to the higher glass transition temperature values of the more highly cross-linked copolymers.

Yenisoy-Karakaş et al. (2004) studied the physical and chemical characteristics of polymer-based spherical activated carbon and its ability to adsorb organics. The polymer-based spherical activated carbon (PAC) is divinylbenzene-based and steam-activated. The divinylbenzene-based-spherical-polymer was produced by a suspension polymerization method. After the spherical polymer was carbonized under nitrogen atmosphere at 450–700 °C, it was activated with water vapor at 800–830°C. The commercial sample (CAC) is pitch-based and steam-activated and was obtained from Kureha Chemical Industry Co. Ltd. (Tokyo, Japan). The particle sizes were between 0.2 and 1.2 mm for the PAC and 0.2–0.8 mm for the CAC.

The characterization of a polymeric spherical activated carbon (PAC) was performed by comparing its adsorption, porosity, functional groups and some of the physical properties with a commercial spherical activated carbon (CAC). The PAC was about 4 times superior to the CAC with respect to the mechanical

strength. The surface areas for PAC and CAC were 1160 and 1170m^2/g respectively. The micropore volume of the PAC was about 5% smaller than that of the CAC. The maximum methylene blue adsorption values of the PAC and the CAC were 32 and 14 mg/g, respectively, which indicated low mesopore volumes. This resulted in the low butane working capacity values for both activated carbons. Adsorption parameters for the Langmuir and the Freundlich isotherm models were determined for all organic substances tested. Both isotherms were suitable models to analyze the equilibrium data for the removal of all organics. However, the Langmuir model fitted better than the Freundlich model and the adsorption capacities of the PAC were somewhat higher than those of the CAC.

2.2 CARBONIZATION AND CHEMICAL ACTIVATION STUDIES

Park et al. (2002) studied on the preparation and structural characterization of cctivated carbons (ACs) based on polymeric resins by chemical activation using KOH as the activating agent. Polystyrene-based cation-exchangeable resin (PSI) by chemical activation with KOH as the activating agent. And the influence of the KOH-to-PSI ratio on the porosity of the ACs studied was investigated by using nitrogen adsorption isotherms at 77 K and a scanning electron microscope (SEM). As a result, PSI could be successfully converted into ACs with well-developed micro and mesopores. The specific surface area and pore volumes increased with an increase in the KOH-to-PSI ratio. However, it was found that the addition of KOH did lead to the transformation of the micropores to the meso- and macropores. From the results of pore size analysis, quite different pore size distributions were observed, resulting from the formation of new pores and the widening of the existing micropores during KOH activation. A scanning electron microscopic (SEM) study

showed that the resulting carbons possessed a well-developed pore structure and the pore size of the ACs studied increased with the KOH-to-PSI ratio.

Puziy et al. (2002) prepared activated carbon starting with synthetic polymer precursors (styrene–divinylbenzene copolymer) using an impregnation weight ratio of 0.75 at various temperatures in the 400–1000°C range by chemical activation with phosphoric acid. Other impregnation ratios (0.93 and 1.11) were also used at a carbonization temperature of 800°C. The resulting carbons were characterized by elemental analysis, cation exchange capacity measurement, infrared spectroscopy, potentiometric titration with calculation of proton affinity spectra, and copper adsorption from solution. The results indicate that the synthetic carbons obtained possess acidic character and show cation-exchange properties similar to those of oxidized carbons. However, the acidic compounds arising from treatment with phosphoric acid are tightly bound to the carbon lattice and are chemically and thermally more stable than those introduced by oxidative treatments. The largest amount of cation-exchange surface groups is introduced after activation at 800°C. Infrared investigations showed that phosphorus compounds may be polyphosphates bound to the carbon lattice.

Proton affinity distribution curves calculated from potentiometric titration experiments showed four types of surface groups on synthetic phosphoric acid activated carbons. Among them phosphorus-containing groups are the most important for the adsorption of heavy metal ions (copper) from acid solutions. Thus, carbons activated with phosphoric acid may be regarded as prospective cation-exchangers for the removal of heavy metals from water solutions.

The porous texture of the resulting carbons was characterized by N_2 adsorption at 219.6°C and CO_2 adsorption at 0°C. All carbons exhibited a multimodal pore size distribution with maxima in the micropore and meso/macropore regions. Maxima in pore volume were attained at 900°C for micropores and at 500 and 900°C for mesopores. The mesopore volume was less sensitive than the micropore volume to changes in the impregnation ratio. It is concluded that the porous texture is not a prime factor in determining the outstanding cation exchange capacities of these carbons.

It was shown that, similarly to the synthetic carbons activated with phosphoric acid obtained in argon, the ones obtained in air possess an acidic character and show considerable cation-exchange properties. The contribution of oxygen-containing surface groups along with phosphorus containing groups to cation exchange capacity (CEC) is higher for carbons obtained in air. Three types of surface groups were identified on carbons prepared at temperatures up to 600°C, and four types on carbons prepared at higher temperatures. These groups were assigned to 'super-acidic' (pK, 0), phosphorus-containing (pK 51.1–1.2), carboxylic (pK 54.7–6.0) and phenolic (pK 58.1– 9.4) groups. The cation-exchange capacity was at a maximum for the carbon prepared at 800°C. Copper adsorption by synthetic carbons activated with phosphoric acid obtained in air at temperatures lower than 800°C is higher than for similar carbons obtained in argon. The increase is due to additional formation of oxygen-containing surface groups. All carbons show a multimodal pore size distribution including simultaneously micropores and mesopores, but the porous texture is not a prime factor in determining the cation-exchange capacities of these carbons. Synthetic phosphoric acid activated carbons show a greater development of porosity when obtained in air as compared to carbons carbonized in argon.

CHAPTER III

THEORETICAL BACKGROUND

3.1 ACTIVATED CARBON

3.1.1 Definition and Properties

Activated carbon is a predominantly amorphous form of carbon that has an extraordinarily large internal surface area and pore volume. These unique characteristics are responsible for its adsorptive properties, which are exploited in many different liquid- and gas-phase applications. Activated carbon is an exceptionally versatile adsorbent because the size and distribution of the pores within the carbon matrix can be controlled to meet the needs of current and emerging markets (Jüntgen, 1977). X-ray analysis of activated carbons shows a structure which is much more disordered than that of graphite, having crystallites only a few layers in thickness and less than 10 nm in width. The spaces between the crystallites of activated carbon constitute the microporous structure with a large internal surface area of 250 -2500 m^2/g. Its chemical structure allows it to preferentially adsorb organic materials and other nonpolar compounds from the gas or liquid streams. Engineering requirements of specific applications are satisfied by producing activated carbons in the form of powders, granules, and shaped products. Through choice of precursor, method of activation, and control of processing conditions, the adsorptive properties of products are tailored since many decades for a wide variety of applications as

the decolorization of sugar and sweeteners, purification of potable water, gold recovery, production of pharmaceuticals, catalytic processes, off gas treatment of waste incinerators, automotive vapor filters, color/odor correction in wines and fruit juices, etc (Smisek and Cerny, 1970; Hassler, 1974).

The removal of impurities from gases and liquids by activated carbon takes place by adsorption. Adsorption is the term used to describe the tendency of molecules from an ambient fluid phase to adhere to the surface of a solid. This is a fundamental property of matter, having its origin in the attractive forces between molecules. The force field creates a region of low potential energy near the solid surface and, as a result, the molecular density close to the surface is generally greater than in the bulk gas (Kirk-Othmer, 2001). Adsorption process can be considered as either physical adsorption or chemisorption. In physical adsorption the impurities are held on the surface of the carbon by weak van der Waal's forces, whereas in chemisorption the forces are relatively strong and adsorption occurs at active sites on the surface. The efficiency of the carbon will therefore, depend upon its accessible surface area, and also upon the presence of active sites on the surface at which chemisorption may occur. The most of the important applications of adsorption depend on the selectivity, i.e., the difference in the affinity of the surface for different components.

The porous structure and chemical nature of an activated carbon is a function of the raw materials used in its preparation, the activation method used and the extent of activation. This is the reason why surface area or pore volume of activated carbons can vary widely from one kind to another. Pore structure of activated carbon using scanning electron microscope (SEM) is shown in Figure 3.1 (Park et. al, 2002).

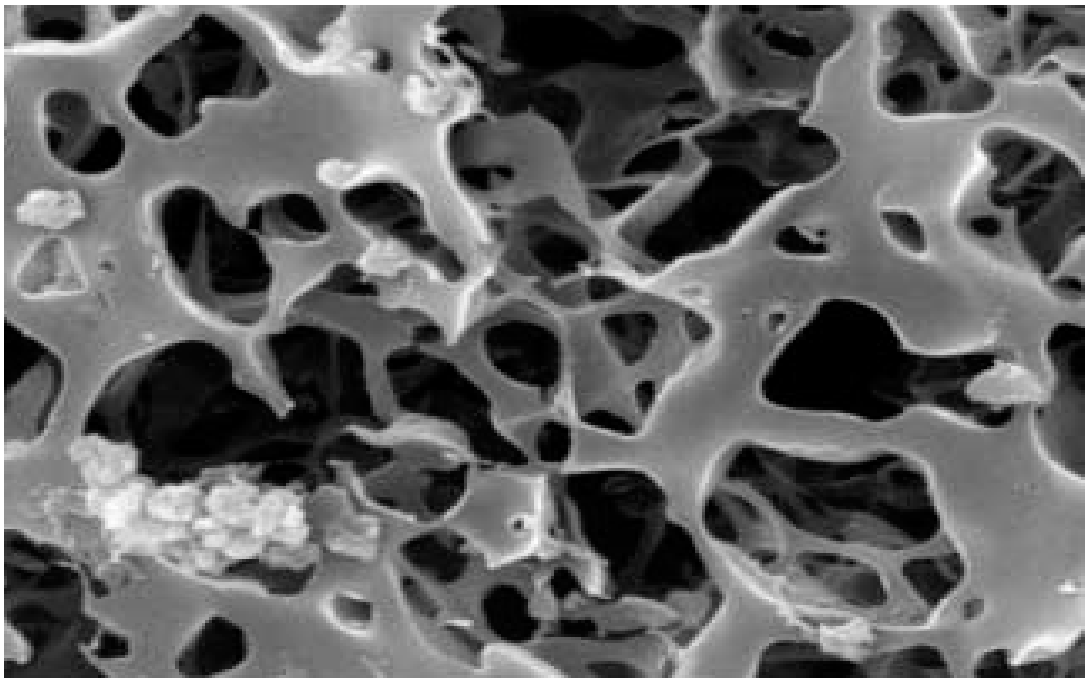

Figure 3.1 Pore Structure of Activated Carbon (SEM)

The internal surface area of activated carbons can be determined by adsorption of nitrogen, but there is no guarantee that the entire surface is available for the adsorption of organic compounds. Since organic molecules are much larger than a nitrogen molecule and if the pores are the same size of molecular dimensions, it is possible to have a sieving action. Thus, it is essential for an adsorptive carbon to have a large accessible surface area which in turn is directly related to its pore size distribution.

3.1.2 History

In 1900, two very significant processes in the development and manufacture of activated carbon products were patented. The first commercial products were produced in Europe under these patents: Eponite, from wood in 1909, and Norit, from peat in 1911. Activated carbon was first produced in the United States in 1913 by Westvaco Corp. under the name Filtchar, using a by-product of the papermaking process (Hassler, 1958). Further milestones in

development were reached as a result of World War I. In response to the need for protective gas masks, a hard, granular activated carbon was produced from coconut shell in 1915. Following the war, large-scale commercial use of activated carbon was extended to refining of beet sugar and corn syrup and to purification of municipal water supplies (Hassler, 1963). The termination of the supply of coconut char from the Philippines and India during World War II forced the development of granular activated carbon products from coal in 1940 (Carrubba et al., 1984). More recent innovations in the manufacture and use of activated carbon products have been driven by the need to recycle resources and to prevent environmental pollution.

3.1.3 Principles of Activation Process

The principle of manufacturing carbonaceous adsorbents is the selective removal of some groups of compounds from a suitable carbon containing material and generation of a highly porous solid matrix containing micropores. Removal of such compounds can be achieved by carbonization and activation of the raw materials.

3.1.3.1 Raw Materials

The quality of the resulting activated carbon is considerably influenced by the starting material. Although the activation procedure employed mainly determines the chemical nature of the surface oxides and the surface area of the resulting product, the structure of the pores and the pore size distributions are largely predetermined by the nature of the starting material. Any cheap substance with a high carbon and low ash content can be used as a raw material. Raw materials for the production of activated carbon include a number

of carbonaceous materials, especially wood, peat, brown coal, bituminous coal, lignite, coconut shells, almond shells, pits from peaches and other fruits, petroleum-based residues, pulp mill residues, and ion exchange resins. (Balcı, 1992)

Since the manufacturing process involves the removal of volatile matter, the economic relationship between price, availability and quality of raw materials on one side and volatile content on the other side, is an important one.

3.1.3.2 Production Methods

Activated carbon can be prepared by one of the following two methods:

1. By carbonizing material of vegetable origin with the addition of activating agents which influence the course of carbonization. The method is generally known as "chemical activation".

2. By allowing the inactive carbonized product prepared by the usual methods of carbonization to react with suitable, usually gaseous (generally steam or carbon dioxide) substance. This procedure is known as "physical activation" or "gas activation".

The terms “chemical” and “physical” activation, though used very frequently in the literature, are both unsuitable and do not express the actual nature of the respective process. Chemical activation is used generally when raw materials with a recent origin (currently grown) are dealt with.

The basic production processes can be combined in different ways. Sometimes the chemically activated carbon is subjected to additional activation with gaseous environment in order to increase the number of wider pores.

In contemporary technologies both types of activation, chemical and physical are widely used. Although high quality products can be obtained by both procedures, sometimes, they are not equally good for all purposes. For example, for the recovery of solvent, chemically activated carbons are preferred, whereas for water treatment, carbon activated with steam appears to be preferable. (Smisek and Cerny, 1970)

3.1.3.2.1 Physical Activation

a. Carbonization

The method of production of the carbonized intermediate product has a marked effect on the quality of the final product. The main purpose of carbonization is to reduce the volatile content of the source material in order to convert it to a suitable form for activation. During the phase of the carbonization, carbon content of the product attains a value of about 80 percent (Balcı, 1992).

During carbonization most of the non-carbon elements, hydrogen and oxygen are first removed in gaseous form by pyrolytic decomposition of the starting material and the freed atoms of elementary carbon are grouped into organized crystallographic formation known as elementary graphitic crystallites.

In the simple carbonization product, the mutual arrangement of the crystallites is irregular, so that free interstices remain between them. However, as a result of deposition and decomposition of tarry substances, these become filled or at least blocked by disorganized (amorphous) carbon. The resulting carbonized product has small adsorption capacity. Presumably, at least for carbonization at lower temperatures, part of the formed tar remains in the pores between the crystallites and on their surface. Such carbonized materials can then be partially activated by removing the tarry products by heating them in a stream of an inert gas, or by extracting them with a suitable solvent, or by a chemical reaction (for example, heating in an atmosphere of sulfur vapor at temperatures lower than those at which reactions with carbon take place). (Smisek and Cerny, 1970; Wigmans, 1985)

b. Activation with Gaseous Agents

A carbon with a large adsorption capacity can also be produced by activating the carbonized material under such conditions that the activating agent reacts with the carbon. Activation takes place in two stages. In the initial stage, when the burn-off is not higher than 10 percent, disorganized carbon is burnt out preferentially and the closed and clogged pores between the crystallites are freed. By the removal of disorganized carbon, the surface of the elementary crystallites becomes exposed to the action of the activation agent. The burning out of the crystallites must proceed at different rates on different parts of the surface exposed to reaction; otherwise new pores can not be formed.

The removal of nonorganized carbon and the non-uniform burnout of elementary crystallites lead to the formation of new pores, and to the

development of macroporous structures. The effect which becomes increasingly significant is the widening of existing pores, or the formation of larger size pores by the complete burnout of the walls between adjacent micropores.

Some difficulties may arise depending on the type of gaseous activation agent. Activation with steam and carbon dioxide are carried out at temperatures between 800°C and 1100°C. The temperature must be chosen carefully to make the determining factor as the chemical reaction between carbon and gaseous agent. At lower temperatures, reactions are too slow. In kinetics control region, reactions take place at interior surface of the carbon. Hence the removing of carbon from the pore walls causes the enlargement of the pores. However at higher temperature reactions become diffusion controlled and occur on the outside of the carbon particle. In gas activation, carbonaceous material is treated at elevated temperatures with suitable gases, the most common being steam, carbon dioxide, oxygen (air) and mixtures thereof. Experiments using graphite have established the reaction velocities: steam has been shown to be eight times as reactive as carbon dioxide. Both gases behave as mild oxidizing agents at 800 – 1000°C, there being several simultaneous reactions:

$H_2O + C \leftrightarrow CO + H_2$ $\quad \Delta H = + 117$ kJ

$2\ H_2O + C \leftrightarrow CO_2 + 2\ H_2$ $\quad \Delta H = + 75$ kJ

$CO_2 + C \rightarrow 2\ CO$ $\quad \Delta H = + 159$ kJ

Due to the endothermic character of these reactions, the carbon particles must be brought into intimate contact with the activating gas which must also be hotter than the required reaction temperature; otherwise, the necessary heat energy will not be provided, or only with difficulty. Below 800°C, the reaction velocity is so seriously reduced that the activation process ceases for all practical

purposes. A useful improvement to the heat supply can be obtained by combustion of gases produced during activation:

$CO + 0.5\ O_2 \rightarrow CO_2$ $\Delta H = -285$ kJ

$H_2 + 0.5\ O_2 \rightarrow H_2O$ $\Delta H = -238$ kJ

Modern furnace construction takes advantage of this fact by introducing oxygen and air at suitable points, which at the same time has the effect of regenerating the activating gases. Thus, the best way of dealing with the carbon monoxide and hydrogen that are produced is by burning them off in the reactor itself. This is necessary for the additional reason that these gases reduce the velocity of activation, carbon monoxide to a noticeable extent and hydrogen very markedly. The reaction mechanism for the gas activation of carbon with steam or carbon dioxide is characterized by an initial adsorption of these gases with subsequent oxidation of the carbon surface as the rate-determining step:

$C + CO_2 \rightarrow C\ (O) + CO$

$C\ (O) \rightarrow CO$

where C (O) signifies surface oxide.

The retarding action of the carbon monoxide and hydrogen can be attributed to the formation of C(CO) and C(H) surface complexes, the latter in particular being much more stable than the C(O) surface complex. Thus, the active sites which could adsorb oxygen are blocked by hydrogen (Ullmann, 2002).

The reaction of oxygen with carbon is exothermic. It may therefore be difficult to maintain the correct temperature in the oven when oxygen is used to activate the carbonized product. Possible local overheating prevents uniform activation. Furthermore, due to the aggressive action of oxygen, burnout is not

limited to pores only but also occurs on the external surface of the grain resulting in great loss. It must be noted that, carbon activated with oxygen has a large amount of surface oxides. Activation by oxygen (air) is rarely used owing to the difficulties and disadvantages just outlined. In a mixture with steam or inert gas, small amounts of oxygen lead to activated material with very large pores. Oxygen reacts with carbon about 100 times as fast as carbon dioxide. This reaction velocity is even further increased by potassium salts, so that potassium-containing raw materials react so vigorously when oxygen is present in the gas that an uncontrolled combustion takes place without producing activation. The chemical condition of the carbon surface, especially the presence of larger or smaller amounts of carbonyl and carboxyl groups, can determine the adsorption properties of the activated carbon and, very importantly, its properties as a catalyst. (Ullmann, 2002)

Acidic surface oxides are formed by heating activated carbon in air or oxygen for a short period below the ignition temperature. If carbon is first heated to 1000°C and then allowed to react with air at room temperature, basic surface oxide groups are formed, although the quantity of these is at most much less than the quantity of acidic groups.

It has long been known that the gas activation of carbonaceous materials is accelerated by small amounts of various compounds, e.g., salts of alkali and alkaline earth metals, almost all chlorides, sulfates, acetates, and carbonates, as well as most acids and hydroxides. The most important catalysts used industrially are caustic potash and potassium carbonate. Amounts between 0.1 % and 5 % are used. The activation accelerators can be used in solid form mixed with the finely powdered carbonaceous substances or added as solutions, sometimes followed by molding into shapes and low-temperature carbonization.

If bituminous coal is activated with addition of alkali metal salts, the gas mixtures containing carbon dioxide must be used for the activation process in preference to pure steam. In addition to these accelerators, the patent literature also refers to compounds of iron, manganese, and aluminum. (Ullmann, 2002)

3.1.3.2.2 Chemical Activation

In this method, the carbonaceous material is carbonized after the addition of substances which restrict the formation of tar. The activating agent added to the raw material is recovered for reuse and to free the pores after carbonization. Through chemical activation, a carbonized product with very good sorption properties can be obtained in a single operation.

Chemical activation is used almost exclusively for carbons produced from materials of recent origin, namely lignocellulosic materials. However, recent researches showed the possibility of activating polymeric resins, as raw materials, for preparing activated carbon. The activation agent influences the pyrolytic process, so that the formation of tar is restricted to a minimum. The yield of carbon in the carbonized product is increased accordingly. Furthermore, temperature needed for pyrolysis is also lower than that needed for activation with gaseous agents in physical activation, and this promotes the development of a porous structure. Under these conditions elementary crystallites of smaller dimensions, (micropores) are formed. (Balcı, 1992)

The most widely used activation agents are zinc chloride, potassium sulphide and phosphoric acid. In some studies, hydroxides of an alkali metal, magnesium and calcium chloride and other substances have also been used. All these chemicals are strong dehydrating agents. (Smisek and Cerny, 1970)

3.1.4 Physical Structure of Activated Carbon

The structure of activated carbon is best described as a twisted network of defective carbon layer planes, cross-linked by aliphatic bridging groups (McEnaney et al., 1989). X-ray diffraction patterns of activated carbon reveal that it is non-graphitic, remaining amorphous because the randomly cross-linked network inhibits reordering of the structure even when heated to 3000°C (Marsh et al., 1988). This property of activated carbon contributes to its most unique feature, namely, the highly developed and accessible internal pore structure. The surface area, dimensions, and distribution of the pores depend on the precursor and on the conditions of carbonization and activation. The structure studies of Franklin (1951) on carbonized materials showed two distinct well-defined classes; nongraphitizing carbons and graphitizing carbon. (Figure 2.1)

In general, nongraphitizing carbon is formed from substances containing little hydrogen or more oxygen. On heating such substances, at low temperature develops a strong system of cross-linking of crystallites forming a porous mass. The graphitizing carbons are prepared from substances containing more hydrogen. The crystallites remain relatively mobile during the early stages of carbonization and cross-linking is much weaker. As a result, a softer and less porous carbon is obtained.

The basic structural character of activated carbon is closely approximated by the structure of pure graphite. The graphite crystal is composed of layers of fused hexagons held approximately 0.335 nm apart by van der Waal's forces. The interatomic distance between the carbon atoms in the individual layer planes is 0.142 nm. (Figure 3.2)

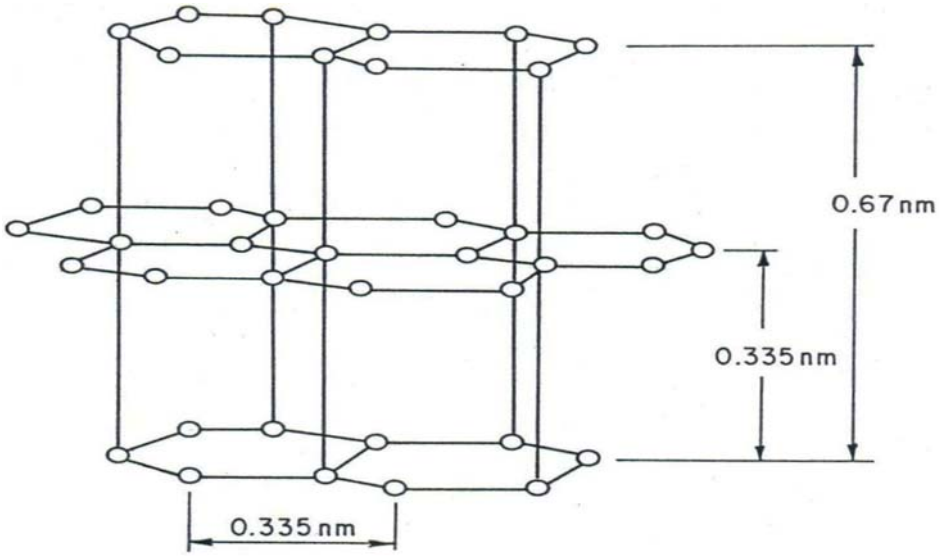

Figure 3.2 Carbon Atom Arrangement in Graphite Crystal (Smisek and Cerny, 1970)

3.1.5 Chemical Properties of Activated Carbon

The adsorptive properties of activated carbon are determined not only by its pore structure, but also by its chemical composition. Activated carbon contains two types of admixtures. One of them is represented by chemically bonded elements, in the first place oxygen and hydrogen. These are derived from the starting material and remain in the structure of activated carbon as a result of imperfect carbonization or become chemically bonded to the surface during activation. The other type of admixture consists of ash, which is an inorganic part of the product.

The elemental composition of activated carbon produced from natural starting materials typically comprises 85-90 % C, 0.5 % H, 0.5 % N, 5 % O, 1 % S, and a balance of 5-6 % representing inorganic (ash) constituents. These values can not, however, serve as specification for the quality or properties of activated carbon. (Faust et al., 1983)

Surface area generated by the more reactive edges of the microcrystallites will contain a wide variety of functional groups and will accordingly be quite heterogeneous in nature. The nature of the relevant functional groups is determined to a large extent by the method of activation as well as by the type of raw material from which the activated carbon is produced. (Balcı, 1992)

Functional groups are formed during activation by interaction of free radicals on the carbon surface with atoms such as oxygen and nitrogen, both from within the precursor and from the atmosphere (Zawadzki et al., 1989). The functional groups render the surface of activated carbon chemically reactive and influence its adsorptive properties (McEnaney et al., 1989). Activated carbon is generally considered to exhibit a low affinity for water, which is an important property with respect to the adsorption of gases in the presence of moisture (Atkinson et al., 1982). However, the functional groups on the carbon surface can interact with water, rendering the carbon surface more hydrophilic (Zawadzki et al., 1989). Surface oxidation, which is an inherent feature of activated carbon production, results in hydroxyl, carbonyl, and carboxylic groups that impart an amphoteric character to the carbon, so that it can be either acidic or basic. The electrokinetic properties of an activated carbon product are, therefore, important with respect to its use as a catalyst support (Solar et al., 1990). As influencing the adsorption of many molecules, surface oxide groups contribute to the reactivity of activated carbons toward certain solvents in solvent recovery applications (Henning et al., 1990).

In addition to surface area, pore size distribution, and surface chemistry, other important properties of commercial activated carbon products include pore

volume, particle size distribution, apparent or bulk density, particle density, abrasion resistance, hardness, and ash content.

3.1.5.1 Oxygen Containing Functional Groups

The oxygen of starting material has a considerable influence on the arrangement and size of the elementary crystallites formed in carbonaceous adsorbents. In adsorbents prepared from materials of high oxygen content, the distance between the parallel graphitic layers is appreciably smaller. Moreover, the course of carbonization and the required carbonization temperature depend very much on the oxygen content of raw material. On the other hand, if oxidizing gases possess oxygen, it can also be chemisorbed and bound as surface oxides on the edge of the layer planes. The presence of chemisorbed oxygen on the surface of activated carbon has important effects on its capacity to adsorb water vapor and vapor of the polar adsorbates.

The oxygen content of activated carbon ranges between 1% and 25% and has been shown to vary considerably with the activation temperature. The amount of oxygen decreases with an increase in the activation temperature.

Carbon activated at low temperatures of 200 to 500°C, termed as L-carbons, will generally develop acidic surface oxides. The acidic surface oxides could mainly include phenolic hydroxyl groups. The carbons activated by chemical treatment in aqueous solutions with such oxidizing agents as chloride, permanganate, persulphate, hydrogen peroxide and nitric acid develop the same characteristics as L-carbon.

The carbons activated at higher temperatures of 800 to 1000°C, termed as H-carbons, will develop basic surface oxides. Adsorption of electrolytes is affected by the presence of basic or acidic surface oxides.

The presence of surface oxygen complexes will also impart a polar character to the activated carbon surface, which should affect preferential adsorption of comparatively polar organic compounds (Balcı, 1992).

3.1.5.2 Hydrogen Containing Functional Groups

Materials prior to activation contain hydrogen in the form of hydrocarbon chains and rings attached to border atoms of the hexagon planes. Most of this hydrogen is removed during activation at temperatures below 950°C, but some hydrogen is still held after activation and is not released unless much higher temperatures are reached. It is to be noted that, the evolution of this latter portion of hydrogen at very high temperatures is paralled by a simultaneous decrease in adsorptive power.

Hydrogen is more strongly chemisorbed than oxygen. Infrared studies show that hydrogen is present in aromatic and aliphatic form. The aromatic hydrogen is suggested to be bonded covalently to the carbon atoms at the periphery of the aromatic basal planes. The aliphatic hydrogen is suggested to be present in the form of aliphatic chains and alicyclic rings attached to the peripheral aromatic rings.

In addition to hydrogen and oxygen, calcined sulphur, nitrogen, chlorine and other elements may also be present in active carbon (Balcı, 1992).

3.1.6 Mechanical Properties of Activated Carbon

Performance characteristics for activated carbon are generally expressed in relation to its mass. If figures on a volume basis are needed, bulk density or tapped density figures are also needed to carry out the conversion calculation.

The bulk density is very much dependent on the filling technique, the geometry of the vessel used, and the grain size of the material. Therefore, a defined tapping or shaking process is usually included in the case of the higher tapped densities.

Another important feature of activated carbon is its grain size distribution. This determines the resistance of a layer of activated carbon to the flow of a liquid or gas. The fineness of grinding of a powdered carbon affects the filtration properties (Ullmann, 2002).

3.1.7 Adsorption Properties and Pore Structure of Activated Carbon

The adsorption properties of activated carbon depend principally on its inner surface area, which in commercial products is 500 – 1500 m^2/g. To make use of the inner surface which is provided by the walls of the pores, the accessibility of this surface is important, that is, the pore size and the pore size distribution. This is determined by various methods, mostly from nitrogen adsorption isotherms, and is represented as integral or differential distribution curves. (Figure 3.3)

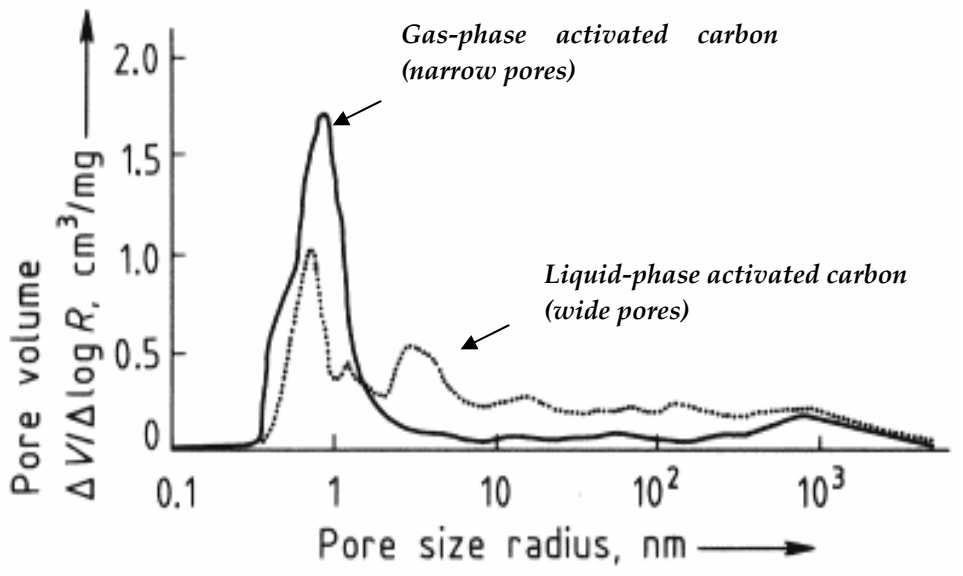

Figure 3.3 Pore Size Distribution of Different Activated Carbons

Commercial adsorbents do not have a smooth surface but are highly porous solids with a very irregular and rugged inner surface. This fact is taken into account by the potential theory which forms the basis of the Dubinin isotherm. At adsorption temperatures below the critical temperature of the component to be adsorbed, the adsorbent pores may fill up with liquid adsorbed. This phenomenon is known as capillary condensation and enhances the adsorption capacity of the adsorbent. Assuming cylindrical pores, capillary condensation can be quantitatively described with the aid of the Kelvin equation, the degree of pore filling being inversely proportional to the pore radius.

In the liquid phase, the empirical Freundlich isotherm is a very helpful tool, as the position and gradient of this isotherm allows conclusions to be drawn regarding carbon properties in practical applications. Often, specific substances like phenol, iodine, or methylene blue are used for characterizing the adsorptive properties of activated carbons.

For commercial adsorption processes not only the equilibrium value, but also the rate at which it is achieved (adsorption kinetics) is of decisive importance. The adsorption kinetics are determined by the following series of individual steps:

- Transfer of molecules to the external surface of the adsorbent
- Boundary layer film diffusion
- Diffusion into the particle
- Actual adsorption step

During the process of activation, the spaces between the elementary crystallites become cleared of various carbonaceous compounds and nonorganized carbon. Carbon is also removed partially from the graphitic layers of the elementary crystallites. The resulting voids are termed as pores. Results seem to indicate that, there are pores with a contracted entrance (ink-bottle shaped) pores in the shape of capillaries open at both ends or with one end closed, pores in the shape of more or less regular slits between two planes, v-shaped, tapered pores, and other forms.

In most cases, however it is difficult to determine the pore shapes reliably. However, the calculation of diameters of pores assuming cylindrical capillary shapes yields values which approach more nearly the actual dimensions of the pores. Activated carbon usually has pores belonging to several groups, each group having a certain range of values for the effective dimensions.

Pores of an effective diameter larger than about 50 nm are classified as macropores. Their volume in the activated carbon is generally between 0.2 cm^3/g and 0.5 cm^3/g and their surface area is 0.5 m^2/g to 2 m^2/g.

Transitional pores are those in which capillary condensation with the formation of a meniscus of the liquefied adsorbate can take place. This phenomenon usually produces the hysteresis loop on the adsorption isotherm. The effective diameters of transitional pores are in the range of 2 nm to 50 nm. Their specific surface area is generally around 5 % of the total surface area of the activated carbon.

Pores with an effective diameter of less than about 2 nm are called micropores. The micropore volume is generally between 0.15 cm^3/g to 0.50 cm^3/g. Usually the specific surface area of micropores amounts to over 90 % of the total specific surface area (Gregg and Sing 1967; Smisek and Cerny, 1970; Rodriguez Reinoso, 1989). Each of these three groups of pores has its specific function in the process of adsorption on activated carbon. According to the type of application, the percentages of the transitional pores and the micropores could be adjusted employing special production procedures.

3.1.8 Applications

The major applications are in water treatment, gas purification, food processing, gold recovery, and solvent recovery (Figure 3.4). (Ullmann, 2002)

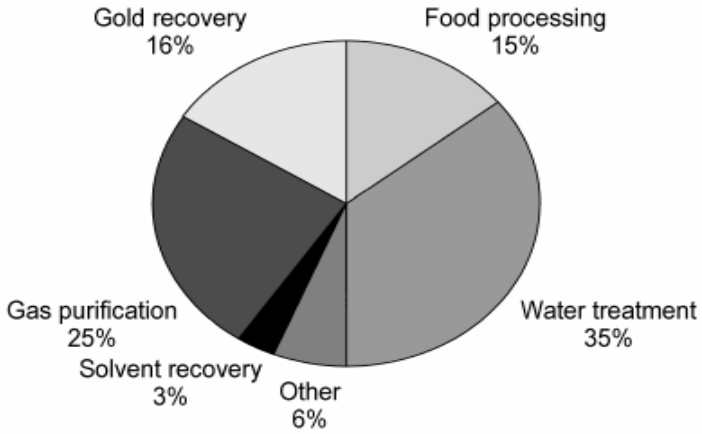

Figure 3.4 Gas and Liquid-phase Applications of Carbonaceous Adsorbents

3.1.8.1 Gas-Phase Applications

The majority of gas- and vapor-phase applications of activated carbon are in process gas purification, air purification, catalysis, flue gas purification, solvent recovery, and automotive emission control, and personal protection (Figure 3.5).(Ullmann, 2002)

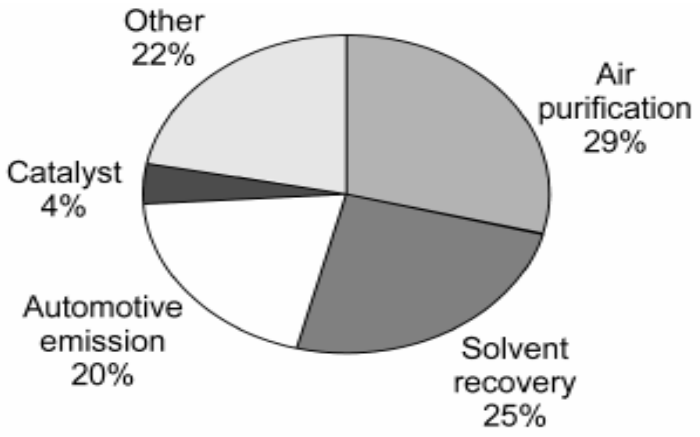

Figure 3.5 Gas-phase Applications of Carbonaceous Adsorbents

Solvent Recovery - Activated carbon can be used advantageously for the removal of organic vapors from gases, its performance being good even at very low partial pressures. Its ability to concentrate a substance is particularly useful for producing extremely pure gases, as well as for protecting the environment. The cost of regeneration, whether by steam, hot gas, or electrical heating, is usually small in comparison to the value of the recovered solvent. The charge of activated carbon retains its effectiveness for a long time if the regeneration is carried out at a sufficiently high temperature. However, fine material which is formed by attrition and thermal or chemical stress must be removed and replaced from time to time. (Ullmann, 2002)

Process-Gas and Air Purification - Many gas purification processes use activated carbon, e.g., for production of pure gases in the chemical industry, in protection against poison gas, in air conditioning, for removal of oil from compressed air, and in purification of waste air. Small traces of unwanted gases or vapors are adsorbed onto activated carbon which is often improved by being specially impregnated, in which case regeneration with recovery of the extracted materials is impossible. Activated carbon is also used to remove resin-forming and other hydrocarbons from gases before passing them over sensitive molecular sieves or catalysts.

Sulfur compounds such as carbon disulfide and organic thiols are removed from moist gases containing excess oxygen at high temperature on alkaline carbon. In air-conditioning installations, activated carbon is used for the purification of air drawn in from outside, e.g., in airports, near chemical plants, or for environmentally controlled rooms of hospitals or museums. In nuclear power installations, activated carbon impregnated with iodine compounds is used to remove radioactive iodine compounds from the air exhausted to the atmosphere. Activated carbon and impregnated activated carbon is also used for many odor emission control applications: wood chip drying, plastic processing (styrene, benzene, etc.), home application (kitchen hood, refrigerator). In cigarette filters and in attachments for tobacco pipes, activated carbon is used to reduce the nicotine and tar content of the smoke. (Ullmann, 2002)

Gas Separation - In 1960 the first pressure-swing adsorption (PSA) plants for gas drying, gas purification and gas separation were built. Several types of product gases can be obtained during the absorption or desorption step. (Ullmann, 2002)

Gasoline Vapor Adsorption - Gasoline vapors evaporate during manufacture, distribution, refueling, and running of cars and enter the environment. To avoid pollution of the environment by gasoline vapor from motor vehicles, installation of an activated carbon filter in the ventilation port of the gasoline tank is required in the United States and Japan. (Ullmann, 2002)

Flue Gas Cleaning - For SO_2 and NO_x removal from flue gases from power plants and waste incineration plants many activated carbon/activated coke processes have been developed. The adsorption capacity of activated carbon and activated coke for sulfur dioxide from flue gas is only a few percent by weight. Therefore, processes are based on the ability of activated coke to oxidize sulfur dioxide in the presence of oxygen, forming sulfuric acid. The spent activated coke can be regenerated thermally at 400 – 500°C in a desorber; the carbon of the activated carbon skeleton is used as a reactant. This carbon consumption results in a larger inner surface area and higher catalytic activity, converting the activated coke to activated carbon. The SO_2-rich gas can be processed to elemental sulfur or sulfuric acid.

The catalytic properties of activated carbon are used for catalytic NO reduction by addition of gaseous ammonia. In waste incineration plants, powdered activated carbon is injected into the flue gas stream through an atomizer. The loaded adsorbent is collected in a fabric filter; further pollutant removal takes place in the filter cake deposited on the fabric. (Ullmann, 2002)

3.1.8.2 Liquid-Phase Applications

Liquid-phase applications are estimated to account for over two-thirds of world activated carbon consumption; both granular and powdered activated

carbons are in use. Percolation through granular carbon is used particularly in the field of water purification and decolorization. Activated carbon and activated coke are often used in combination with other filter materials in multilayer filters for wastewater and drinking water treatment. (Ullmann, 2002)

Water Treatment - Water treatment (35 % of world consumption) can be divided into drinking water, industrial and municipal wastewater, and groundwater. In drinking water, activated carbon is used to remove unpleasant odors and tastes and reduce the concentration of compounds constituting a health hazard (pesticides, chlorinated hydrocarbons, etc.). Powdered activated carbon is often used to solve temporary pollution problems. When granular activated carbon is used to purify drinking water, after a rapid gravity sand filtration (removal of suspended solids) the percolation process is used almost exclusively, and in addition to the adsorptive purification, the catalytic decomposition of the oxidizing agents chlorine, chlorine dioxide, and ozone plays an important role. (Ullmann, 2002)

Micellaneous Liquid-Phase Applications - Both powdered and granular activated carbons made from a variety of raw materials are used in food and beverage processing. Wood-based chemically activated carbons are preferable for the removal of large color bodies and other high molecular mass impurities. Peat- and coal-based steam-activated carbons are used for decolorization and removal of unpleasant tastes, odors, and other low and medium molecular mass impurities. Microporous coconut-shell activated carbons are less efficient in decolorization. Powdered grades are used in batch processes which already require a filtration stage and where the dosage needs to be varied according to different process conditions. Some products which are purified with

activated carbon are: alcoholic beverages, soft drinks, sugar and sweeteners, chemicals and pharmaceutical products, etc…

Activated carbon processes have been developed for gold recovery from low-grade ores. Activated coconut carbon or extruded granular carbon, with high attrition and abrasion resistance, are used.

One of the oldest uses is in medicine for the adsorption of harmful bacteria and their metabolic products in the gastrointestinal tract. For blood dialysis treatment in cases of kidney and liver diseases or poisoning, granular activated carbon with a semi permeable coating is used. (Ullmann, 2002)

Impregnated Activated Carbon - Impregnated activated carbon is predominantly used in the following applications: gas purification, civil and military gas protection, catalysis. For these applications the manufacturers offer various qualities of impregnated activated carbon. (Ullmann,2002)

Catalysts and Catalyst Supports – The catalytic action of activated carbon is due to the crystalline structure of the skeleton, which consists of a mixture of amorphous and graphitic carbon. On the rims of the layers, there are many unsaturated edges and ridges which act as lattice vacancies. On the internal activated carbon surface, there are surface oxides, which have been identified as carbonyl groups, lactone groups, phenolic hydroxyl groups, and carboxyl groups. These surface oxides can participate in redox reactions, and they are a reason for the effectiveness of activated carbon catalysts in oxidation reactions. Activated carbon serves as a catalyst in the synthesis of phosgene from carbon monoxide and chlorine and in the synthesis of sulfuryl chloride from sulfur dioxide and chlorine. (Ullmann, 2002)

3.2 ION EXCHANGERS

3.2.1. Definition and Principles

Ion exchange is a process in which cations or anions in a liquid are exchanged with cations or anions on a solid sorbent in such a way that electroneutrality is maintained in both the liquid and solid phases. The solid matrix is mostly a resinous organic skeleton though inorganic ion exchangers are also present. The process is reversible, which allows extended use of the sorbent resin before replacement is necessary.

The ion exchanger may be a salt, acid, or base in solid form that is insoluble in water but hydrated. Exchange reactions take place in the water, retained by the ion exchanger; this is generally termed swelling water or gel water. Figure 3.6 shows the partial structure of a cation exchanger; each positive or negative ion is surrounded by water molecules. (Kirk-Othmer, 2001)

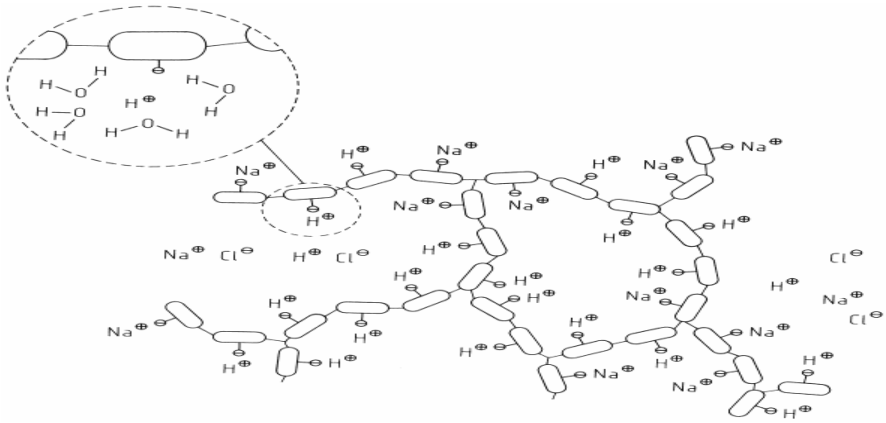

Figure 3.6 Structure of a Cation Exchanger of H^+ Ions for Na^+ Ones (Swelling Water is represented in the Insert)

Ion exchange forms the basis of a large number of chemical processes which can be divided into three main categories: substitution, separation, and removal of ions.

3.2.2. Historical Aspects

Many naturally occurring inorganic and organic materials have ion-exchange properties. The discovery of ion exchange dates from the middle of the nineteenth century when Thomson and Way noticed in 1850 that ammonium sulfate was transformed into calcium sulfate after percolation through a tube filled with soil. In 1905, Gans softened water for the first time by passing it through a column of sodium aluminosilicate that could be regenerated with sodium chloride solution.

Synthetic organic ion-exchange resins became available in the late 1930s with the introduction of phenolic-type products. In 1935, Liebknecht and Smit discovered that certain types of coal could be sulphonated to give a chemically and mechanically stable cation exchanger. In addition, Adams and Holmes in 1935 produced the first synthetic cation and anion exchangers by polycondensation of phenol with formaldehyde and a polyamine, respectively. Demineralization then became possible. Styrenic resins appeared in the mid-1940s and acrylic resins about 20 years later. The ion-exchange market of the early to middle 1990s is dominated by the styrenic resins, but acrylic resins are becoming increasingly important. Phenolic-based resins have almost disappeared. A few other resin types are available commercially but have not made a significant impact. Inorganic materials retain importance in a number of areas where synthetic organic ion-exchange resins are not normally used. At present, aluminosilicates and phenol-formaldehyde resins are reserved for special applications and sulphonated coal has been replaced by sulphonated polystyrene. (Kirk-Othmer, 2001)

Macroporous Resins - Two of the problems encountered in the use of ion-exchange resins are the fouling of the resin by natural organic acids present in surface waters and the mechanical stress imposed by plants operating at high flow rates. To cope with these, manufacturers produced resins with a high degree of cross-linking but containing artificial open pores in the form of channels with diameters up to 150 nm that can adsorb large molecules. Resins in which the polymer is artificially expanded by the addition of a nonpolymerizable compound that is soluble in the monomer are known as macroporous or macroreticular resins. Other naturally porous resins are known as gel resins.

3.2.3. Structures of Ion-Exchange Resins

A synthetic ion exchanger consists of a polymeric matrix and functional groups that interact with the ions.

3.2.3.1. Polymer Matrices

The polymer matrix is the insoluble solid backbone of the ion exchange resin. There are numerous polymers employed for this purpose, such as polyacrylates obtained by polymerizing an acrylate, a methacrylate, or an acrylonitrile, any of which can be cross-linked with divinylbenzene, phenol formaldehyde resins which show interesting adsorption properties, and polyalkylamine resins, obtained from polyamines, which gives an anion exchanger directly in a single step. The most well known and by far the most important commercial polymeric matrix is, however, based on polystyrene crosslinked with divinylbenzene to yield a porous structure.

Polystyrene Matrix - The polymerization of styrene (vinyl benzene) under the influence of a catalyst (usually an inorganic peroxide) yields linear polystyrene. Linear polystyrene is a clear moldable plastic, which is soluble in certain solvents (e.g., styrene or toluene) and has a well-defined softening point. If a proportion of divinylbenzene is mixed with styrene, the resultant polymer becomes crosslinked and is then completely insoluble. A sketch of structure for cross-linked polystyrene is given in Fig. 3.7.

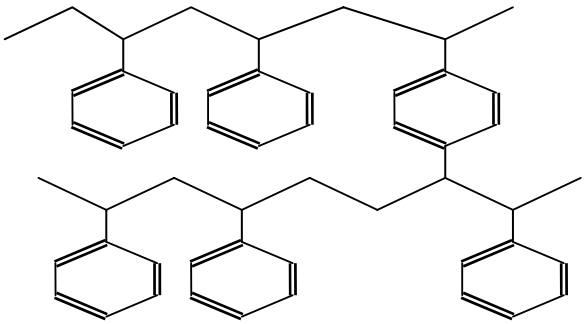

Figure 3.7 Cross-linked Polystyrene

In the manufacture of ion-exchange resins, polymerization generally occurs in suspension. Monomer droplets are formed in water and, upon completion of the polymerization process, become hard spherical beads of the polymer.

3.2.3.2. Functional Groups

3.2.3.2.1. Cation-Exchange Resins

Copolymers do not have the ability to exchange ions. Such properties are imparted by chemically bonding acidic or basic functional groups to the aromatic rings of styrenic copolymers, or by modifying the carboxyl groups of the acrylic copolymers. Cation-exchange resins in current use can be separated into two

classes according to their active groups: (1) strongly acidic (sulphonic groups) and (2) weakly acidic (carboxylic groups).

Strongly Acidic Cation-Exchange Resins – All strong acid-type resins are made from styrene-DVB copolymers, with the exception of a minor quantity of phenolic resin. Chemically inert, crosslinked polystyrene beads are treated with concentrated sulfuric or chlorosulfonic acid to give cross-linked polystyrene 3 sulfonic acid. This material is the most widely used cation-exchange resin and is strongly acidic. A schematic representation is presented in Fig. 3.8.

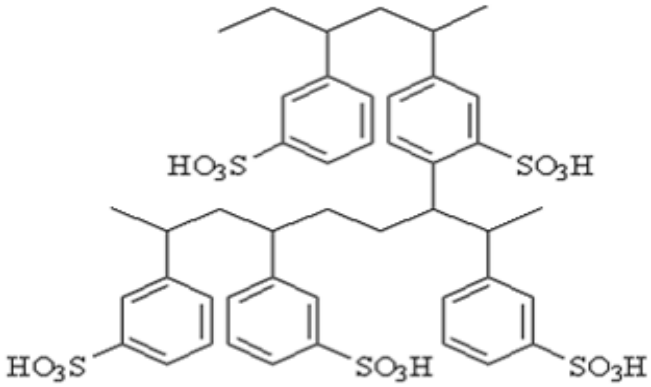

Figure 3.8 Cross-linked Polystyrene 3-Sulfonic Acid

Commercial demand for strong acid resins is greatest for those having microporous properties and a copolymer DVB content of 8%. Resins having greater cross-linking are generally preferred in processes where significant oxidative attack is expected because these are more resistant to deterioration.

Weakly Acidic Carboxylic Cation-Exchange Resins - The weakly acidic resins are almost always obtained by hydrolysis of polymethylacrylate or polyacrylonitrile to give a poly (acrylic acid) matrix.

3.2.4. Properties

3.2.4.1. Degree of Cross-Linking and Porosity

Porosity is more dependent on the solvent used when manufacturing the copolymer than on the degree of cross-linking. Porosity of a resin is controlled by varying the amount of divinylbenzene (DVB) which is incorporated into the matrix. The lower the degree of cross-linkage the more the ion-exchange resin will swell in an aqueous medium, approaching the density of water in swollen state. The volumetric capacity of the product is correspondingly decreased. The beads of particles of resin become softer and less resistant to deformation and oxidation. They also swell and shrink more during regeneration and exhaustion.

In contrast, highly cross-linked products have maximum volume capacity, stability, density, and resistance to deformation and particle breakage. An increase in the degree of cross-linking (i.e., the weight percentage of DVB based on the total amount of monomer prior to polymerization) produces harder, less elastic resins. Resins with higher degrees of cross-linking show more resistance to oxidizing conditions which tend to de-crosslink the polymer. Above 10-12% DVB, however, the structure becomes too hard and dense. Ion exchanging process becomes more difficult because access to the interior of the bead is hindered by the high density of the matrix. In addition, osmotic stress can not be adsorbed by the elasticity of the structure, which causes the bead to shatter. Finally, the rate of exchange increases in proportion to the mobility of the ions inside the exchanger bead: if the structure is too dense, ionic motion is slowed down, thus reducing the operating capacity of the resin. For sulphonic resins, maximum operating capacity is obtained with approximately 8% DVB. (Ullmann, 2002)

Cross-Linking and Affinity - The greater the ionic mobility in the resin, the poorer is the differentiation between the adsorption of ionic species with the same charge. Consequently, the degree of cross-linking in the resin must be increased when greater differences in ionic affinity are required.

In water treatment, the sulphonated polystyrene resins usually have an approximate DVB concentration of 8%. Resins with a slightly higher degree of cross-linking (10-12%) are sometimes used to increase the retention of mineral ions when water of very high purity is being produced. Resins with slightly lower levels of cross-linking (5-7%) may be chosen when easier desorption and, hence, better regeneration efficiency are required, especially in water softening.

Non-uniformity in the Matrix - Cross-linking reduces the retention of water in ion-exchange resins. The volume occupied by this water is a measure of the resin's porosity. Cross-linking is not uniform because the DVB - DVB reaction is more rapid than that between DVB and styrene. Polymerization begins to occur around the catalyst molecules, and polymer growth is faster at sites rich in DVB than at those rich in styrene. Material with an average of 8% DVB may therefore contain local microscopic regions with more than 20% DVB, whereas other regions may have less than 4%.

Macroporous Resins, also called macroreticular, are made by mixing the monomers with a compound (e.g., heptane, saturated fatty acids, C_4 – C_{10} alcohols or polyalcohols, or low molecular mass linear polystyrene) which expands the resin. The substance does not itself polymerize and, thus, although it acts as a solvent for the monomers, it causes the polymer to precipitate from the liquid. Macroporous resins have a measurable porosity which does not disappear when the resin is dry.

Macroporous cation exchangers usually have 12 to 25% DVB. They are particularly useful in applications where oxidative attack is severe. They are also beneficial in non-aqueous systems. A substantially larger number of functional groups, or exchange sites, are available along the internal surfaces present in macroporous-type resins, compared to just those sites on the outer surface of an un-swollen microporous resin.

Channels are formed inside the beads, producing an artificially high porosity. Resins containing such channels are described as macroporous, whereas other resins with natural porosity, usually microporous, are known as gel resins (Fig. 3.9). Porosity of this type resin cannot be measured by standard techniques. Gel resins are porous when the particles are swollen with water or another solvent. That is these resins have no porosity when the resin is dry. Microporosity is inversely proportional to the degree of cross-linking. Large ions migrate through a low cross-linked resin faster than through the less porous, higher crosslinked resins.

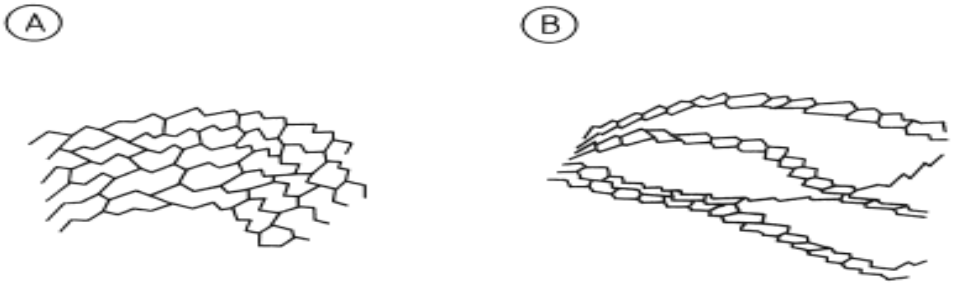

Figure 3.9 Arrangement of Structural Units in Gel (A) and Macroporous (B) Resins. (Ullmann, 2002)

Macroporous resins have a higher degree of cross-linking than gel resins to strengthen the matrix and compensate for voids left by the added solvent. The porosity and mechanical strength of the resin can be modified by varying the degree of cross-linking or the amount of solvent added. Therefore, various

macroporous resins are available, with different moisture-holding capacities and internal structures.

The pore diameter in a macroporous resin is around 100 nm, in contrast to a diameter of about 1 nm in a gel resin. The macropores form a network of channels filled with free water, and large molecules can move freely in the resin into the centre of a bead. Once inside the resin, ions generally have a much shorter distance to travel before they encounter an active group: around 100 nm in macroporous resins and up to 500 μm in gel resins. Exchange is thus faster in a macroporous resin. (Ullmann, 2002)

Macroporous resins are highly resistant to physical stress and generally withstand osmotic shock very well. They are, therefore, used in systems where mechanical and osmotic stress would otherwise cause gel resins to deteriorate rapidly, such as those involving circulation of resin, fluidized beds, high flow rates, oxidizing conditions, concentrated solutions, and short cycles. Finally, macroporous resins are used when reversible uptake of large molecules is necessary, without fouling the resin.

3.2.4.2. Exchange Capacity

Total Capacity - The total exchange capacity of a resin, expressed in equivalents per unit weight (or per unit volume), represents the number of active sites available. In polystyrene exchangers, the maximum number of active sites corresponds to the "grafting" of one active group per benzene ring. The capacity is expressed in equivalents (eq) per kilogram of dry resin (the weight capacity C_p) or equivalents per liter of wet settled resin (the volume capacity C_v).

The actual capacity is however less than this maximum since it is difficult to attach active groups to every benzene ring in the matrix.

Operating Capacity - The operating capacity is defined as the proportion of total capacity used during the exchange process. It can amount to a large or small proportion of the total capacity and depends on a number of process variables including

1) concentration and type of ions to be absorbed,
2) rate of percolation,
3) temperature,
4) depth of resin bed, and
5) type, concentration, and quantity of regenerant.

3.2.4.3. Stability and Service Life

Because ion-exchange resins must give several years of service, their stability over long periods of time is of prime importance.

Chemical Stability of the Matrix - Industrially available resins have a degree of cross-linking high enough to make them insoluble. Highly oxidizing conditions (presence of chlorine or chromic acid) can attack the matrix and destroy cross-linking. When oxidizing agents are present, highly cross-linked resins with a greater resistance to oxidation, such as the macroporous resins, should be used.

Thermal Stability of Active Groups - The sulphonic group of cation-exchange resins is extremely stable. Anion-exchange resins, on the other hand, are temperature-sensitive.

Mechanical Stability – Polycondensation-type resins that are manufactured in bulk and broken up into irregular grains are comparatively fragile and used only in fixed beds. Polystyrene and polyacrylic resins made by suspension polymerization are perfect spheres and suffer little damage when used in continuous moving-bed ion-exchange plants. Macroporous resins are often the strongest of all and are used widely for the most severe stress conditions.

The less elastic resins, i.e., those with the higher degree of cross-linking (gel resins with >8% DVB and macroporous resins with >15% DVB), have the disadvantage that, when they do break, they explode into minute fragments, whereas other resins break into two or three usable pieces.

3.2.4.4. Density

Resin density is an important property because it determines the hydrodynamic behavior in counterflow systems. Resin density normally lies in the following ranges (figures in parentheses are the most common values for standard resins). (Ullmann, 2002)

Strongly acidic cation exchangers	1.18-1.38 (1.28 g/cm^3)
Weakly acidic cation exchangers	1.13-1.20 (1.18 g/cm^3)
Strongly basic anion exchangers	1.07-1.12 (1.10 g/cm^3)
Weakly basic anion exchangers	1.02-1.10 (1.05 g/cm^3)

By choosing suitable particle sizes, several different types of resin can be used in the same column. If necessary, they can be kept separate by an up flow of water. This is used mainly in layered beds.

3.2.4.5. Particle Size

The ion–exchange particles have a different volume in the dry and the wet states and therefore also have different particle sizes. This difference is due to the moisture-holding capacity of the exchange resins and depends on the nature of the functional group and the degree of cross-linking.

For industrial use, particle size is a compromise between the speed of the exchange reaction (which is greater with small beads) and high flow rates (which require coarse particles to minimize the head loss). Standard resins contain particles with diameters from 0.3 to 1.2 mm, but coarser or finer grades are available.

The size of the polymer droplets formed during polymerization and, hence, the sizes of the resin beads are determined by the suspension medium, the monomer concentration, and the rate of stirring. The beads always have a range of particle sizes rather than a uniform size (Table 3.1). (Ullmann, 2002)

Table 3.1 A Typical Particle-Size Distribution of Ion Exchange Resins

Sieve aperture, mm	Noncumulative total (between sieves), %
> 1.25	0.6
-1.25/+1.00	4.9
-1.00/+0.80	20.4
-0.80/+0.63	33.3
-0.63/+0.50	30.8
-0.50/+0.40	8.5
-0.4/+0.315	1.3
<0.315	0.2

Effective particle size 0.50 mm, mean diameter 0.68 mm

3.2.4.6. Moisture Content

Ion-exchange resins carry both fixed and mobile ions which are always surrounded by water molecules located in the interior of the resin beads. The water retention capacity governs the kinetics, exchange capacity, and mechanical strength of ion-exchange resins.

The moisture content or moisture-holding capacity (MHC) is defined as

$MHC = (W_{Hydr} - W_{Dry}) / W_{Hydr}$

Where W_{Hydr} is the weight of the hydrated resin sample, and W_{Dry} the weight of the same sample after drying.

The MHC of an ion-exchange resin is an inverse function of the degree of cross-linking unless the porosity or degree of cross-linking in the polymer is artificially increased (as in macroporous resins).

In all cases, the ionic form of the resin at the time of measurement should be quoted.

CHAPTER IV

PHYSICAL CHARACTERIZATION METHODS OF ACTIVATED CARBON

4.1. GENERAL

There are numerous techniques and methods for the characterization of pore structure of activated carbon. Since by nature the size of the pores vary in a wide range, (e.g. macro, meso, micro) there is not a single technique to provide information in all ranges of pores. Therefore, in most cases a combination of different methods are used. For the quantitative characterization of the pore structures; estimation of pore surface area, pore volume, and pore size distribution together with the true and apparent density determinations are needed. For this purpose; the adsorption of gases and vapors by standard gravimetric or volumetric techniques and mercury porosimetry are still classical and convenient approaches to the general characterization of porosity in activated carbon. Other, complementary techniques such as, small angle scattering (X-rays or Neutrons), transmission electron microscopy, etc. are also used or the characterization of pores. (Şenel, 1994)

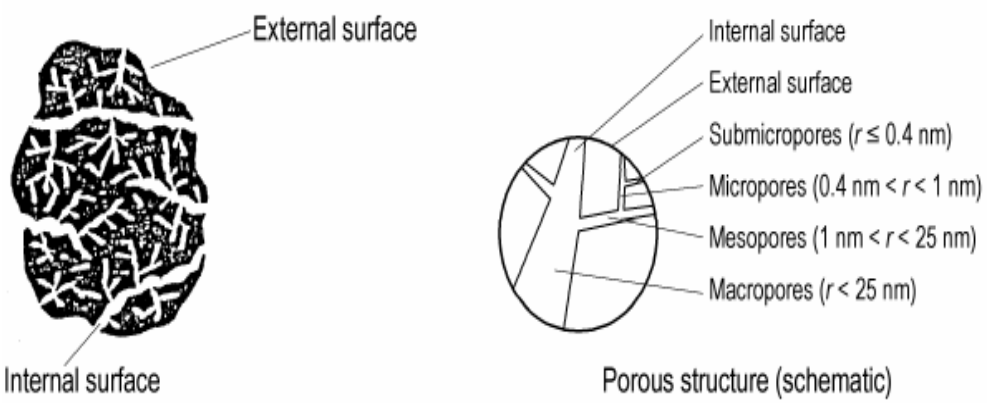

Figure 4.1 Micropore, Mesopore and Macropore Regions of Activated Carbon

Figure 4.1 shows micro, meso and macropore regions of activated carbon. In the following sections of this chapter, the main theory and methods involved in these characterization tests are given.

4.2. ADSORPTION PHENOMENA AND STANDARD ISOTHERMS

When a gas (adsorbate) is confined in a closed space, in the presence of an outgassed solid (adsorbent), an adsorption process begins. The gas molecules are transferred and accumulated on and in the solid material as a result of the forces between the solid surface and the adsorbate. Physical adsorption includes attractive dispersion forces and at very short distances repulsive forces as well as the contribution from the polarization and electrostatic forces between the permanent electric moment and the electric field of the solid.

The amount adsorbed on a solid surface will depend upon the temperature, pressure and the interaction potential between the vapor and the surface. Therefore, at some equilibrium pressure and temperature, a plot of weight of gas adsorbed per unit weight of adsorbent versus pressure is referred to as the sorption isotherm of a particular vapor-solid interface.

Brunauer et al. (1940), based upon an extensive literature survey, found that most of the adsorption isotherms fit into one of the five types shown in Figure 4.2. Type I isotherm indicates that the pores are microporous. Type II isotherms are most frequently encountered when adsorption occurs on nonporous powders or on powders with pore diameters larger than micropores. The inflection point of the isotherm usually occurs near the completion of the first adsorbed monolayer and with increasing relative pressure, second and higher layers are completed until at saturation the number of adsorbed layers becomes infinite.

Type III isotherms are observed when the adsorbate interaction with an adsorbed layer is greater than the interaction with the adsorbent surface. Type IV isotherms occur on porous adsorbents possessing pores mainly in mesopore range. The slope increases at higher pressures as it is true for the Type II, the knee generally occurs near the completion of the first monolayer. Type V isotherms result from small adsorbate-adsorbent interaction potentials similar to the Type III isotherms. However, they are also associated with the pores in the same range as those of the Type IV isotherms. A new rare type of isotherm, Type VI recently has been found which exhibits a series of steps.

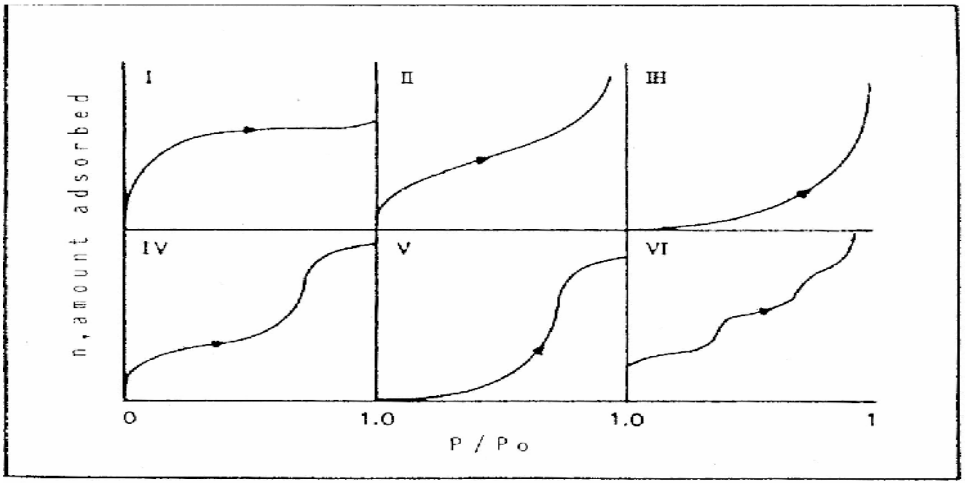

Figure 4.2 Schematic Representations of Different Types of Adsorption Isotherms

4.2.1. The Brunauer, Emmett and Teller (BET) Theory

Although derived over sixty years ago, the BET theory continues to be almost universally used because of its simplicity, and its ability to accommodate each of the five isotherm types. The BET model extends the monolayer Langmuir model to multilayer adsorption. It assumes that the surface is homogeneous and that the different layers of molecules do not interact. Each adsorbed molecule in the monolayer is assumed to be adsorption site for second layer of molecules, and so on as the relative pressure increases, until bulk condensation occurs.

In the region of relative pressures near the completion of monolayer, the BET theory and experimental isotherms do agree very well leading to a powerful and extremely useful method for the estimation of surface areas of various materials including activated carbon, coal and coal chars as well. In the final form it is given as;

$$\frac{P}{V\left[P_O - P\right]} = \frac{1}{VmC} + \frac{C-1}{V_m C}\frac{P}{P_O} \qquad (4.2.1)$$

where; V and V_m are the volume adsorbed, at the relative equilibrium pressure P/Po, and the monolayer capacity respectively, C is a constant, which is related exponentially to the heat of adsorption at the first and subsequent layers by the equation

$$C = \exp\left[\left(q_1 - q_2\right)/RT\right] \qquad (4.2.2)$$

where; q_1 is the heat of adsorption of the first layer, q_2, is the heat of adsorption of the second and subsequent layers. The determination of surface areas from the BET theory is a straightforward application of equation (4.2.1). A plot of P/V(P-Po) versus P/Po, will yield a straight line usually in the range of 0.05 < P/Po < 0.35. The slope S and the intercept of I of a BET plot will give

$$S = \frac{[C-1]}{V_m C} \quad \text{and} \quad I = \frac{1}{V_m C} \tag{4.2.3}$$

Solving the preceding equations for V_m and C gives;

$$V_m = \frac{1}{S} + I \quad \text{and} \quad C = S + \frac{1}{I} \tag{4.2.4}$$

The BET equation usually gives a good representation of the frequently appearing Type II and IV isotherms within the range of relative pressures 0.05-0.3, and this range is generally used in practice for measurement of the surface area. At higher relative pressures, the BET equation is usually inaccurate because of capillary condensation effect, while at P/Po values below about 0.05, the amount of adsorbed gas is too small to be measured with sufficient accuracy. A poorer description is obtained for the type I, III and V isotherms, but in practice, they are often analyzed by the BET method. In order to calculate the surface area, it is necessary to know the mean cross-sectional area A_m occupied by one molecule of adsorbate gas. The specific surface area is calculated from the equation,

$$S_{BET} = \frac{V_m N_A A_m}{V_{mol}} \tag{4.2.5}$$

in which; V_m is volume of monolayer, N_A is the Avagadro's constant and V_{mol} is the molar volume of the gas. The cross-sectional area of any adsorbed gas molecule can be estimated from the density of the condensed phase of the gas. (Şenel, 1994)

For surface area determinations, nitrogen as being the ideal adsorbate, exhibits the unusual property that on almost all surfaces its C value is sufficiently small to prevent localized adsorption and yet adequately large to prevent the adsorbed layer from behaving as a two dimensional gas. Thus, the unique

properties of nitrogen have led to its acceptance as a universal, standard adsorbate with an assigned cross sectional area of 0.162 nm^2 at its boiling point of -195.6^oC (Livingstone, 1949). Using BET it is possible to measure pores down to 10^oA (1 nm).

4.2.2. Pore Analysis by Adsorption / Desorption

Another way to get information on the porous texture of the adsorbent is to look at the shape of the desorption isotherm. It is commonly found for porous solids that the adsorption and desorption branches are not coincident over the whole pressure range. At relative pressures above 0.3, De Boer (1958), has identified four types of hysteresis loops which is correlated with various pore shapes, Figure 4.3 shows idealization of the four types of hysteresis (Gregg and Sing, 1982).

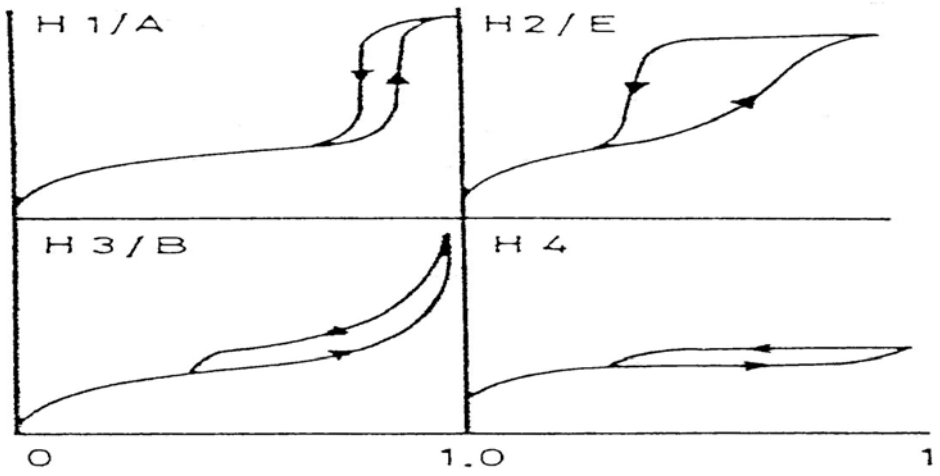

Figure 4.3 Types of Adsorption-Desorption Hysteresis Loops

Type I hysteresis is often associated with capillary condensation in open-ended cylindrical-shaped pores. The formation of a cylindrical meniscus occurs at a higher P/Po than the emptying process, which proceeds through the evaporation from a hemispherical meniscus. Type II corresponds to spheroidal cavities or voids as well as to "ink- bottle" pores. The liquid trapped in the body

of the pore until P/Po is reduced to allow evaporation from the neck; therefore, the release of condensate is limited by the neck radius. Type III hysteresis exhibits no limiting adsorption at P/Po = 1 indicating the existence of slit shaped pores. Type IV hysteresis is associated with Type I isotherms, that is with microporous adsorbents.

The hysteresis part of the isotherms contains information about the mesopores. There is a relationship between shape and position of the isotherm and the pore geometry, due to condensation and evaporation phenomena. These can be described by Kelvin's capillary condensation equation (Gregg and Sing, 1967) as;

$$r_P = \frac{-2\sigma V_{mol} Cos\ \theta}{RT \ln\left[P / P_o\right]} \qquad (4.2.6)$$

where, r_p is the mean radius of the liquid meniscus, σ is the surface tension, R is the gas constant ,T is the absolute temperature, (θ) is the angle of contact between the condensed phase and the surface of the solid. In finding the pore radius by the Kelvin equation it is necessary to take into consideration the thickness t of the adsorbate layer. Then, the actual pore radius r_p is given by,

$$r_p = r_k + t \qquad (4.2.7)$$

The term r_k indicates the radius into which condensation occurs at the required relative pressure. This radius, called the Kelvin radius or the critical radius, is not the actual pore radius since some adsorption has already occurred on the pore wall prior to condensation, leaving a center core or radius, r_k. Alternatively, during desorption, an adsorbed film remains on the pore wall when evaporation of the center core takes place. Halsey (1948) set up a useful analytical expression for the thickness of the layer t as a function of the relative

pressure,

$$t = t_m \left[\frac{5}{\ln \left(P / P_o \right)} \right]^{1/3} \qquad (4.2.8)$$

Here, "t_m" is the thickness of the monolayer. Thus, replacing equation (4.2.6) and (4.2.8) into (4.2.7) for nitrogen as the adsorbate at its normal boiling point of -195.6°C, with t_m as 0.354 nm, the following equation is obtained:

$$r_P = \frac{4.15}{\log \left(P_O / P \right)} + 3.54 \left[\frac{5}{2.303 \log \left(P_O / P \right)} \right] \qquad (4.2.9)$$

Here, a closely packed hexagonal liquid structure is assumed for the nitrogen molecules. The question of whether or not the adsorption or desorption branch is better suited for calculation of the mesopore size has not yet been answered definitely.

For a symmetrical pore geometry, calculation of the size distribution of the mesopores from the adsorption or desorption data permits a simple determination of the mesopore surface area. The gas volumes adsorbed or desorbed upon a change of the relative pressure are taken from the isotherms, and Equation (4.2.9) is used to calculate the corresponding mesopore radius. Assuming certain pore geometry, the contribution to the surface area from the pores of various sizes can be found from the pore radius distribution.

Stepwise computational methods for finding the pore radius distribution and the mesopore surface area and volume are described by several investigators (Pierce, 1953; Orr, 1959; Broekhoff, 1970). One computational method (BJH) method, proposed by Barrett, Joyner and Halenda (1951), was frequently used in practice. Derivations of the related equations are given in Appendix B. 1.

4.2.3. Characterization of Microporosity

Adsorption in microporous solids is not very well understood in comparison with non-porous or mesoporous solids. Pore sizes of similar order of magnitude as the sizes of the adsorbate molecules lead neither to the progressive completion of a monolayer nor to multilayer adsorption but to the filling up of the micropore volume with the adsorbate in a liquid like condition. A major development in understanding adsorption of gases and vapors on microporous carbons was provided by the potential theory of adsorption of Polanyi (1932).

Potential theory assumes that at the adsorbent surface the molecules of gases are compressed by attractive forces acting between the surface and the molecules and these forces of attraction decrease with increasing distance from the surface. Polanyi described the adsorption space as a series of equipotential surfaces, each with the adsorption potential E_i, and each enclosing a volume W_i. As one moves away from the surface the values of adsorption potential decrease until it falls to zero and the adsorption space increases up to a limiting value W_o (zero potential). At the surface, W=O and $E_i=E_{max}$. The building up of the volume enclosed within the adsorption space may be described by the function of the type E = f(W).

Polanyi assumed that since dispersion and electrostatic forces are independent of temperature, the adsorption potential at constant volume filling is also temperature independent. This means that the curve E = f(W) should be the same as for a given gas and a given adsorbent at all temperatures. This relationship between E and W is called the characteristic curve. Polanyi expressed the adsorption potential for a volume filling as the amount of work

necessary to compress the adsorbate from its equilibrium vapor pressure P_1 to the compressed adsorbate pressure, P_2.

$$E = \int_{P_1}^{P_2} \frac{RT}{P} dP = RT \ln \frac{P_2}{P_1} \quad (4.2.10)$$

Thus, E is equal to the ΔG "equivalent free energy change". The state of the compressed adsorbate in the adsorption space depends on the temperature. Polanyi distinguished three different cases. (i) when the temperature is well below the critical temperature of the adsorption, T_C, adsorbed vapor may be considered as liquid like. (ii) when the temperature is just below the T_C most of the adsorbate will be as liquid like but also the adsorbate may be as compressed gas. (iii) when the temperature is above the T_c, the adsorbate will be as compressed gas. The first case is, by far, the most common one. Therefore the adsorption potential will take the form

$$E = RT \ln \frac{P_O}{P} \quad (4.2.11)$$

In this equation it is assumed that the liquefied adsorbate is incompressible and has the normal density of the liquid at the given adsorption temperature, then it is possible to obtain the volume filled adsorption space by

$$W = \frac{nM}{\rho} = nV_{mol} \quad (4.2.12)$$

where, n is the amount adsorbed in moles, M is the molecular weight of the adsorbate and ρ is the liquid density. The temperature-invariance of the adsorption potential which is the fundamental postulate of the Polanyi's theory, has been demonstrated, mainly by Dubinin and co-workers (1966) and they have added a second postulate. They stated that for an identical degree of filling of the volume of adsorption space, the ratio of adsorption potentials for any two

vapors is constant which is called the affinity coefficient, β. Dubinin's treatment has been modified by Kaganer to yield a method for calculation of specific surface from the isotherm. Using the experimental data and assuming that pore size distribution is Gaussian, Dubinin and Radushkevich, 1947, arrived at an expression which is known as "Dubinin Radushkevich", (D-R) equation;

$$\log W = \log W_O - D \log^2 \left(\frac{P_O}{P} \right) \qquad (4.2.13)$$

where D is 2.303 K (RT / β)^2. A plot of log W against log (Po/P) will be straight line having an intercept equal to micropore volume, W_o. Dubinin and Astakhov (1971), assuming a Weibull distribution of pore sizes, rather than a Gaussian, obtained the following "Dubinin - Astakhov, (D-A)" equation;

$$\log W = \log W_O - D' \log^n \left(\frac{P_O}{P} \right) \qquad (4.2.14)$$

where D'= 2.303$^{(n-1)}$ (RT/E)^n. It follows from the equation (4.2.14), that "DR" equation is a special case of "D-A" equation (4.2.13), when n=2. The lower limit of CO_2 adsorption technique is down to 4-5^{o}A.

4.3. MERCURY INTRUSION POROSIMETRY

Washburn in 1921 first suggested the use of Mercury intrusion under pressure to determine the pore size distribution of porous solids. The principle of the mercury intrusion technique is based on forcing the mercury under increasing pressure into successively smaller pores.

An important feature of mercury utilized in this technique is that it exhibits a contact angle of greater than 90° with most materials. This means that mercury will neither penetrate the openings of particles nor pore space within the material unless forced. The volume of mercury penetrated into the

solid is measured as a function of the applied pressure which is related by the Washburn equation as,

$$rp = \frac{-2\gamma Cos\theta}{P} \quad (4.2.15)$$

where; r_p is the radius of circular pore, γ is the surface tension of mercury in the pore, θ is the angle of wetting of the pore wall by mercury P is the total pressure exerted under which mercury is made to penetrate the pores. From this, the pore volume and pore surface area distributions can be calculated. The lower limit of this technique is down to 60°A. Derivation of the above equation is given in Appendix A.1.

4.4. DENSITY AND TOTAL PORE VOLUME DETERMINATIONS

The total pore volume and porosity of activated carbon can be determined by using the combination of apparent and true density measurements.

True density of a porous solid is defined as the ratio of the mass to the volume occupied by that mass. Therefore, contribution to the volume made by pores or internal voids must be excluded when measuring the true density. To determine the true density of a solid, one needs to have a non interacting fluid which completely fills all the pores. In reality, no fluid completely fills the pore volume of activated carbons. Therefore, the term, true density should be treated in this way.

Helium is the smallest molecule available with an atomic diameter of 1.7°A. Therefore, it has the best chance of penetrating the entire porosity of activated carbon. Apparent density is defined as the weight of the solid divided

by the volume including the internal pores of that solid. Apparent density measurement is most commonly determined from the volume of mercury displaced under pressure to fill the interparticle (interstitial space) void volume only. Then, total pore volume and total porosity of the activated carbon can be evaluated as

$$\text{Total pore volume } (cm^3/g) = \frac{1}{\rho_{Hg}} - \frac{1}{\rho_{He}} \qquad (4.2.16)$$

$$\text{Total porosity} = 1 - \frac{\rho_{Hg}}{\rho_{He}} \qquad (4.2.17)$$

Figure 4.4 depicts a block-diagram of the overall experimental approach. The physical characterization of activated carbon samples was studied according to the following scheme. (Şenel, 1994)

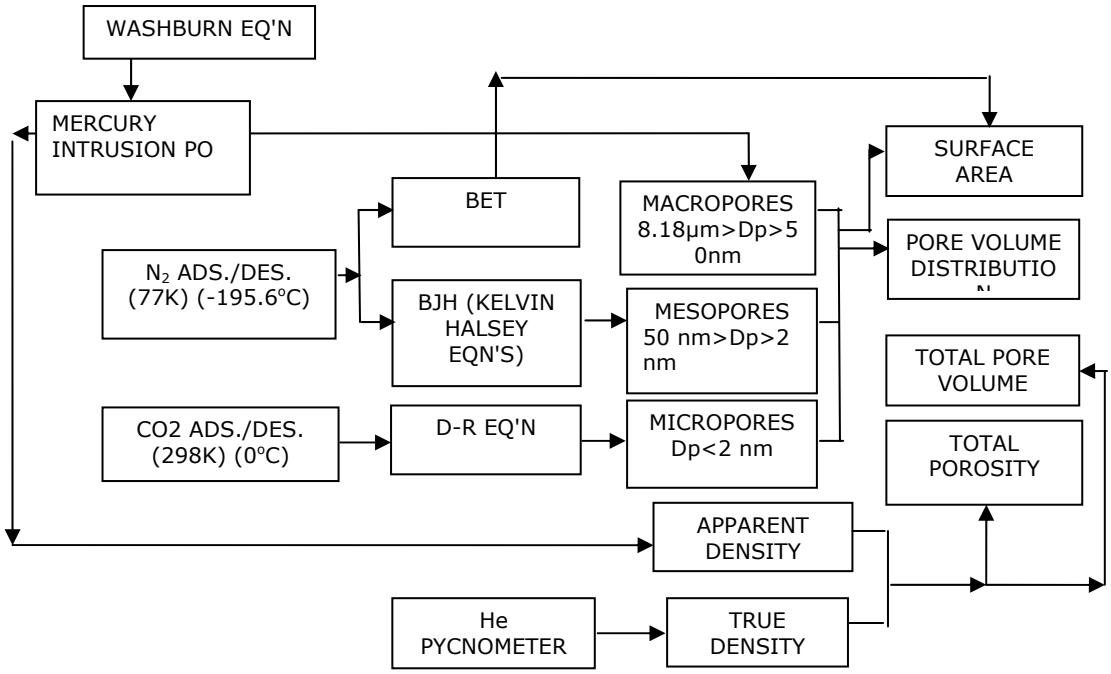

Figure 4.4 Block-Diagram of the Overall Experimental Approach

CHAPTER V

EXPERIMENTAL WORK

One of the major objectives of this study was to investigate the pore structure of activated carbon produced from carbonized and steam activated sulphonated styrene-divinylbenzene copolymer.

5.1 MATERIALS

A macroporous resin, Lewatit MonoPlus SP 112 H, was used as the starting material. The resin – manufactured by SYBRON Chemicals Inc. - is a strong cation exchanger originally in H^+ form. The Experimental study was carried out in accordance with the procedure outlined in Figure 5.1.

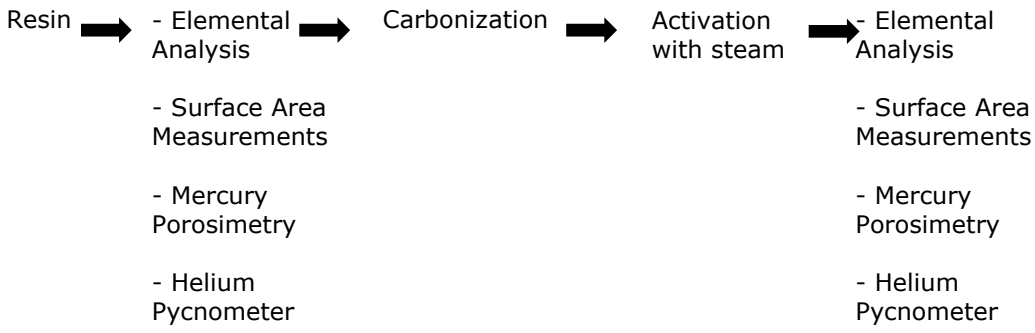

Figure 5.1 Schematic Diagram of Experimental Procedure

5.2 PREPARATION OF THE SAMPLES

The original material to start with was reported to be a strongly acidic, macroporous-type cation exchange resin of uniform particle size (monodispersed) based on a styrene-divinylbenzene copolymer, originally in H^+ form. The resins had a uniformly distributed bead size of 0.69-0.70mm.

5.3 CHEMICAL ANALYSIS OF ION-EXCHANGERS AND CHARS

5.3.1 Water Retention and Total Exchange Capacities

The water retention capacities and the total exchange capacities of the original ion-exchangers, from the manufacturer's manual, are 57–59% by weight and 1.6 eq/L respectively..

5.4. ELEMENTAL ANALYSIS

The carbon, hydrogen and sulfur contents of original ion-exchangers together with the samples obtained both after carbonization and activation experiments of selected ion-exchangers were determined using two elemental analyzers; LECO-CHN-600 for carbon, hydrogen and nitrogen, and for sulfur. Ash contents of some samples were determined by thermogravimetric analysis (TGA). The results of elemental analysis (on dry basis) of original ion-exchangers are given in Table 5.1.

Table 5.1 Elemental Analysis of Original Ion-Exchangers

C %(wt)	H %(wt)	N %(wt)	S %(wt)	O %(wt)	Ash %(wt)
50.20	4.78	0.07	16.00	28.47	0.48

5.5. CARBONIZATION AND ACTIVATION STUDIES

5.5.1. Experimental Set-Up

Carbonization and activation experiments were conducted in an electrically heated "Lenton Unit C2" horizontal tubular furnace, using approximately 10 grams of oven-dried resins. The experimental set-up is shown in Figure 5.2. Nitrogen was used for carbonization at a 100 cm^3/min flow rate, with the help of a rotameter. Steam was sent into the system by using a water bath (bubbler) through which the carrier nitrogen gas was passed at a flow rate of 200cm^3/min to ensure good activation. Sample container consisted of a quartz tube, 20 mm inside (24 mm outside) diameter and 90 cm length, and placed horizontally in the furnace. Oven was heated from room temperature (25°C) to the final carbonization temperature at a heating rate of 20°C /min. A cold trap was placed after the furnace to collect the condensables. After cooling, the outlet gases purged to hood by a heat resistant hose.

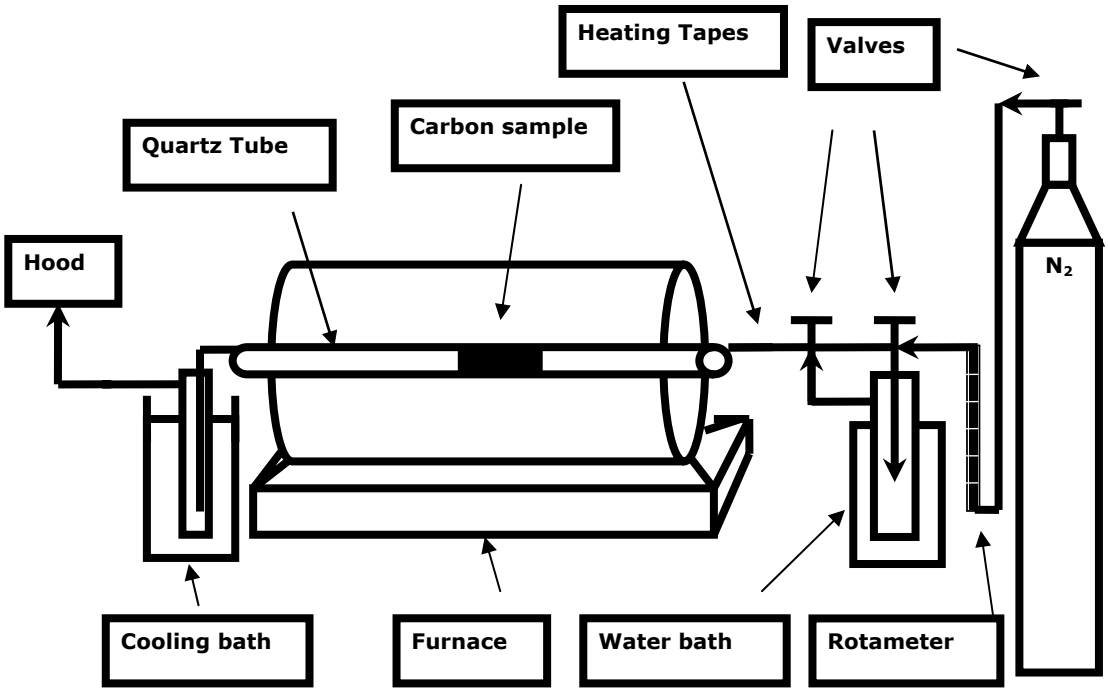

Figure 5.2 Experimental Set-Up

In carbonization experiments, two sets (1 and 2) were performed in which time and temperature were varied in order to study their effects on the BET surface areas of the products. In activation experiments (Set 3), carbonized ion-exchangers (600 °C, 1 hr) were activated with steam at 900°C, changing the time of activation and the steam flow rate. The experimental conditions and abbreviations of all sets are given in table 5.2.

Table 5.2 Abbreviations of Experiments

<table>
<tr><th>Set</th><th colspan="2">Experimental Constants</th><th colspan="3">Experimental Variables</th></tr>
<tr><td rowspan="4">Set 1</td><td>Particle Size</td><td>0.7 mm</td><td colspan="3" rowspan="4">Carbonization Time
(hr)
0.5, 1, 1.5, 2, 2.5 & 3</td></tr>
<tr><td>N_2 Flow Rate</td><td>100 cm^3/min</td></tr>
<tr><td>Heating Rate</td><td>~20°C/min</td></tr>
<tr><td>Carbonization Temp.</td><td>750°C</td></tr>
<tr><td rowspan="4">Set 2</td><td>Particle Size</td><td>0.7 mm</td><td colspan="3" rowspan="4">Carbonization Temperature (°C)
450, 600 & 750</td></tr>
<tr><td>N_2 Flow Rate</td><td>100 cm^3/min</td></tr>
<tr><td>Heating Rate</td><td>~20°C/min</td></tr>
<tr><td>Carbonization Time</td><td>1.5 hrs</td></tr>
<tr><td rowspan="15">Set 3</td><td rowspan="5">Particle Size</td><td rowspan="5">0.7 mm</td><td colspan="3">Activation Period, hr, Series 1</td></tr>
<tr><td rowspan="4">Water Bath Temp.
60°C</td><td>1</td><td>AC6.1</td></tr>
<tr><td>4</td><td>AC6.4</td></tr>
<tr><td>6</td><td>AC6.6</td></tr>
<tr><td>8</td><td>AC6.8</td></tr>
<tr><td rowspan="5">N_2 Flow Rate</td><td rowspan="5">200 cm^3/min</td><td>10</td><td>AC6.10</td></tr>
<tr><td colspan="3">Activation Period, hr, Series 2</td></tr>
<tr><td rowspan="3">Water Bath Temp.
80°C</td><td>1</td><td>AC8.1</td></tr>
<tr><td>3</td><td>AC8.3</td></tr>
<tr><td>4</td><td>AC8.4</td></tr>
<tr><td rowspan="5">Heating Rate</td><td rowspan="5">~20°C/min</td><td>6</td><td>AC8.6</td></tr>
<tr><td colspan="3">Activation Period, hr, Series 3</td></tr>
<tr><td rowspan="3">Water Bath Temp.
90°C</td><td>1</td><td>AC9.1</td></tr>
<tr><td>1.5</td><td>AC9.1.5</td></tr>
<tr><td>2</td><td>AC9.2</td></tr>
</table>

At the end of the carbonization and activation experiments, the system was cooled to room temperature under N_2 flow. The cooled char was removed from the sample chamber, weighed, and stored in small sealed containers for physical characterization tests.

5.6. PHYSICAL CHARACTERIZATION TESTS

For the characterization of the products of Set 3, BET surface areas and solid and apparent densities were measured, then porosities and total pore volumes were calculated. For Set 1 and 2 samples, BET surface area measurements were enough.

Prior to making all characterization tests, the samples were first oven dried at 110°C for two hours and then out-gassed under vacuum (10^{-3} mm Hg) at 110°C until no change in vacuum level was obtained in the automatic degassing port of an automated volumetric gas adsorption equipment (ASAP 2000, Micromeritics Co.), the details of which are given below.

5.6.1. Analysis of the Pore Structure

The pore size distribution of the samples by different methods was analyzed. Macro and meso pore size distributions of the products were examined by using a commercial automated high pressure mercury intrusion porosimeter (Micromeritics Porosizer 9310, Micromeritics Inst. Co., USA). The porosimeter uses a technique of forcing mercury into successively smaller pores under increasing pressure. Due to its high surface tension, mercury does not wet the solid surface. The porosimeter used in this study, enables to detect the pores

with pore diameters from 180 μm down to 0.006 μm. Calculation of apparent and solid densities and porosities are given in Appendix A.

5.6.2. Nitrogen Gas Adsorption Measurements

A commercial volumetric gas adsorption apparatus, "ASAP 2000", Accelerated Surface Area and Porosimetry System manufactured by Micromeritics Co., USA was used to characterize the BET surface area of products.

To determine the BET areas of the samples, nitrogen gas adsorption and desorption isotherms were obtained at -195.6°C. For each experimental point, an equilibrium time of about 15 minutes was allowed. The cross sectional area of the nitrogen molecule was taken as 0.162 nm^2 (Walker et al., 1968). Surface areas of the samples were determined by using BET equation in the relative pressure range of 0.05 to 0.999. The area and the volumes of the pores as well as their distributions were evaluated from the nitrogen adsorption isotherms using the Barrett, Joyner and Halenda (BJH) method, considering the IUPAC mesopore range from 50 nm down to 2 nm in terms of pore diameters of the cylindrical shaped pores. (Barrett et al., 1951)

5.6.3. CO_2 Gas Adsorption Measurements

The micropore volumes of the samples were estimated by application of the Dubinin- Radushkevich (DR) equation to carbon dioxide adsorption at 0°C using the same "ASAP 2000" system. At least half an hour was allowed for equilibrium to be established at each point of the CO2 isotherm. Micropore surface area of the samples were calculated from the DR micropore volume,

taking the cross sectional area and the density of a CO_2 molecule as 0.17 nm^2 and 1.181 g/cm^3 respectively. The saturation vapor pressure was taken as 26142.000 mm Hg at the analysis temperature of 0°C (Micromeritics ASAP 2000, User Manual, Appendix C, 1993).

5.6.4. True Density and Total Pore Volume Determinations

True (Helium) density of samples were determined by using a commercial pycnometry, "The Multivolume Pycnometer, Model 1305" manufactured by Micromeritics. Schematic diagram of this apparatus is given in Figure D.1. The He Pycnometer instrument consisted essentially of a sample-holding vessel, a cylinder fitted with a movable piston, the relative position of which is indicated on the front panel dial to five decimal places and a pressure detector. A dial light reveals whether the pressure in the system is the same as that in the detector.

In a typical run, 0.1-0.2 g degassed sample was placed into a propylene cup and then, both were evacuated in the pycnometer chamber for a sufficient time. After filling the system with helium, chamber was opened to atmosphere by means of a 4 position valve. By this way, enough helium is allowed to escape into the system in order to reduce pressure in the system to the atmospheric reference pressure.

After some time, the valve was turned to gauge position for sealing the helium in the system at atmospheric reference pressure. Once the valve in gauge position, the variable volume chamber, sample chamber and pressure detector are connected and sealed off as a closed system. When the variable volume is changed so as to decrease the volume of the system, the pressure increases to the point where contact is broken between the bellows of the

pressure detector and an electric contact in the detector. This indicates where the reading should be taken. After obtaining three values; for empty cup, for standard volume and for sample as V_{CELL}, V_{EXP} and V_{SAMP} values, respectively, true density of the sample was determined using the known weight of sample according to procedure given in Appendix D. Total pore volumes and total porosities were then calculated combining the true and apparent density values by means of the equations 4.2.16 and 4.2.17, respectively.

5.6.5. Scanning Electron Microscope (SEM) Analysis

For microscopic structural studies, the structure of the carbonized product and sample AC6.6 (Water bath Temperature=60^{o}C, Activation Time= 6hours) were investigated using a NORTAN INSTRUMENTS- JSM-6400 scanning electron microscope.

CHAPTER VI

RESULTS AND DISCUSSION

The main objective of this study was to produce and characterize activated carbon from strong cation exchange resins (sulphonated styrene-divinylbenzene copolymers) by physical activation technique using steam as the activating agent at relatively high temperatures. Another aim was to investigate the effect of carbonization time and temperature on the structure of the resins.

The pore structures of the products were characterized by different physical techniques; nitrogen adsorption at -195.6°C, carbon dioxide adsorption at 0°C, mercury porosimetry and helium pycnometry.

In terms of chemical characterization, the analyses were limited to determination of C, H, N, O and S elements analysis; to provide information with respect to elemental composition.

6.1. CHEMICAL ANALYSIS OF PRODUCTS

Elemental analyses of the twelve activated carbons of set 3 and the carbonized material were carried out and were given out in Figure 6.1 and Table E.1. As it is seen from this figure, activated carbons produced in this study

contain about 91.80– 95.20 % carbon, 0.30- 0.90 % H , 0.32- 0.59% N, 1.6 - 2.2% S, and no oxygen.

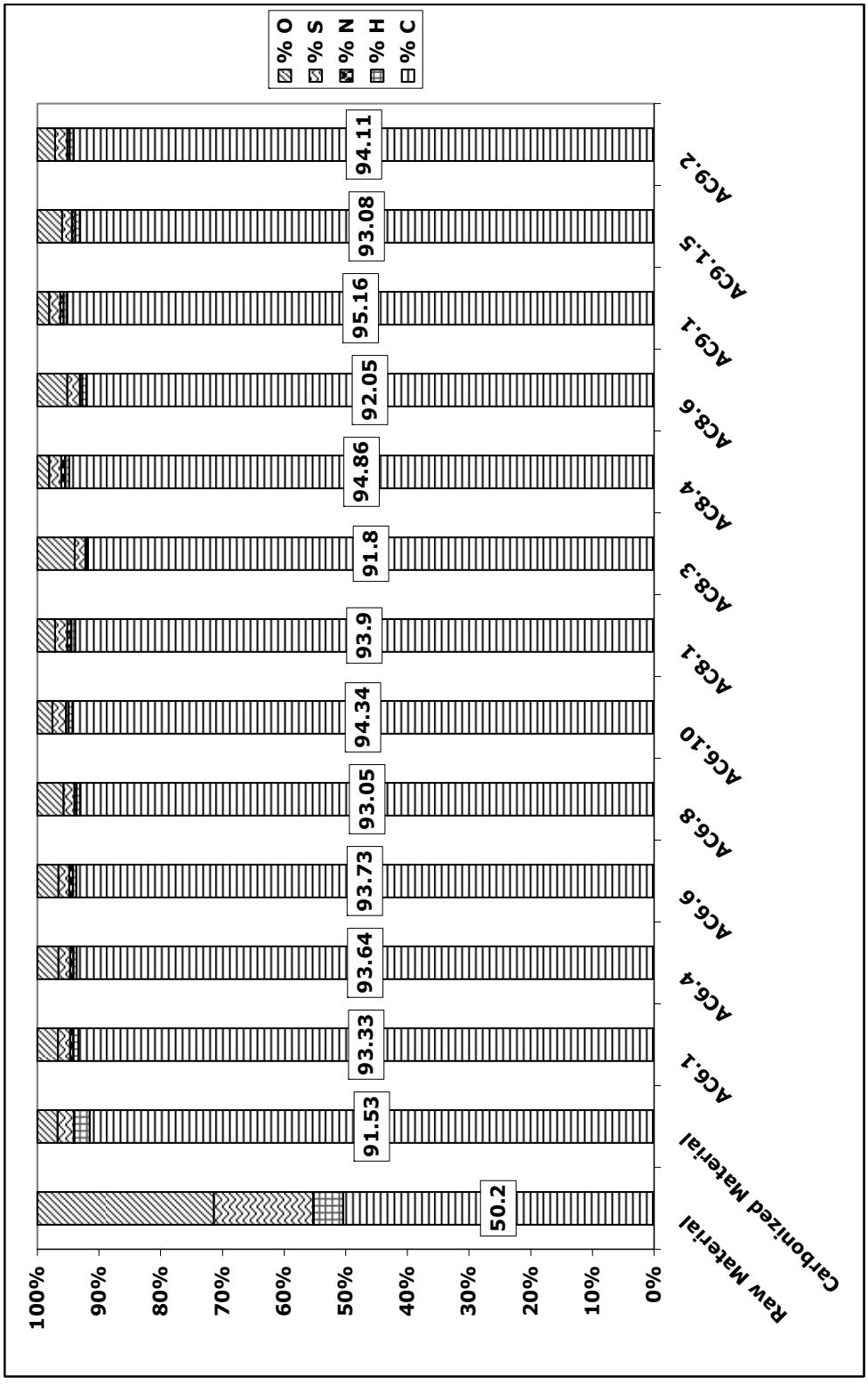

Figure 6.1 Chemical Compositions of Activated Carbons

6.1.1. Carbon Content

Data reported in Figure 6.1 indicates that, the least carbon content (50.20%) was observed for the raw material. After carbonization the carbon content increased to 91.53%. This shows that carbonization reduces the volatile content of the source material efficiently. The carbon content increases after activation from a minimum of 91.8% for AC8.3 sample to a maximum of 95.16% for AC9.1 sample. The C content of activated carbon produced by steam activation from same raw material under similar conditions ranges between 95 to 97% (Karakaş, 2004). BET area is the most important parameter for activated carbons. High carbon content value is desired to achieve high BET surface area.

6.1.2. Oxygen and Hydrogen Content

The presence of oxygen and hydrogen influence the adsorptive properties of activated carbon. As discussed in Section 3.1.5 these elements are combined with the atoms of carbon by chemical bonds. The oxygen and hydrogen functional groups provide sites where molecules of water and other polar substances or easily polarizable gases and vapors are adsorbed (Smisek and Cerny, 1970; Hassler, 1971).

The oxygen content of the starting material was about 28.48%. This value decreased down to a value between 0.5 and 6.1% after carbonization and activation of the products. H contents of the products of the three series of set 3 are almost similar to those of literature ranging from 0.30% to 0.90%. The H content of activated carbon produced by steam activation from same raw material under similar conditions ranges between 0.38 to 0.58% (Karakaş,

2004). For a typical activated carbon the recommended oxygen content is around 5% and the hydrogen content is 1% (Faust and Aly, 1983).

6.1.3. Nitrogen Content

For a typical activated carbon, nitrogen content is less than 1 %. All the products obtained from the physical activation of the ion exchange resins have maximum nitrogen content of 0.59% (Figure 6.1). During carbonization in nitrogen atmosphere, small amount of nitrogen can be chemisorbed. (Smisek and Cerny, 1970)

6.1.4. Sulfur Content

The sulfur contents of the samples decreased from a high initial value of 16% due to the existence of sulfonic groups to 2.62% after carbonization and then to a value between 1.6 and 2.2 after activation. The sulfur content range of the products is small enough proving that their sulfur contents are almost the same.

6.1.5. Ash content

A good activated carbon must have low ash content. A small increase in ash content causes a decrease in adsorptive properties of activated carbon. The raw material has ash content of about 0.48%. The ash analysis was done for some samples using the thermogravimetric analyzer (TGA). Only one activated product (AC6.6) was characterized for ash contents by TGA and showed a higher value than that of a commercial activated carbon obtained from Kureha Chemical Industry Co. Ltd. (Tokyo, Japan). This difference can be explained by the type of

starting material, the procedure and the conditions available in the preparation of the activated carbon.

6.1.5.1 Thermal Gravimetric Analysis (TGA)

TGA experiments were carried out by burning the samples in air up to 900°C so as to obtain the ash contents for each of the carbonized product and one activated sample (AC6.6) of set 3, and also for the starting material Lewatit SP112H and for the commercial activated carbon (Kureha Chemical Industry Co. Ltd.) and compare it with the results of elemental analysis, the TGA figures of which are given in Appendix G. Ash contents of the samples are given in Table 6.1.

Table 6.1 Ash Contents (%) of Samples

	Lewatit SP112H	Carbonized Sample	AC 6.6	Commercial AC
% Ash	0.48	0.571	3.810	1.143

6.2. PHYSICAL CHARACTERIZATION OF THE PRODUCTS

The physical characterization of the both sets 1 and 2 of activated carbons was confined to BET surface area measurement. On the other hand, the physical characterization of the twelve activated carbons produced in set 3 and the carbonized one was carried out according to the experimental procedures given in Figure 2.15. These samples were characterized by determination of their pore size distribution, total pore volume, apparent and solid density, mesopore area, micropore area, macropore area, macropore volume, mesopore volume, micropore volume and surface area. Mercury intrusion porosimetry, BET (N_2) surface area measurement, Helium pycnometry and D-R method (CO_2) are used to determine these values.

6.2.1. Nitrogen Gas Adsorption Measurements

The nitrogen adsorption measurements of the Set 1 and 2 samples were limited at determining the BET surface area, S_{BET}. While for set 3 samples, the measurements included the determination of the (I) BET surface area, S_{BET}, (II) volume of mesopores, V_{MESO}, and (III) cumulative surface area of mesopores, S_{MESO}.

BET surface area values of the samples in Set 1 and 2 are are shown in Figure 6.2 and Figure 6.3 respectively. The main aim of this part of study was to investigate the effect of time and temperature on the BET surface area of the products of carbonization.

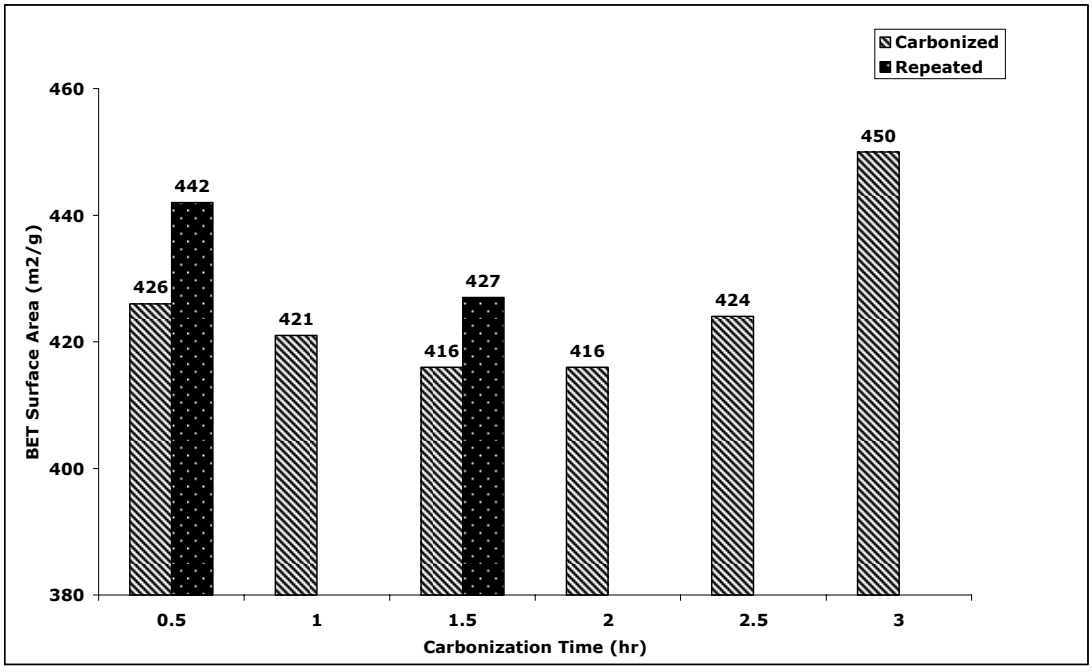

Figure 6.2 Variation of BET Surface Area with Carbonization Time (Set 1)

Figure 6.2 shows that the BET surface areas of the six different carbonization times give almost the same value with a maximum deviation of 5% from the average. In other words, the change in carbonization time showed

no significant effect on the BET surface areas of the products. Two experiments (0.5hr and 1.5hrs) were repeated to check reproducibility and the deviation was approximately 4% from the average. Three different temperatures (450, 600, 750°C) were chosen in reference to related earlier works (Bothe, 1979 and Neely, 1981) to study the effect of temperature on the BET surface areas of the products.

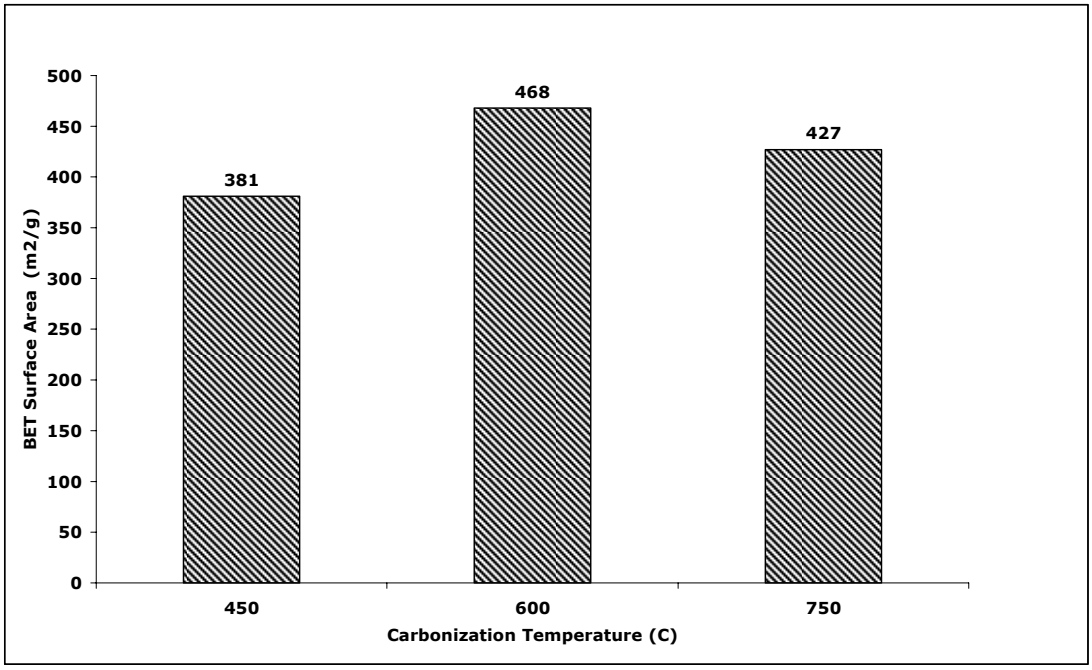

Figure 6.3 Variation of BET Surface Area with Carbonization Temperature(Set 2)

Figure 6.3 shows the BET surface areas of the carbonized resins at these temperatures for 1.5hours. The reason of choosing 1.5 hrs for this set was to compare the results with an earlier work (Öztürk,1999) where the same type of resins were used under the same conditions (750^{o}C, 1.5hrs). The resins gave a higher surface area of 427m^2/g at a carbonization temperature of 750°C compared to 359m^2/g of Öztürk. At 450^{o}C, the surface area was low indicating that 450°C is insufficient to produce a good starting material for activation. At temperatures in the range of 300 - 500°C, the H content of the sample is high enough to prevent the production of new carbon- carbon bonds, and thus

preventing the development of pores. The majority of the weight loss above 500°C is hydrogen (Neely, 1981). Hence, a minimum temperature of 500°C must be used for the production of these bonds. The BET surface areas at 600°C and 750°C showed close values proving that increasing the temperature above 600°C have no significant effect.

Abbreviations and results such as steam amount, burn-off % and BET surface area values of the samples of Set 3 and the carbonized one are shown in Table 6.2. The carbonization temperature and time were chosen in accordance with Set 2 results as 600°C and 1hour respectively. The activation temperature was taken as 900°C, a feasible temperature for steam activation of activated carbon raw materials (Ullmann, 2002). The steam flow rate calculation is given in appendix F.

Table 6.2 Abbreviations and Results of Carbonized and Set 3 Samples

Sample Code	Activation time (hr)	Steam Amount (g)	Burn-off (%)	BET surface area (m^2/g)
Carbonized Material	-	-	67	473
Series 1 (2.2 g/hr Steam Flow Rate)				
AC6.1	1	2.23	17	636
AC6.4	4	8.90	34	978
AC6.6	6	13.36	48	1570
AC6.8	8	17.81	59	1292
AC6.10	10	22.26	64	1141
Series 2 (8.6 g/hr Steam Flow Rate)				
AC8.1	1	8.59	18	700
AC8.3	3	25.76	52	1333
AC8.4	4	34.35	57	1367
AC8.6	6	51.52	90	2130
Series 3 (26.3 g/hr Steam Flow Rate)				
AC9.1	1	26.30	36	960
AC9.1.5	1.5	39.45	51	1281
AC9.2	2	52.61	70	1572

Figure 6.4 shows the variation of BET surface area as a function of activation time. Sample AC8.6 (90% burn-off) had the highest BET area, 2130 m^2/g and sample AC6.1 (17% burn-off) had the lowest BET area 636 m^2/g. An increase in BET areas is noticed as the temperature of water bath increases for all series except series 1 which shows a slow increase till it reaches a maximum of this series at AC6.6 (50% burn-off) and then declines gradually. The reason of this behavior is the saturation percent of water vapor sent to the system. At 60°C water bath temperature, the pores were not developed enough proving that the water vapor sent to the furnace (~2.2g/hr) is a relatively small amount to activate ~3 grams of starting material. The decrease of BET areas of the samples can also be contributed to the enlargement of the pores diameters down to 10A^o for an activation time up to 10 hours. During this enlargement, the pores with diameters smaller than 10A^o can not be measured with N_2, so surface area of the smaller pores are not measurable.

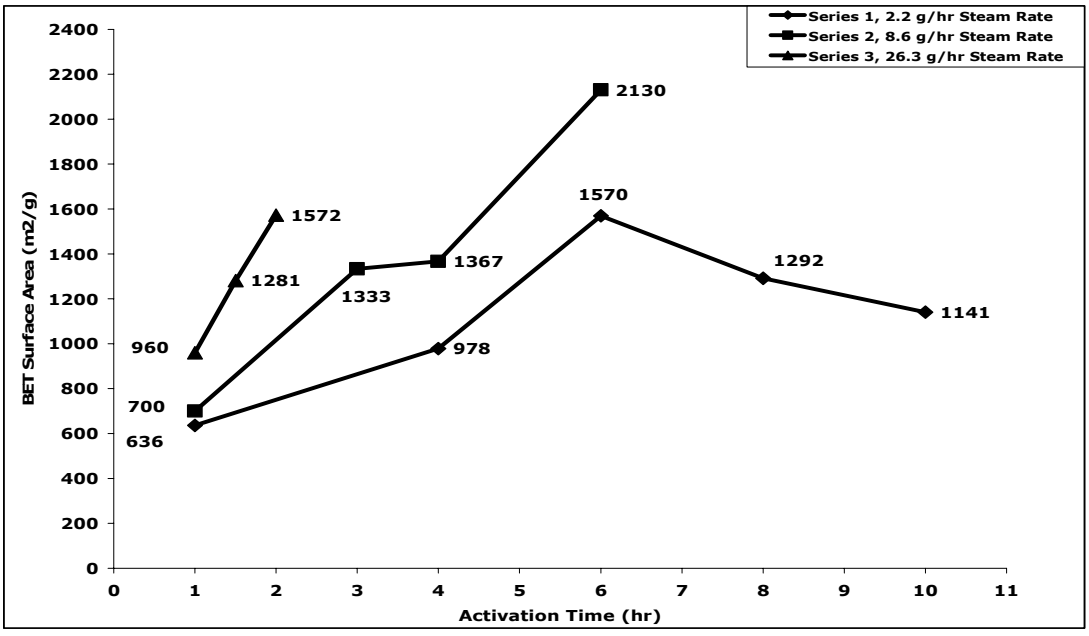

Figure 6.4 BET Surface Areas versus Time of Activation (Set 3)

The BET areas of the samples are higher than those of literature values (BET areas of activated carbons produced from same starting materials and under similar conditions were in the range of 600-1200 m^2/g (Karakaş, 2004). Series 2 and 3 show a continuous increase in the areas as the activation temperature increases. This indicates that 60°C water bath temperature was not enough to attain saturation needed for activation.

Figure 6.5 shows the variation of BET surface areas of Set 3 as a function of burn-off percentage. There is an increase in the areas except for series 1 where a decline is seen after 50% burn-off. Moreover, Figure 6.6 shows the amount of the samples left after steam activation versus the time of carbonization. Considering all series of this figure, it seems that the efficient pore structure can only be developed when more activation is carried on, and thus more burn-off (which is not preferred). The slope of the decline increases as the temperature of the steam increases. For series 1, the slope has the least decline and its best surface area- 1570 m^2/g - is reached only at 50% burn-off. The burn-off of this series was 17 % after 1 hour of activation and reaches 64 % after 10 hrs of activation. For series 2, the burn-off reaches 90 % burn-off after 6 hours of activation, starting from 18 % after 1 hour of activation. The highest surface area among all series is noticed here for 90 % burn-off. The product of this sample were powder while for all others were granular. At 50 % burn-off of this series, a well developed surface area product of 1333 m^2/g was achieved after 3 hours of activation. For series 3, the burn-off percent started at 36 % after 1 hour of activation giving a surface area 960 m^2/g, and reached a maximum of 70 % burn-off and gave a surface area of 1572 m^2/g after two hours of activation. At 50 % burn-off of the same series, a surface area of 1281 m^2/g was achieved after 1.5 hours of activation. Regarding the changes in the slopes of these series and from table 6.2 data, it is seen that the more steam is

sent to the system the more the surface area increases- except for series 1 after 50 % burn-off as mentioned before.

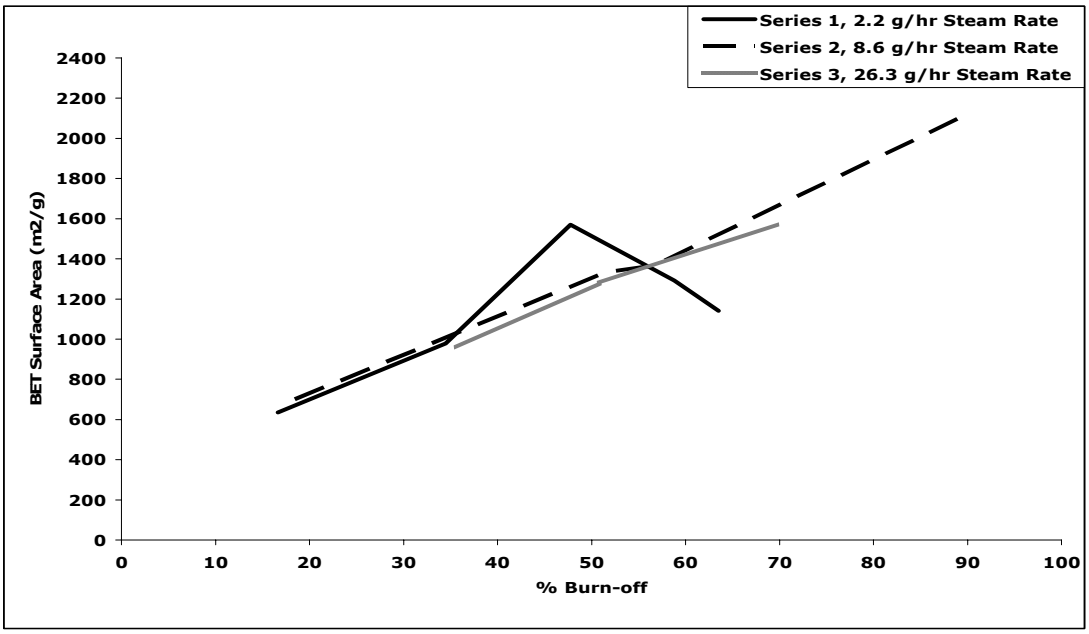

Figure 6.5 BET Surface Areas versus % Burn-off (Set 3)

The reproducibility of the experiments was checked by repeating activation experiments i.e. AC6.6 and characterize them using BET, and the results were found to be almost the same (1572 m^2/g, 1570 m^2/g). For the carbonized samples, the BET areas had a maximum deviation of 5% from the average.

Mesopore areas of the samples range between 64 to 984 m2/g calculated from BJH adsorption-desorption isotherms between the range 20 and500A^0. For Set 3 samples mesopore areas are around 8- 53 % of the BET surface areas as seen in Figure 6.7. It is shown from the values of all series that the mesopores are developed with the increase in surface areas of the samples. It can also be seen from the N_2 adsorption/desorption isotherms (Figure 6.10, 11 and 12) that the hysteresis at the end of adsorption isotherm assures the existence of well developed mesopore pores in the samples. Mesopore surface area values of the

samples are high enough to allow its usage in liquid phase processes (such as sugar decolorization).

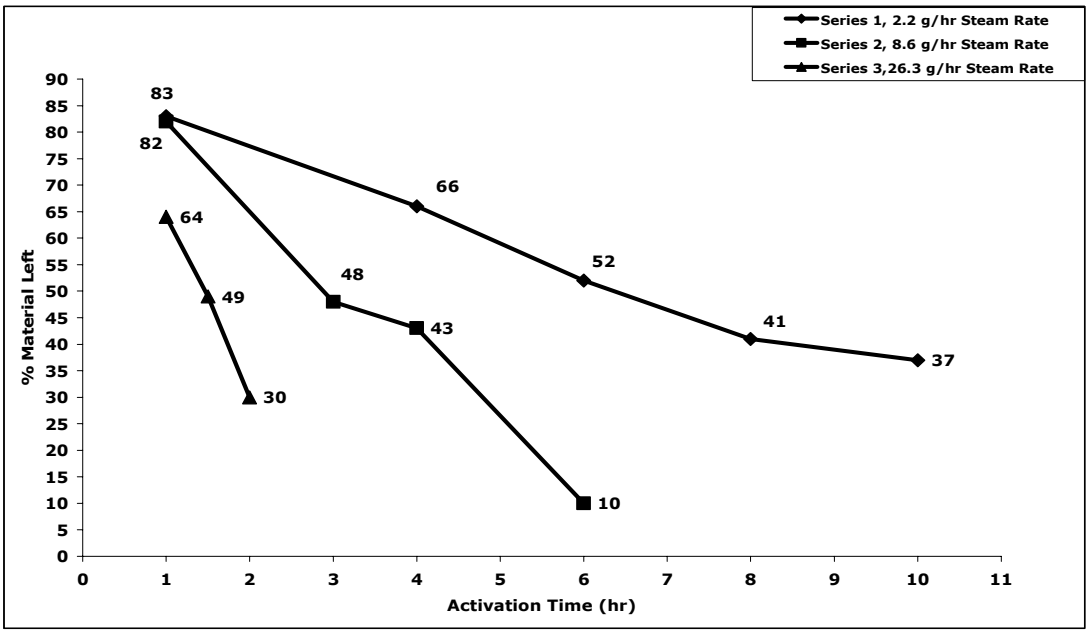

Figure 6.6 % Material left versus Time of Activation (Set 3)

As it is shown in the Figure 6.8 mesopore volumes of the samples are in the range of 0.11 - 0.83 cm^3/g. Mesopore volumes are between 23 – 48 % of the total pores.

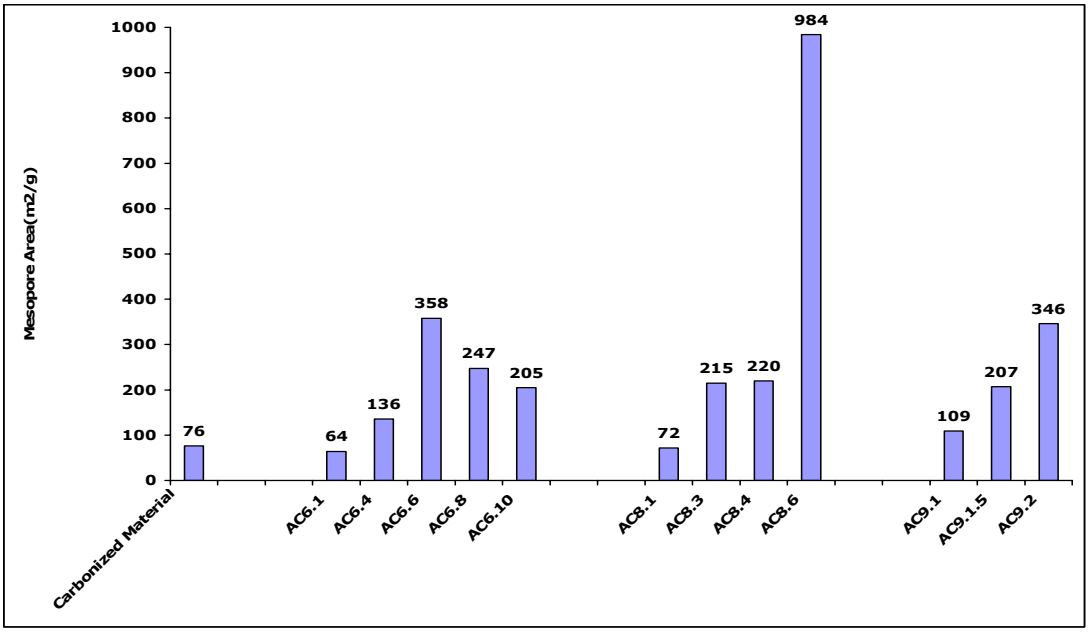

Figure 6.7 BJH Mesopore Areas of the Samples

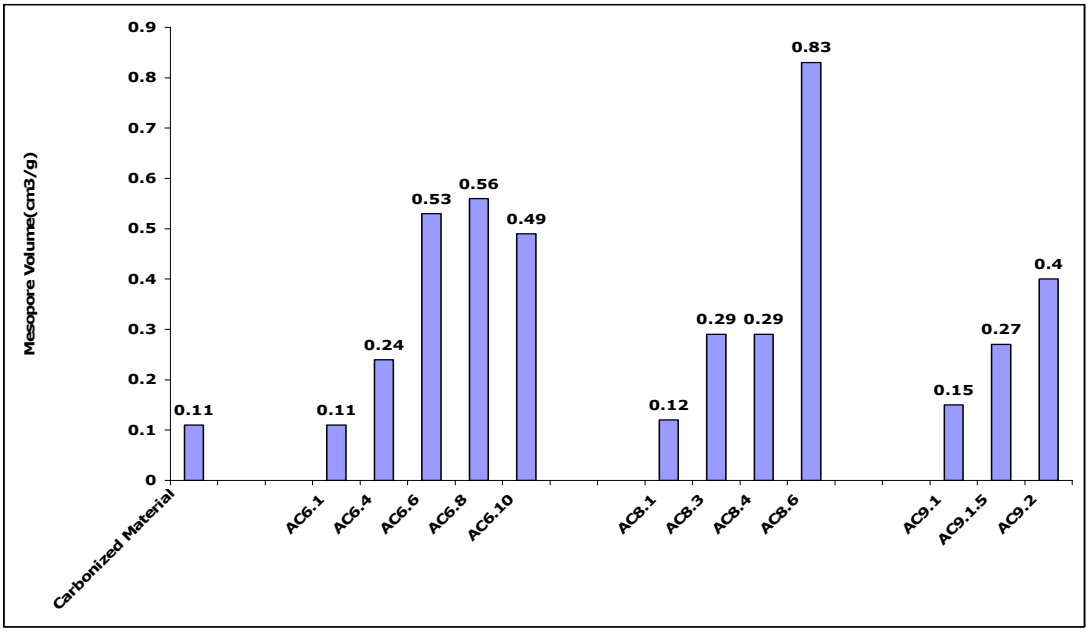

Figure 6.8 Mesopore Volumes of the Samples

Isotherm shapes in the literature which were originally defined by Brunauer et al. (1943) and classified into 6 well-known groups, (as shown in Figure 4.2) one may say that almost all products show similar isotherms to type I isotherm with hysteresis of type IV. According to Brunauer, this type of isotherm is observed in the case of microporous solids.

As discussed in section 4.2.2, another way of obtaining information on the porous texture of the solids is to compare the shape of the hysteresis loop of adsorption-desorption isotherms (Figure 4.3) with the shape of adsorption and desorption branches of the standard shapes which were originally classified by De Boer (1958).

Figures 6.9, 6.10, 6.11 and 6.12 show the N_2 adsorption / desorption isotherms of the carbonized sample (600^{o}C, 1hr) and Set 3 samples. The hysteresis seen at the start of desorption isotherm is ought to be a sign of the mesopores available in the products.

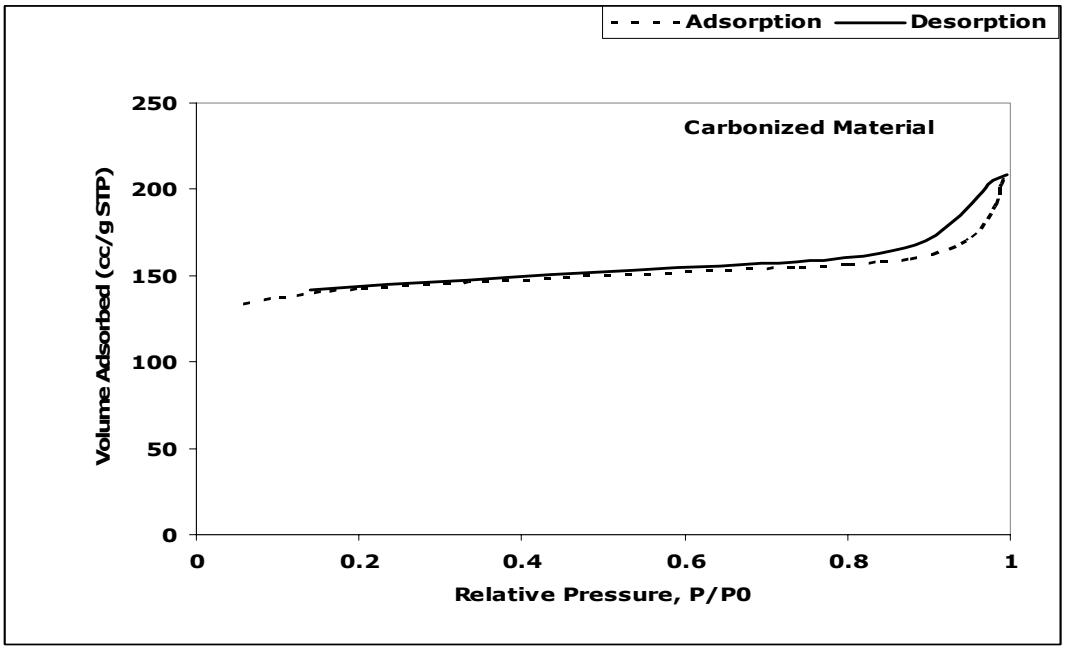

Figure 6.9 N_2 Adsorption/Desorption Isotherms of the carbonized sample

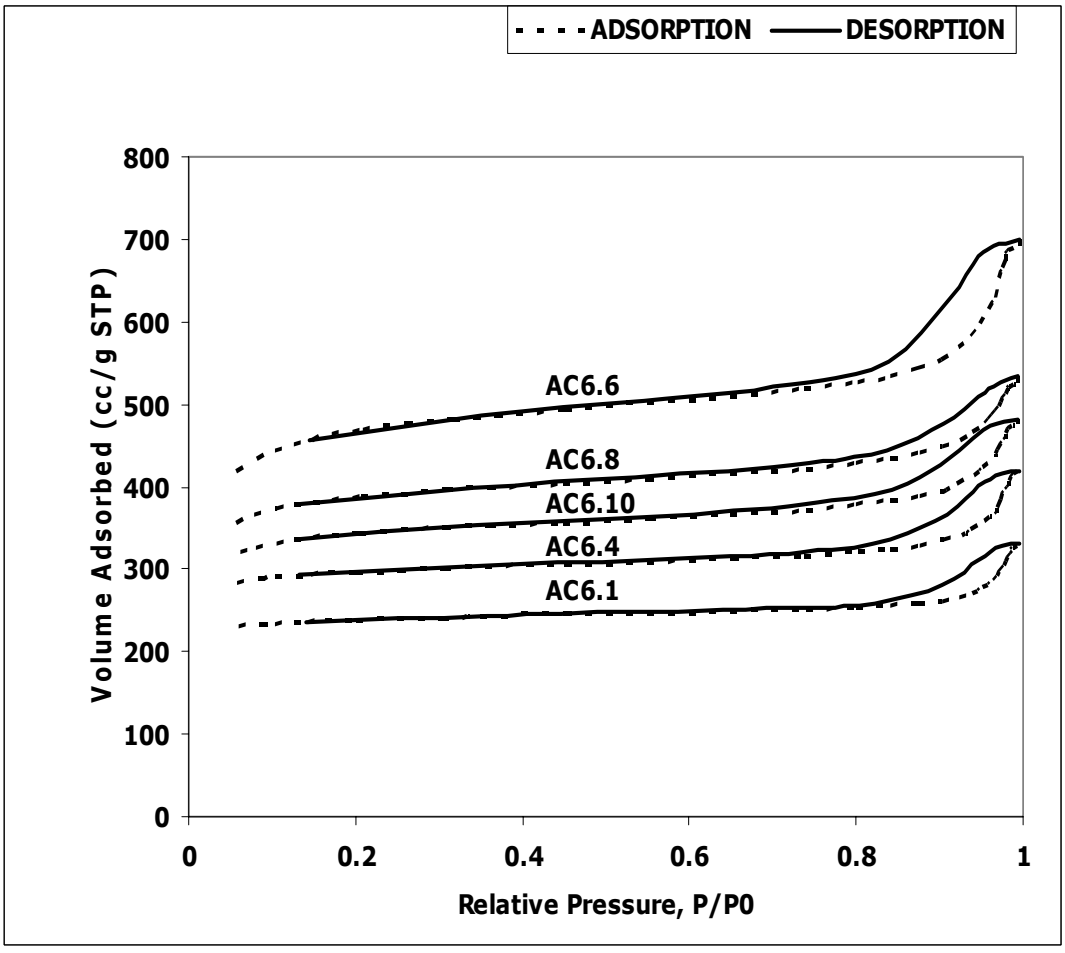

Figure 6.10 N_2 Adsorption/Desorption Isotherms of Series 1 (Set 3)

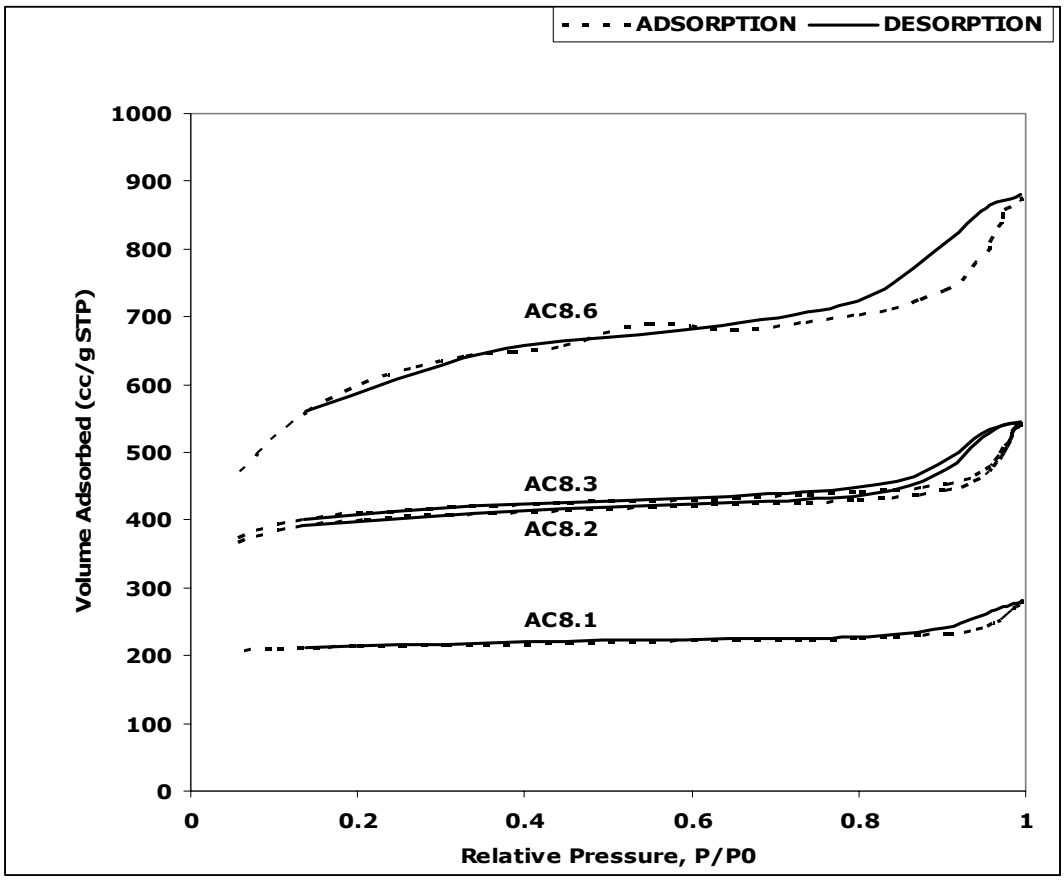

Figure 6.11 N_2 Adsorption/Desorption Isotherms of Series 2 (Set 3)

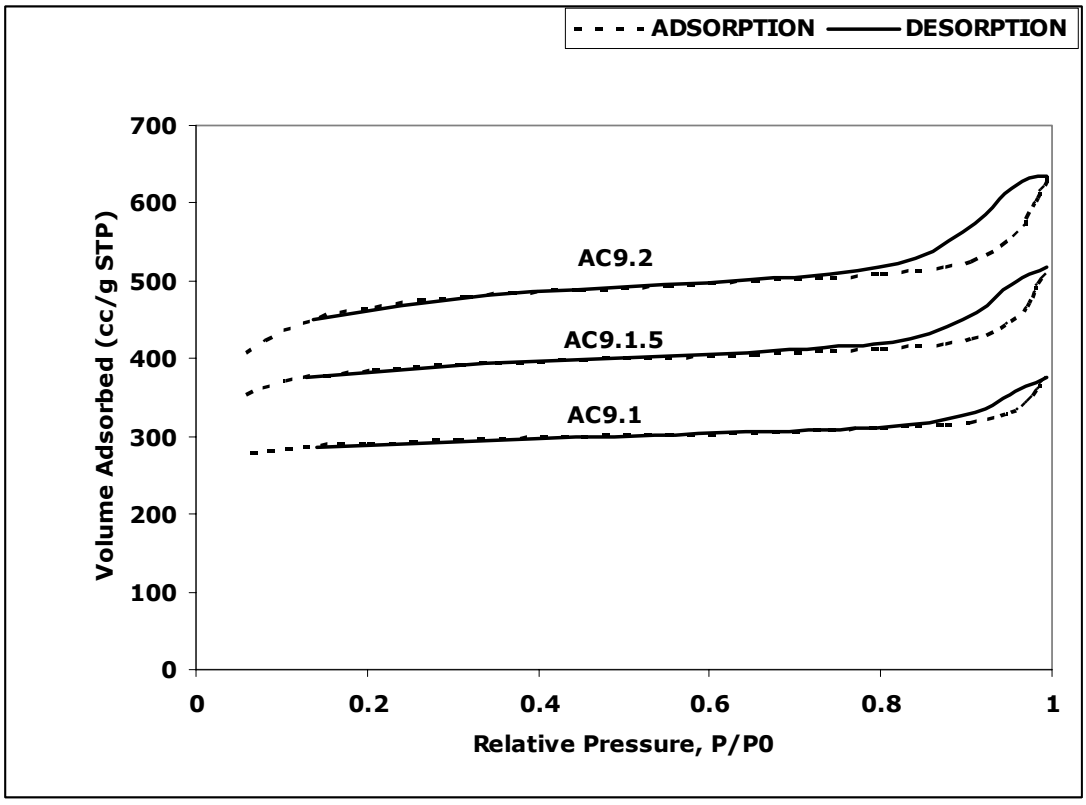

Figure 6.12 N_2 Adsorption/Desorption Isotherms of Series 3 (Set 3)

6.2.2. Carbon Dioxide Gas Adsorption Measurements

Micropore analysis of the samples was carried out by CO_2 adsorption studies at 0°C as described in section 3.6.3. The micropore volumes were calculated using the Dubinin-Radushkevich (D-R) equation. The relative pressures, P/P_o employed in all measurements were in the range of 1.10^{-4} to 1.10^{-2}. Micropore areas values of the samples are shown in the Figure 6.13. Almost similar to BET areas, the highest micropore area, 966 m^2/g, was obtained for the AC8.3 sample and the lowest micropore area 761 m^2/g, was obtained for the AC6.1 sample. For series 1 and 3, the area increases with activation while for series 2 there is a decrease after 6 hours of activation.

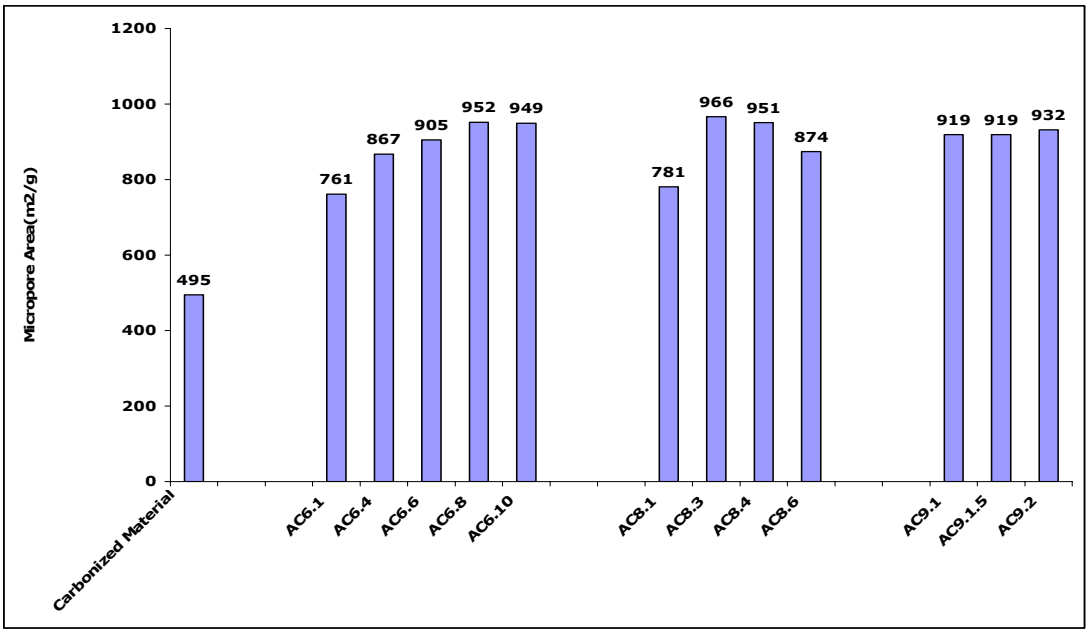

Figure 6.13 Micropore Area Values From CO_2 Adsorption at 0°C

Micropore volume of the samples are shown in Figure 6.14. Micropore volume values are in the range of 0.26-0.96 cm^3/g. As it is shown from the figure micropore volume values are proportional to micropore area values except for AC8.6 sample. This behavior may be explained by coalescence in which widening of the pores occurs for a specific volume and thus the total surface area gets smaller.

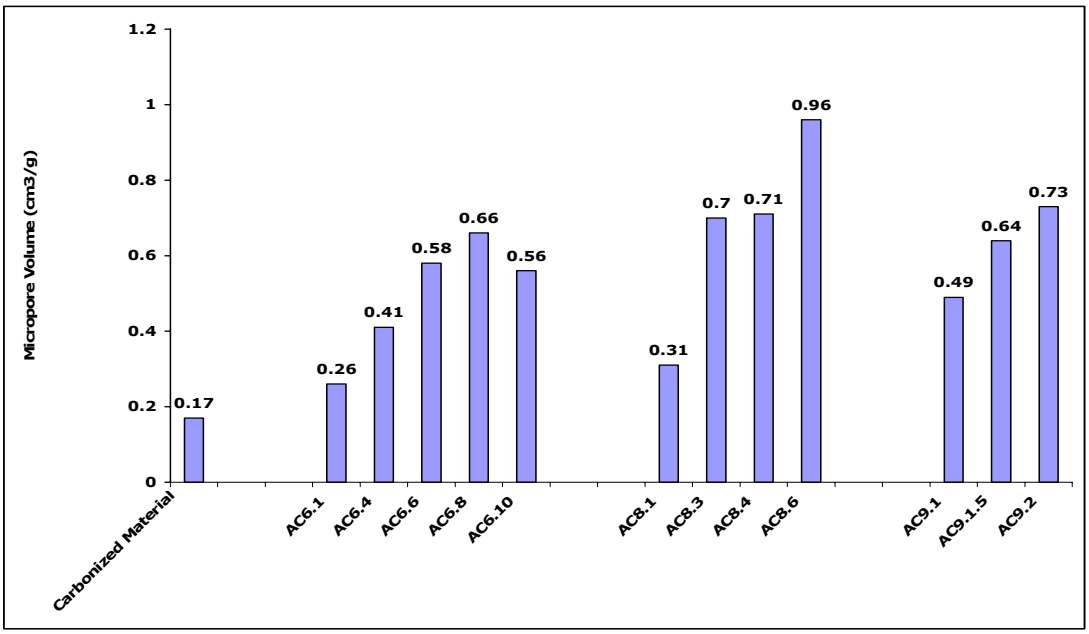

Figure 6.14 Micropore Volume Values From CO_2 Adsorption at 0°C

BET equation has been used extensively to determine surface areas of activated carbons from nitrogen adsorption isotherms measured at -195.6°C. It is now generally agreed that N_2 adsorption at -195.6°C does not measure the total surface area of activated carbons for two important reasons. First, due to the activated diffusion limitations, N_2 molecules at -195.6°C do not posses enough kinetic energy to readily penetrate into the micropores. Thus, impractically long periods are required for equilibrium to establish. Secondly, the micropores undergo some decrease in their size at low temperatures. On the other hand, in some cases, the CO_2 areas greatly exceed those determined from N_2 adsorption at -195.6°C because the kinetic energy of CO_2 molecules at the adsorption temperatures used far exceeds that of N_2 molecules at -195.6°C. Consequently, rate of diffusion of CO_2 into the activated carbon micropores will be significantly higher than that of N_2. Other interpretations have also been found in literature that CO_2 adsorption may be influenced by the spelling moment of CO_2 molecule interacting with the oxygen functionalities present on the carbon surface and that higher surface area may be caused by a CO_2 induced

swelling effect (Şenel, 1994). CO_2 can measure pores down to 4-5 ^oA while BET can measure pores down to 10 ^oA.

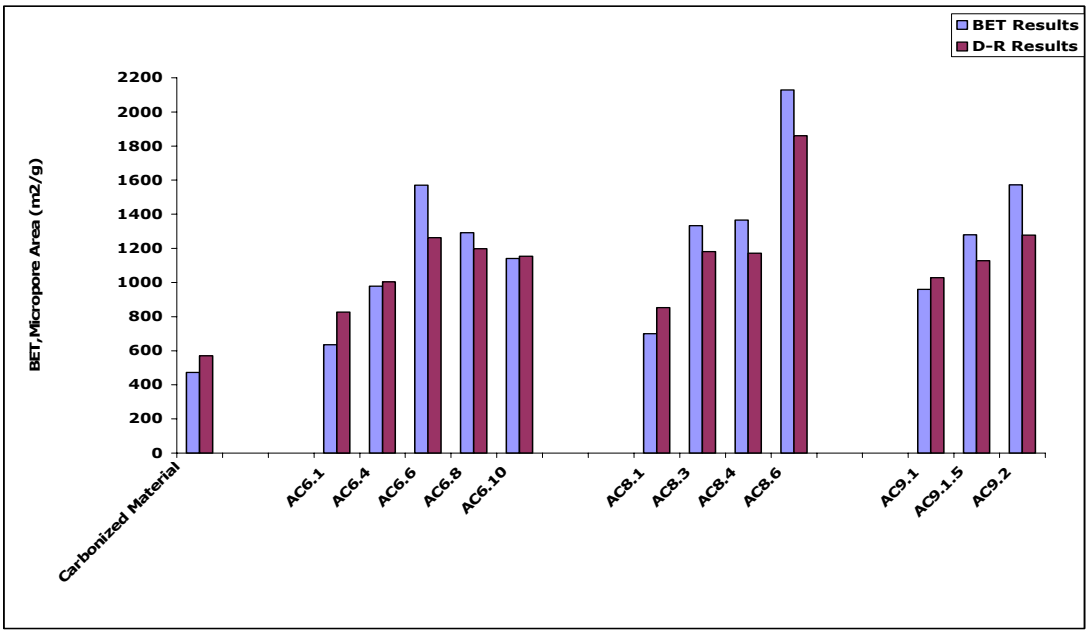

Figure 6.15 Comparison of BET and D-R Areas

As it is shown in Figure 6.15, there is a small difference between BET areas and Dubinin Radushkevich (D-R) ones. This may be a result of pore-limit of the characterization process used. BET method limits the range of the pores of diameter $10A^0$ (mesopore range) while D-R method decreases the limit down to 5 A^0.

6.2.3. Characterization of Activated Carbons by Mercury Intrusion Porosimetry

Macropore volume, macropore surface area and the apparent density values of the samples are given in Table 6.3. The macropore area and volume values of the samples are in the ranges of 0.00-0.96 m^2/g and 0.05-0.233 cm^3/g, respectively. It can be said that, there is no significant contribution of macropore surface area of the samples to the total surface area. However,

macropore volumes of the samples are 4-16% of the total pore volume and these ratios have a significant contribution to the total pore volume of the samples.

Table 6.3 Mercury Porosimetry Results of Activated Carbons

Sample	S_{macro} (m^2/g)	V_{macro} (cm^3/g)	Apparent Density (g/cm^3)
Carbonized Material	0.26	0.059	1.46
Series 1 (2.2 g/hr Steam Flow Rate)			
AC6.1	0.82	0.06	1.21
AC6.4	0.27	0.07	0.92
AC6.6	0.82	0.08	0.73
AC6.8	0.00	0.10	0.82
AC6.10	0.31	0.12	0.93
Series 2 (8.6 g/hr Steam Flow Rate)			
AC8.1	0.23	0.08	0.93
AC8.3	0.01	0.06	0.77
AC8.4	0.58	0.06	1.06
AC8.6	2.36	0.23	0.65
Series 3 (26.3 g/hr Steam Flow Rate)			
AC9.1	0.33	0.04	0.82
AC9.1.5	0.94	0.05	0.99
AC9.2	0.96	0.05	1.01

6.2.4. Pore Volume Distribution of the Activated Carbons

The pore volume and areas of the activated carbons determined as described above, in the macro, meso and micropore ranges are given in Tables 6.4 and 6.5, respectively. In these tables pore volumes and areas of all products and percentages corresponding to each pore range are given. As seen in Table 6.4, all the samples have at least 47% micropore volume of the total volume and 47% micropore area of the total surface area. As indicated in nitrogen adsorption isotherms, this values show that majority of pores are in micropore region. Percentage of mesopore volume of the samples does not change significantly and ranges between 25-45% of the total volume.

Table 6.4 Pore Volume Distributions of Activated Carbons

Sample Code	V_{Micro}	V_{Meso}	V_{Macro}	V_{Total}	$\%V_{Micro}$	$\%V_{Meso}$	$\%V_{Macro}$
Carbonized Material	0.17	0.11	0.06	0.34	50.1	32.5	17.4
Series 1 (2.2 g/hr Steam Flow Rate)							
AC6.1	0.26	0.11	0.06	0.43	60.6	25.6	13.8
AC6.4	0.41	0.24	0.07	0.72	57.1	33.4	9.5
AC6.6	0.58	0.53	0.08	1.19	48.7	44.5	6.9
AC6.8	0.66	0.56	0.10	1.32	50.1	42.5	7.3
AC6.10	0.56	0.49	0.12	1.17	47.8	41.8	10.4
Series 2 (8.6 g/hr Steam Flow Rate)							
AC8.1	0.31	0.12	0.08	0.51	60.7	23.5	15.9
AC8.3	0.7	0.29	0.06	1.05	66.8	27.7	5.5
AC8.4	0.71	0.29	0.06	1.06	67.3	27.5	5.2
AC8.6	0.96	0.83	0.23	2.02	47.5	41.0	11.5
Series 3 (26.3 g/hr Steam Flow Rate)							
AC9.1	0.49	0.15	0.04	0.68	71.6	21.9	6.4
AC9.1.5	0.64	0.27	0.05	0.96	66.7	28.1	5.2
AC9.2	0.73	0.4	0.05	1.18	61.8	33.9	4.3

Table 6.5 Pore Area Distributions of Activated Carbons

Sample Code	S_{Micro}	S_{Meso}	S_{Macro}	S_{Total}	$\%S_{Micro}$	$\%S_{Meso}$	$\%S_{Macro}$
Carbonized Material	495	76	0.26	571	86.7	13.3	0.05
Series 1 (2.2 g/hr Steam Flow Rate)							
AC6.1	761	64	0.82	826	92.2	7.8	0.10
AC6.4	867	221	0.27	1003	86.4	13.6	0.03
AC6.6	905	350	0.82	1264	71.6	28.3	0.06
AC6.8	952	384	0.00	1199	79.4	20.6	0.00
AC6.10	949	305	0.31	1154	82.2	17.8	0.03
Series 2 (8.6 g/hr Steam Flow Rate)							
AC8.1	781	72	0.23	853	91.5	8.4	0.03
AC8.3	966	215	0.01	1181	81.8	18.2	0.00
AC8.4	951	220	0.58	1172	81.2	18.8	0.05
AC8.6	874	984	2.36	1860	46.9	52.9	0.13
Series 3 (26.3 g/hr Steam Flow Rate)							
AC9.1	919	109	0.33	1028	89.4	10.6	0.03
AC9.1.5	919	207	0.94	1127	81.6	18.4	0.08
AC9.2	932	346	0.96	1279	72.9	27.1	0.08

6.2.5. Density and Total Pore Volume Determinations

True densities values of the activated carbons are determined at room temperature by Helium Pycnometry as explained in section 5.6.4 and are shown in Figure 6.16.

As it is shown in the figure true density values of the samples are in the range of 1-1.8 g/cm^3 and no significant deviation from the average is noticed. Using true and apparent densities of the products, total open pore volume and porosities of the activated carbons were calculated as described in Section 4.4 and are given in Table 6.6.

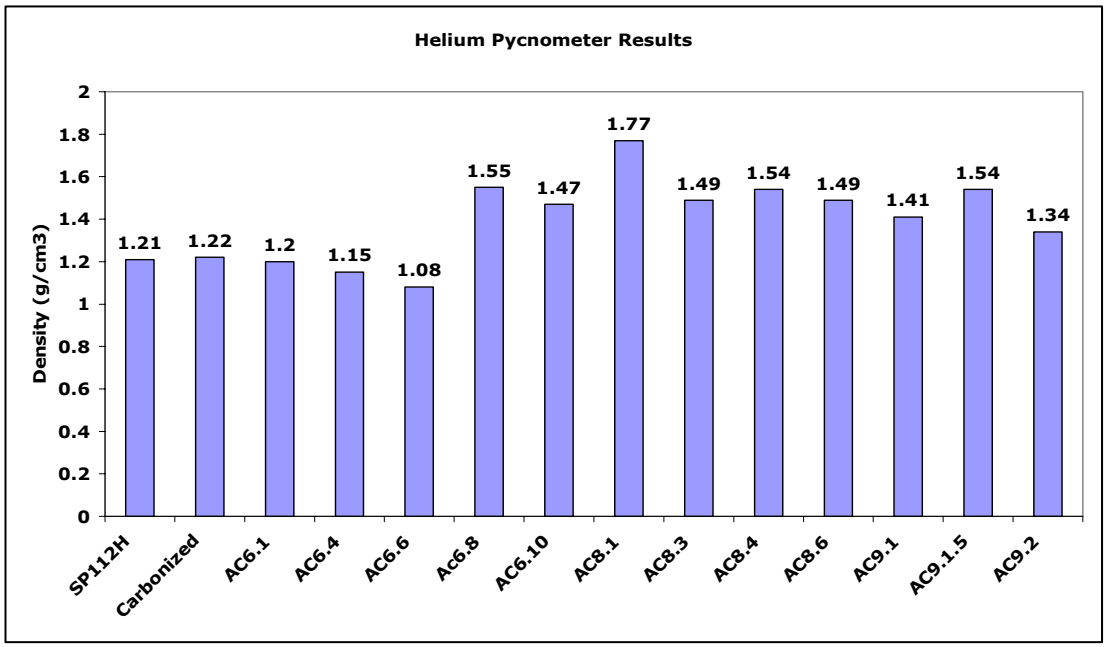

Figure 6.16 True Density Values of the Activated Carbons

Table 6.6 Densities and Total Pore Volumes of the Samples

Sample	Apparent Density (g/cm^3)	True Density (g/cm^3)	Porosity (%)	Total Pore Volume (cm^3/g)
SP112H	1.02	1.21	16	0.15
Carbonized	0.95	1.22	22	0.23
AC6.1	1.21	1.30	7	0.06
AC6.4	0.92	1.15	20	0.22
AC6.6	0.73	1.08	33	0.45
AC6.8	0.82	1.55	47	0.57
AC6.10	0.93	1.47	37	0.40
AC8.1	0.93	1.77	47	0.51
AC8.3	0.77	1.49	48	0.63
AC8.4	1.06	1.54	31	0.29
AC8.6	0.65	1.49	57	0.88
AC9.1	0.82	1.41	42	0.52
AC9.1.5	0.99	1.54	35	0.35
AC9.2	1.01	1.34	25	0.24

The total pore volume evaluated in this method has shown close values with that obtained from the cumulative pore volumes (by adding macro, meso and micropore volumes). Table 6.7 shows the total pore volume calculated by using equation 4.2.16 and total pore volume calculated by adding macro, meso and micropore volumes.

Table 6.7 Comparison of Total Pore Volumes of the Samples

Sample Code	Total Pore Volume Calculated Using Eqn.4.2.16 (cm^3/g)	Total Pore Volume Calculated By Adding Volumes (cm^3/g)
Carbonized	0.36	0.23
AC6.1	0.13	0.06
AC6.4	0.41	0.22
AC6.6	0.66	0.45
Ac6.8	0.51	0.57
AC6.10	0.39	0.40
AC8.1	0.34	0.51
AC8.3	0.63	0.63
AC8.4	0.23	0.29
AC8.6	0.87	0.88
AC9.1	0.51	0.52
AC9.1.5	0.29	0.35
AC9.2	0.24	0.24

6.2.6. Scanning Electron Microscope (SEM) Analysis

Figures 6.18 and 6.19 were taken for the carbonized product and Figures 6.20 and 6.21 for AC6.6 product. The shape of the products in Figure 6.17 and 6.20 shows spherical activated carbons with smooth surfaces, and as expected the sizes of the spheres decrease from about 0.7 mm starting material to about 0.37 mm after carbonization, and to a value between 0.23-0.30 mm after activation for 6 hours with a steam flow rate of 2.7 g/hr. Carbonized and activated char grains seen through the scanning electron microscopes have a little spalled outer surface and a smooth fracture surface and there are well developed pores at the surface (Fig. 6.19 and 6.21). It is obvious from both figures that the pores develop in a better way after activation where the surface of the carbonized grains shows smoother surface than the activated ones where a better pore openings occur.

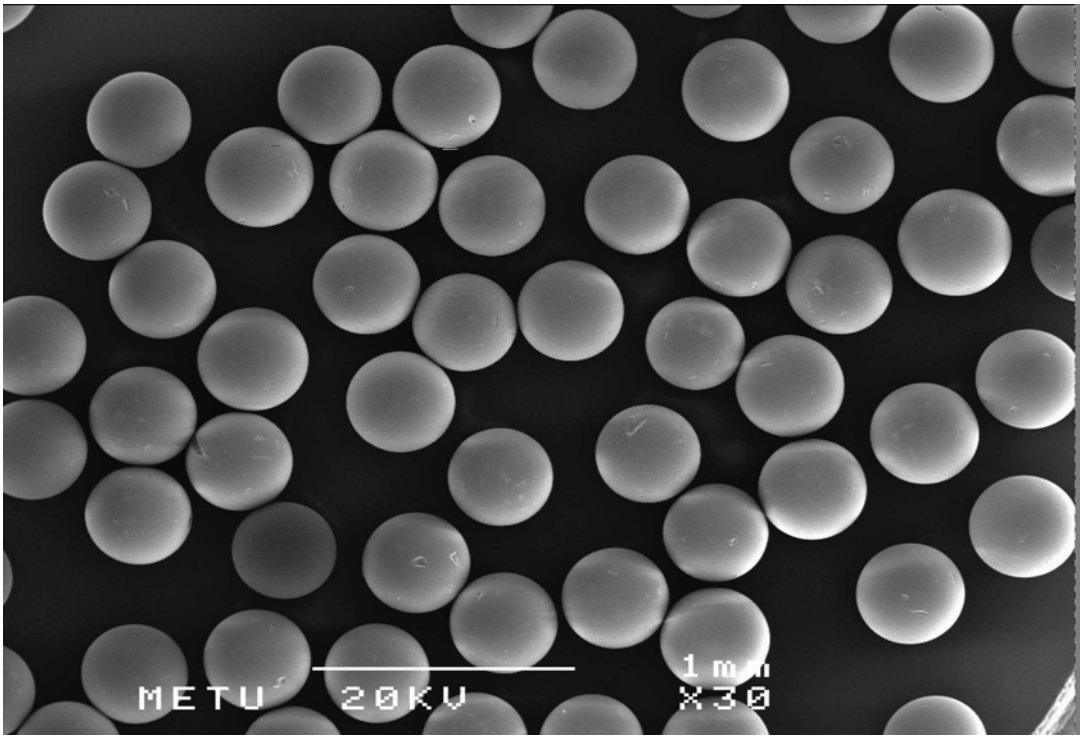

Figure 6.17 SEM of the carbonized product

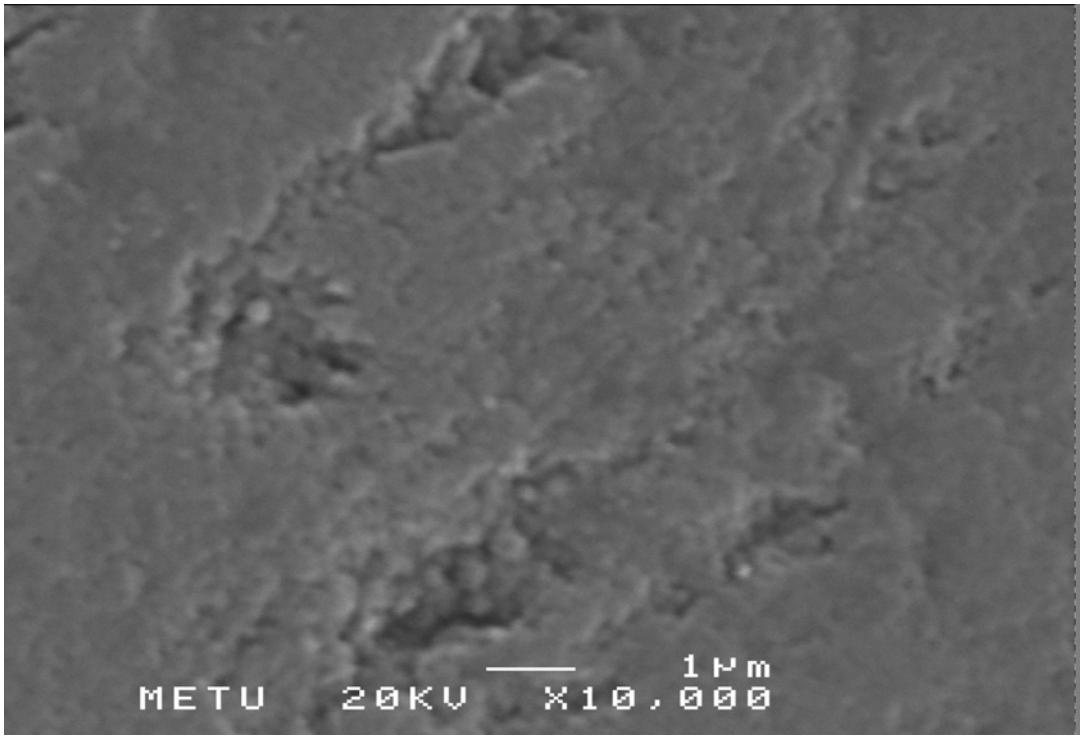

Figure 6.18 SEM of the carbonized product

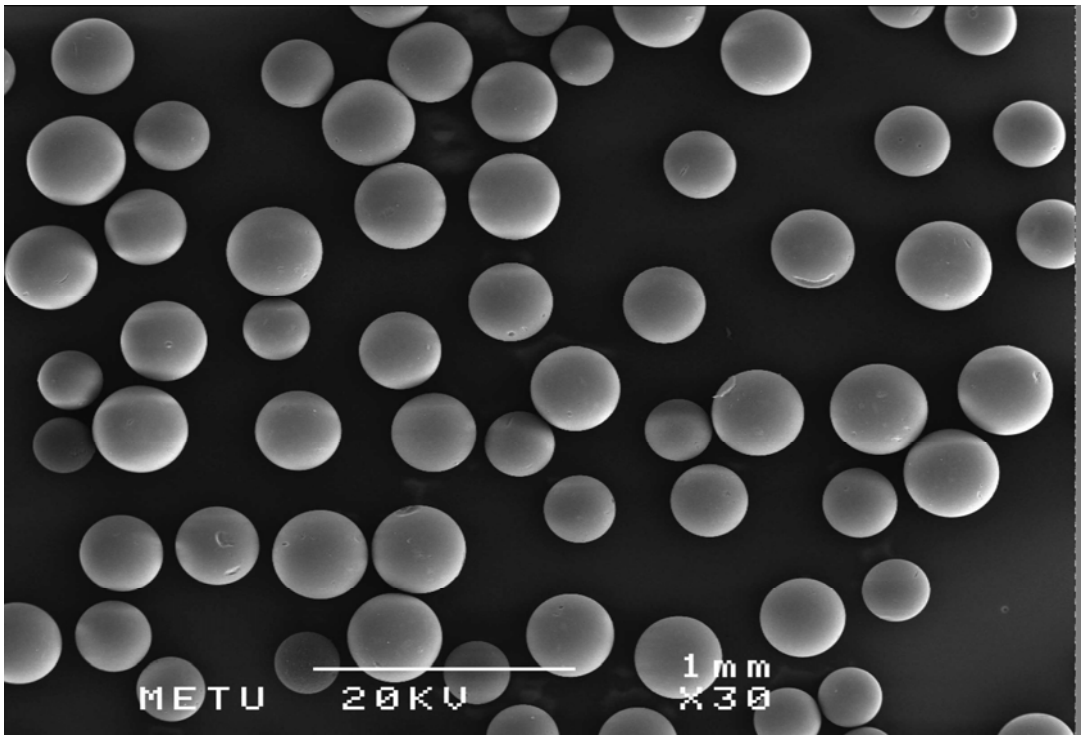

Figure 6.19 SEM of the activated AC6.6 product

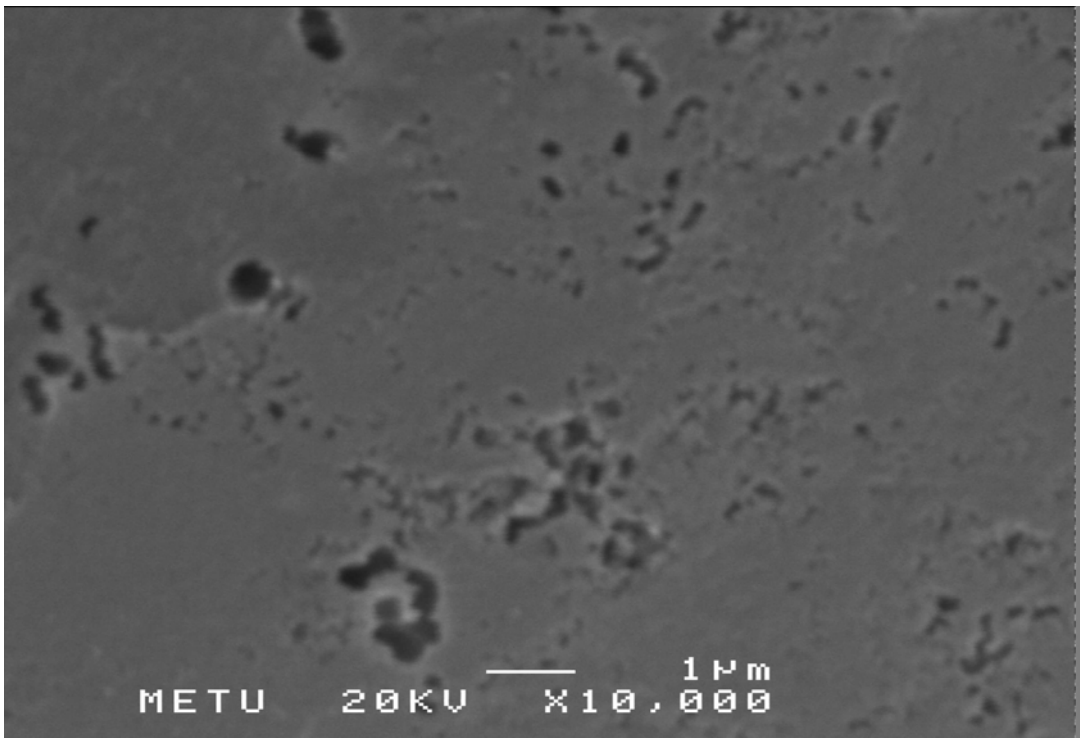

Figure 6.20 SEM of the activated AC6.6 product

CHAPTER VII

CONCLUSION

From the results of this study, it was concluded that polymer precursors based ion exchange resins are suitable raw materials for the production of activated carbons. N_2 and CO_2 isotherms, together with the mercury porosimetry measurements showed that activated carbons obtained from styrene-divinylbenzene copolymers, by physical activation technique, have a high degree of porosity, located mainly in micro size of pores.

The carbonization time has no significant effect on the BET surface areas of the products. A temperature of 600°C is a feasible one for carbonization while 450°C is insufficient to produce a starting material for activation and 750°C shows no difference than that of 600°C.

Results showed that, activation of the samples with steam increased the surface area tremendously if compared to activating with carbon dioxide due to the aggressive reactivity of steam with the bone of the carbon material. The products obtained from steam activating styrene-divinyl benzene copolymers gave surface area values over 2100 m^2/g at water bath temperature of 80^oC after 6 hours of activation.

Steam activation improved the micropore structure and over 70- 90 percent of the surface areas of the products were found to correspond to pores having diameters less than 2 nm. The remaining 10- 30 percent of the surface areas of the products were found to correspond to pores having diameters between 2 and 50 nm. The structure of the products informs us that they can be used for applications involving gases and vapors due to their well developed micopores and are also suitable to be used in adsorption from liquid phase because of their well developed mesopores.

From the chemical analysis of the products it is concluded that, ash contents are slightly higher than typical values. Activation process slightly increased the carbon content of the products which ranged between 92- 95%.

CO_2 adsorption results showed that micropore area values for the products increase proportionally with mesopores defeating the idea that the mesopores are transforming into micropores with further activation. The reason for this behavior has already been mentioned to occur due to the coalescence of the pores upon activation.

CHAPTER VIII

RECOMMENDATIONS

Activated carbon has several industrial applications depending on its porous structure and adsorption capacity. To increase the BET surface area value of the activated carbon produced from steam activated synthetic carbons, it is recommended to carry out experiments with different experimental parameters such as; the steam flow rate, heating rate, and activation temperature and time.

The future efforts in this field should include the investigation of the effect of steam on the carbonaceous material. To get more idea about the kinetics of activation of sample, it is better to analyze the gaseous products.

For further studies on furnace experiments, either a rotating horizontal sample chamber or a vertical bed, which can be fluidized also, is recommended. In either case a better contact between carrier gas and samples may be accomplished, which also helps removal of volatile products from the chamber. To decrease the ash content value, it is recommended to change the heating rate. Also adding salts such as $ZnCl_2$ may help to reserve the stability of the material after activation.

REFERENCES

Atkinson D., McLeod A. I., Sing K. S. W., and Capon A., Carbon 20, 339-343 (1982).

Balcı, S., "Kinetics of Activated Carbon Production from Almond Shell, Hazelnut Shell and Beech Wood and Characterization of Products", Ph.D. Thesis in Chemical Engineering, Middle East Technical University, Ankara, Turkey. (1992)

Balcı, S., Doğu, T. And Yücel, H., "Characterization of Activated Carbon Produced from Almond Shell and Hazelnut Shell", J. Chem. Tech. Biotechnol. Vol.60, pp.419-426. (1994)

Benaddi, 2000 : Benaddi, H., Bandosz, T. J., Jagiello, J., Schwarz, J. A., Rouzaud, J. N., Legras, D. and Béguin, F., "Surface Functionality and Porosity of Activated Carbons Obtained from Chemical Activation of Wood", Carbon Vol. 38, pp.669-674. (2000)

Bothe, N., Döscher, F., Klein J. and Widdecke, H., "Thermal Stability of Sulfonated Styrene-Divinylbenzene Resins", Polymer, Vol. 20, pp 850-854. (1979)

Brunauer, S., Demming, L. S., Demming, W. S. and Teller, E., J. Am. Chem. Soc., Vol. 62, pp.1723. (1940)

Broekhoff, J. C. P. and Linsen, B. G., Physical and Chemical Aspects of Adsorbents and Catalysts, ed. B. G. Linsen, Academic Press, New York. (1970)

Carrubba R. V., Urbanic J. E., Wagner N. J., and Zanitsch R. H., AIChE Symp. Ser. 80, 76-83. (1984)

Dubinin, M. M. And Radushkevich, L. V., Proc. Acad. Sci., SSSR., Vol.55, pp.331. (1947)

Dubinin, M. M., "On Methods for Estimating Micropore Parameters of Carbon Adsorbents", Carbon, Vol. 26, pp.97-110. (1988)

Faust S. D., and Aly, O. M., Chemistry of Water Treatment, Butterworth Pub., Woburn. (1983)

Gregg S. J., and Sign K.S.W., Adsorption, Surface and Porosity, New York Academic Press. (1967)

Gregg, S. J. and Sign, K.S.W., Adsorption, Surface and Porosity, 2nd Edn, New York Academic Press. (1982)

Hashimoto, K, Miura, K, Yoshikawa, F, and Imai, 1., "Change in Para Structure of Carbonaceous Materials during Activation and Adsorption Performance of Activated Carbon", Ind. Eng. Chem. Process Des. Dev. voI.18, No.1, pp.72-78. (1979)

Hassler J. W., Forest Products J. 8, 25A-27A. (1958)

Hassler J. W., Activated Carbon, Chemical Publishing Co., Inc., New York, pp. 1-14. (1963)

Hassler J. W., Purification with Activated Carbon, Chem. Pub. Co., New York. (1974)

Henning K. D., Bongartz W., and Degel J., 19th Biennial Conference on Carbon, Penn State University, Pa., June 25-30, extended abstracts, pp. 94, 95. (1990)

Jüntgen H., Carbon 15, 273-283 (1977)

Kirk Othmer, Kirk-Othmer Encyclopedia of Chemical Technology, Vol. 4, Bearing Materials, John Wiley and sons Inc. (2001)

Kocırık M., Brych J., Hradil J., "Carbonization of bead-shaped polymers for application in adsorption and in composite membranes", Carbon 39, pp.1919–1928. (2001)

Kolarz, B. N., Wojaczynska, M., Kaczmarczyk, J., Siemienıeewska, T. and Tomkow, K., "Influence of Heat Treatment Conditions on the Porosity Changes of Sulfonated Styrene / Divinylbenzene Copolymers", Journal of Polymer Science: Part B: Polymer physics, Vol.32, pp 1977-1990. (1994)

Marsh H., Butler J., Unger K. K., Rouquerol J., Sing K. S. W., and Kral H., Characterization of Porous Solids, Proceedings of the IUPAC Symposium (COPS I), Bad Soden a.Ts., FRG, Apr. 26-29, 1987, Elsevier, Amsterdam, The Netherlands, pp. 139-149. (1988)

Matsuda M., Funabashi K., Nishi T. and Yusa H., "Decomposition of Ion Exchange Resins by Pyrolysis", Nuclear Technology, Vol. 75, pp 187-192. (1986)

McEnaney B. and Mays T. J., Marsh H., ed., Introduction to Carbon Science, Butterworths, London, pp. 153-196. (1989)

Miura, K., and Hashimoto, K., "A Model Representing the Change of Pore Structure during the Activation of Carbonaceous Materials", Ind. Eng. Chem. Process Des. Dev., Vol.23, pp 138-145. (1984)

Neely, J. W., 1981, "Characterization of Polymer Carbons Derived from Porous Sulfonated Polystyrene" , Carbon, Vol.19, pp 27-36. (1981)

Orr C. and Dalla V. J. M., Fine Particle Measurement, Mc Millian, New York. (1959)

Öztürk, A., MSc. Thesis in Chemical Engineering, Middle East Technical University, Ankara, Turkey. (1999)

Park et al. (2002),"Characterization of Activated Carbons Based on Polymeric Resin", Journal of Colloid and Interface Science 250, 196–200 (2002)

Pierce, 1953; Pierce, C., Smith, R. N., J. Phys. Chem., Vol. 57, pp.56. (1953)

Puziy A. M., Poddubanya O. I., Martinez-Alanso A., Suarez- Garcia F.,Tascon J.M.D., "Characterization of synthetic carbons activated with phosphoric acid", Applied Surface Science 200, pp. 196-202. (2002)

Rodriguez Reinoso, F., "An Overview of Methods for the Characterization of Activated Carbons", Pure and Appl. Chem. Vol. 61, No.11, pp.1859-1866. (1989)

Ruthven, D. M., Principle of Adsorption and Adsorption Process, John Wiley and Sons, New York, (1984)

Shelley, S., "Reduce the risk of Adsorbent Bed Fires during Vapor Recovery", Chemical Engineering, pp 127. (December 1994)

Smisek, M. And Cerny, S., Active Carbon Manufacture, Properties and Aplications, Elsevier Pub., Comp., New York. (1970)

Solar J. M., Leon y Leon C. A., Osseo-Asare K., and Radovic L. R., Carbon 28, 369-375. (1990)

Şenel, G. İ., Ph.D. Thesis in Chemical Engineering, Middle East Technical University, Ankara, Turkey. (1994)

Ullmann, " Ullmann's Encyclopedia of Industrial Chemistry", 6th Edition, WILEY-VCH Publishers. (2002)

Walker, P. L. and Shelef, M., Chemistry and Physics of Carbon, Vol.4, pp. 287-383. (1968)

Wigmans, T., Carbon and Coal Gasification. (Edited by Figueriedo, J. L. and Moulijn, J. A.,), pp.559-601, Martinus Nijhoff Pub., Lancaster. (1985)

Winslow, F. H. and Matreyek, W., "Pyrolysis of Crosslinked Styrene Polymers", Journal of Polymer Science, Vol. 22, pp 315-324. (1956)

Wolff W. F., "A Model of Active Carbon", J. Phys. Chem. Vol. 63, pp.653-659. (1959)

Yağşi N. U., MSc. Thesis in Chemical Engineering, Middle East Technical University, Ankara, Turkey. (2004)

Yenisoy-Karakas S. , Aygün A., Güneş M., Tahtasakal E., Physical and chemical characteristics of polymer-based spherical activated carbon and its ability to adsorb organics, Carbon 42, pp. 477–484. (2004)

Zawadzki J., in P. A. Thrower, ed., Chemistry and Physics of Carbon, Vol. 21, Marcel Dekker, Inc., New York, pp. 147-380. (1989)

APPENDIX A

ANALYSIS OF MERCURY POROSIMETRY DATA

A.1. ANALYSIS OF MACROPORES

In the present study, analysis of macropore volume and areas were determined by using a commercial mercury porosimeter which involves the technique of forcing mercury under increasing pressure into successively smaller pores of the sample.

If a pore or void space is considered to be circular in cross section, the surface tension γ of the mercury acts along the circle of contact for a length equal to perimeter of the circle. If r_p is the pore radius, the force tending to squeeze the liquid out of the pore normal to the plane of the circle of contact may be written $-2\pi r_p \gamma \cos\theta$, where θ is contact angle (Ritter and Drake, 1945). The negative sign enters because for θ greater than 90°, the term $2\pi r_p \gamma \cos\theta$, is intrinsically positive. The opposing force, the force due to an externally applied pressure, acts over the area of the circle of contact and is $\Pi r_p^2 P$ where P is the applied pressure. At equilibrium the opposing forces are equal; thus

$$-2\pi r_p \gamma \cos\theta = \Pi r_p P \qquad \text{(A.1)}$$

or, replacing $D_p = 2r_p$, Washburn equation can be obtained (Washburn, 1921).

$$Dp = \frac{-4\gamma Cos\ \theta}{P} \quad \text{(A.2)}$$

Taking the γ and θ values as 485 dynes/cm and 130° (Orr, 1959) respectively, and substituting info the equation A.1,

$$Dp\ (\mu m) = \frac{-4\,x\,485\ (\frac{dynes}{cm})\,x10^{4}\,(\frac{\mu m}{cm})\,x\,-0.6428}{P\,(psia)\,x\,6.8948\ \ x10^{4}\,(\frac{dynes}{cm\ .\ psia})} \quad \text{(A.3)}$$

which, in simplified form, can be given as;

$$Dp = \frac{180\ (\mu m\ .\ psia)}{P\,(psia)} \quad \text{(A.4)}$$

Pore surface area can be calculated from the PV work expanded in forcing mercury into the pores. The work dW required to immerse an area dA of pore wall is expressed by

$$dW = \gamma\ \text{Cos}\ \theta\ dS = -\ P\ dV \quad \text{(A.5)}$$

The total cumulative area up to V_{max} is then

$$S = \frac{1}{\gamma Cos\ \theta} \int_{0}^{V\ max} PdV \quad \text{(A.6)}$$

Taking the surface tension and contact angle values given above, surface area per unit weight of material,

$$S = \frac{0.0225}{m} \int_{V\ min}^{V\ max} PdV \quad \text{(A.7)}$$

In the present study, mercury intrusion pressures of 3600 psia and 22 psia were taken as the upper and the lower limits for the determination of the macropores; they correspond to pores diameters of 0.05 and 8.18 μm,

respectively, according to equation A.4. Then, cumulatively obtained volume and area values were used to estimate the macropore volume and areas.

$$Vmacro = \left[Vcum \left|_{dp=0.05\ \mu m}^{P=3600\ psi} - Vcum \left|_{dp=8.18\ \mu m}^{P=22\ psi} \right. \right] (cm^3 / g) \quad \text{(A.8)}$$

$$Smacro = \left[Scum \left|_{dp=0.05\ \mu m}^{P=3600\ psi} - Scum \left|_{dp=8.18\ \mu m}^{P=22\ psi} \right. \right] (m^2 / g) \quad \text{(A.9)}$$

A.2. DETERMINATION OF APPARENT DENSITY

About 0.20- 0.3 g of sample was placed into a glass penetrometer. After weighing, penetrometer was assembled to the low pressure manifold and degassing until a sufficient vacuum level was attained (less than 30 μm Hg). Then, triply distilled mercury was introduced into the penetrometer until penetrometer was filled. Pressure was gradually increased to 22 psi with the increments of 2 psi for the low pressure port of the test (up to 22psi). Mercury filled penetrometer was weighed and replaced to the high pressure compartment and pressure was stepwise increased to a final pressure of 27000 psi. Sufficient equilibration time was allowed for each intrusion points. Thus, a complete analysis lasted 2 to 3 hours for taking about 30 intrusion points. The recorded electrical capacitance data were converted to volumes of pores by multiplying them with the stem conversion factor of the penetrometer. Pores which are in the pressure range of 22 psia (d_{pore}=8180 nm) to 3600 psia (d_{pore}=50 nm) can be considered as macropores, by applying the Washburn equation (eqn. 4.2.15) and considering the IUPAC definition. Apparent density values were calculated from the measurements of mercury displaced by the samples at 22 psia since, in the determination of apparent density, in interparticle voids should be excluded while internal pores should be included. In the determination of apparent density the following procedure was used:

1- Weight of sample= W_s

2- Weight of sealed, empty penetrometer = W_p

3- Weight of penetrometer and sample = W_s+W_p

4- Weight of sample, penetrometer and mercury: = $W_s+W_p+W_{Hg}$

5- Weight of mercury (4-3): = $W_{Hg}= (W_s+W_p+W_{Hg})-(W_s+W_p)$

6- Volume of mercury (Weight of mercury / density of mercury):

$$V_{Hg} = W_{Hg} / \rho_{Hg} \quad (A.10)$$

7 - Volume of Penetrometer = V_p

Volume of penetrometer was obtained from the calibration runs, by measuring the mercury displaced in empty penetrometer.

8- Volume of sample (7-6) = $V_s= V_p- V_{Hg}$

9- Pore volume, mercury displaced in penetrometer stern at 22 psi= V_{pore}

10- Apparent density of the sample at 22 psi:

$$\rho_{Hg} =W_s / (V_s-V_{pore}) \quad (A.11)$$

A.3. SAMPLE CALCULATION

Sample Code: AC 6.6
(Water bath Temperature=60^{o}C, Activation Time= 6hours)

A.3.1. Calculation of Macropore Volume and Area

Cumulative Volume Intruded up to 3600 psia (down to D_p=0.05μm) = 0.0498 cm^3/g

Cumulative Volume Intruded up to 22 psia (down to D_p= 8.18μm) = 0.0299 cm^3/g

Replacing these quantities into equation A.8:

V_{macro}= 0.0498-0.0299=0.0199 cm^3/g

Cumulative Pore Surface Area up to 3600 psia (down to D_p=0.05μm)=0.8215 m^2/g

Cumulative Pore Surface Area up to 22 psia(down to D_p=8.18μm)=0.0036m^2/g

Replacing these quantities into equation A.9:

S_{macro}= 0.8215-0.0036 = 0.818 m^2/g

A.3.2. Calculation of Apparent Density

1- W_s= 0.1544 g

2- W_p= 69.6726 g

3- W_s+W_p= 69.8270 g

4- $W_s+W_p+W_{Hg}$= 109.1343 g

5- W_{Hg}=($W_s+W_p+W_{Hg}$)-(W_s+W_p)= 39.3073 g

Density of Mercury = 13.5413 g/ cm^3 (at 22°C)

6- V_{Hg}= 2.9027 cm^3

7- V_p= 3.1153 cm^3

8- V_s= 0.2125 cm^3

9- Pore volume, mercury displaced in penetrometer stem at 22 psi:

V_{pore}= 0.3797 cm^3/g x 0.1544=0.052863 cm^3

10- Apparent density of the sample at 22 psi:

ρ_{Hg} =0.1544/ (0.2125-0.05863) = 1.003 g/ cm^3

APPENDIX B

ANALYSIS OF N_2 SORPTION DATA

B.1. ANALYSIS OF MESOPORES

Adsorption studies reading to measurements of pore sizes and pore size distributions generally make use of the Kelvin equation B.1 which relates the equilibrium vapor pressure of a curved surface such as that of a liquid in a capillary or pore, to the equilibrium pressure of the same liquid on a plane surface (Gregg and Sing, 1982).

$$\ln \frac{P}{Po} = \frac{-2\gamma V mol Cos\ \theta}{r_p RT} \qquad \text{(B.1)}$$

where P is the equilibrium vapor pressure of the liquid contained in a narrow pore of radius r_p and Po is the equilibrium pressure of the same liquid at a plane surface. The terms γ and V_{mol} are surface tension and molar volume of the liquid, respectively. θ is the contact (wetting) angle with which the liquid meets the pore wall.

If the transfer of d_n moles of vapor in equilibrium with the bulk liquid at pressure Po into a pore where the equilibrium pressure P is considered, this process consists of three steps: evaporation from the bulk liquid, expansion of the vapor from Po to P and condensation into the pore. The first and third of these steps are equilibrium processes and are therefore accompanied by a zero free energy change, whereas the free energy change for the second step is

described by

$$dG = \left(RT \ln\left(\frac{P}{Po} \right) \right) dn \tag{B.2}$$

When the adsorbate condenses in the pore

$$dG = -(\gamma Cos \quad \theta) dS \tag{B.3}$$

where dS is the change in the film-vapor interfacial area and θ is the wetting angle which is taken to be zero since the liquid is assumed to wet completely the adsorbed film. Equations B.2 and B.3, when combined

$$\frac{dn}{dS} = \frac{-\gamma}{RT \ln(P/Po)} \tag{B.4}$$

The volume of liquid adsorbate which condenses in a pore of volume V_p is given by

$$dVp = Vmoldn \tag{B.5}$$

Substituting equation B.4 into B.5 gives

$$\frac{dVp}{dS} = \frac{- \gamma Vmol}{RT \quad \ln (P / Po)} \tag{B.6}$$

The ratio of volume to area within a pore depends upon the geometry. When the shapes of the pores are highly irregular or consisting of a mixture of regular geometries, the volume to area ratio can be too complex to express mathematically. In these cases, or in the absence of specific knowledge of the pore geometry, the assumption of cylindrical pores is usually made. Since the ratio of volume to area for cylinders is r/2, the equation B.6 gives the Kelvin equation;

$$\ln\left(\frac{P}{Po} \right) = \frac{- 2\gamma Vmol}{rRT} \tag{B.7}$$

For nitrogen as the adsorbate at its normal boiling point of -195.6°C, the Kelvin equation can be written as

$$r_k = \frac{2\left(8.85\ \frac{erg}{cm^2}\right)\left(34.6\ \frac{cm^3}{mol}\right)\left(\frac{10^8\ ^oA}{cm}\right)}{\left(8.314\ x10^7\ \frac{erg}{Kmol}\right)(77\ K)(2.303)\log\left(P_o\ /\ P\right)} \qquad \text{(B.8)}$$

where 8.85 erg/cm^2 is the surface tension and 34.6 cm^3 is the molar volume of liquid nitrogen at -195.6°C. Then equation B.9 can be found as

$$r_k = \frac{4.15}{\log\left(P_o / P\right)} \qquad \text{(B.9)}$$

The term r_k indicates the radius into which condensation occurs at the required relative pressure. This radius, called the Kelvin radius or the critical radius, is not the actual pore radius since some adsorption has already occurred on the pore wall prior to condensation, leaving a center core or radius r_k. Alternatively, during desorption, an adsorbed film remains on the pore wall when evaporation of the center core takes place. If the depth of the film when condensation or evaporation occurs is t, then the actual pore radius r_p is given by

$$r_p = r_k + t \qquad \text{(B.10)}$$

This equation can be used to calculate r_p but some means of evaluating t is required if the pore radius is to be determined. Using the assumption that the adsorbed film depth in a pore is the same as that on a plane surface for any value of relative pressure, one can write

$$t = \left(\frac{W_a}{W_m}\right)\tau \qquad \text{(B.11)}$$

where W_a and W_m are, respectively, the quantity adsorbed at a particular relative pressure and the weight corresponding to the BET monolayer. Essentially

equation B.11 asserts that the thickness of the adsorbed film is simply the number of layers times the thickness τ of one layer regardless of whether the film is in a pore or on a plane surface. The t value of τ can be calculated by considering the area S and volume V_{mol} occupied by one mole of liquid nitrogen if it were spread over a surface to the depth of one molecular layer

$$\tau = \frac{V_{mol}}{S} = \frac{\left(34.6 \times 10^{24}\right) A^3}{\left(16.2 \frac{A^2}{mol}\right)\left(6.02 \times 10^{23} \frac{1}{mol}\right)} = 3.54\ A \qquad \text{(B.12)}$$

On nonporous surfaces it has been shown that when the quantity W_a/W_m is plotted versus P/P_o the data all approximately fit a common type II curve above a relative pressure of 0.3 (Cranston and Inkley, 1957). The common curve is described closely by Halsey, (1948) equation which for nitrogen can be written as

$$t = 3.54\left(\frac{5}{2.303 \log\left(P_o / P\right)}\right)^{1/3} \qquad \text{(B.13)}$$

The thickness of the adsorbed layer which is calculated for a particular relative pressure from the above equation which becomes thicker and thicker with successive increase in pressure, so that the measured quantity of gas adsorbed in a step is composed of a quantity equivalent to the liquid cores formed in that step plus the quantity adsorbed by the pore walls of pores whose cores have been formed in that and previous steps. Barrett Joyner and Halenda developed the method (BJH) which incorporates these ideas. The algorithm used on the ASAP 2000; the N_2 adsorption apparatus used in the present work, is an implementation of the BJH method. According to this method, ΔV_{gas}, the incremental volume: the change in adsorbed volume between two successive P/P_o values can be determined by subtracting the successive values. The ΔV_{gas}

then, can be converted to ΔV_{liq} by multiplying by the liquid molar volume for nitrogen at standard temperature and pressure. This is given by

$$\Delta V_{liq} = \frac{\Delta V_{gas}\left(cm^3/g\right)}{22414\left(cm^3/mol - STP\right)}\left(34.6\left(cm^3/mol\right)\right) = \Delta V_{gas}\left(1.54\,x10^{-3}\right) \quad \text{(B.14)}$$

The actual pore volume was evaluated by

$$\Delta V_{liq} = \pi r^2{}_{KAVE} + \Delta t \sum S \quad \text{(B.15)}$$

In this equation r_{KAVE} is the average Kelvin radius and the term $\Delta t\,\Sigma S$ is the product of the film area and the increase in the film depth, and since,

$$V_p = \pi r^2{}_{PAVE} \quad L \quad \text{(B.16)}$$

where L is the pore length, by combining the equations, B.15 and B.16

$$V_p = \left(\frac{r_{PAVE}}{r_{KAVE}}\right)^2 \left[\Delta V_{liq} - \left(\Delta t \sum S\right)\left(10^{-4}\right)\right] (cm^3) \quad \text{(B.17)}$$

The surface area of the pore walls can be calculated from the pore volume by

$$S = \frac{2V_p}{r_{PAVE}}\left(10^4\right) (m^2) \quad \text{(B.18)}$$

Then, mesopore volume and surface areas were calculated by using the incremental pore volume and surface area values evaluated from the equations B.17 and B.18:

$$V_{meso} = \left[\sum V_p\Big|_{d_p=0.002\mu m} - \sum V_p\Big|_{d_p=0.05\mu m}\right] (cm^3/g) \quad \text{(B.19)}$$

$$S_{meso} = \left[\sum S\Big|_{d_p=0.002\,\mu m} - \sum S\Big|_{d_p=0.05\,\mu m}\right] (m^2/g) \quad \text{(B.20)}$$

Figure B.1 shows a schematic representation of the surface analyzing apparatus.

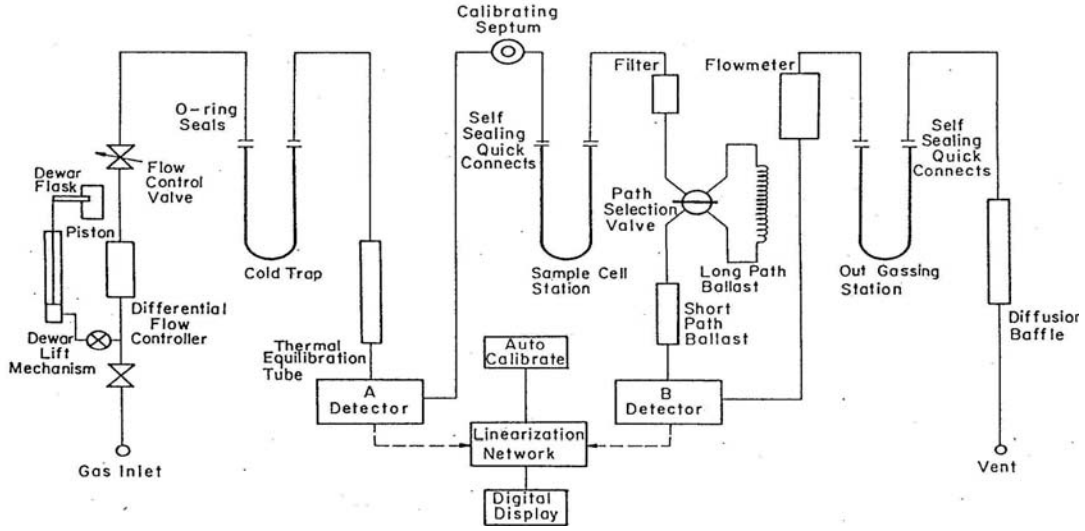

Figure B.1 Schematic Representation of the Surface Analyzer (Şenel, 1994)

B.2. DETERMINATION OF BET SURFACE AREA

BET surface areas of the samples can be obtained from the plot of $P/V(P_o-P)$ versus P/P_o plot, in the relative pressure range 0-0.2, using the following relation (Brunauer et al., 1938).

$$\frac{P}{V\left[P_O - P\right]} = \frac{1}{VmC} + \frac{C - 1}{V_m C}\frac{P}{P_O} \qquad \text{(B.21)}$$

The slope and intercept of this plot which are given as

$$S = \frac{C - 1}{V_m C} \quad \text{and} \quad I = \frac{1}{VmC} \qquad \text{(B.22)}$$

And can be used to evaluate BET surface area by the equation

$$S_{BET} = \frac{\left[\left(CSA_{N_2}\, nm^2\right)\left(6.023x10^{23}\left(1/mol\right)\right)\right]}{\left[\left(22414\left(cm^3/mol - STP\right)\right)\left(10^{18}\left(nm^2/m^2\right)\right)\left(\left(S+I\right)\left(g/cm^3 - STP\right)\right)\right]} \qquad \text{(B.23)}$$

where CSA_{N2} is the cross sectional area of a nitrogen molecule.

B.3. SAMPLE CALCULATION

Sample Code: AC 6.6
(Water bath Temperature=60^{o}C, Activation Time= 6hours)

B.3.1. Calculation of Mesopore Volume and Area

Cumulative Mesopore Volume up to d_p=20 ^{o}A (2 nm)= 0.513933 cm^3/g

Cumulative Mesopore Volume up to d_p=500 ^{o}A (50 nm)= 0.014651 cm^3/g

Replacing these quantities into equation B.19:

V_{meso}= 0.513933 -0.014651 =0.499 cm^3/g

Cumulative Pore Surface Area up to d_p=20 ^{o}A (2 nm)= 359.88 m^2/g

Cumulative Pore Surface Area up to d_p=500 ^{o}A (50 nm)= 1.248497 m^2/g

Replacing these quantities into equation B.20:

S_{meso}= 359.88 -1.248497 = 358.6315 m^2/g

B.3.2. Calculation of BET Surface Area

S=Slope= 0.002012

I=Intercept= 0.000025

CSA_{N_2} =0.162 nm^2 (Walker et al., 1968)

Replacing these quantities into equation B.23:

S_{BET}= 2137.1 m^2/g

APPENDIX C

ANALYSIS OF CO_2 ADSORPTION DATA

C.1. ANALYSIS OF MICROPORES

The micropore volume of the samples calculated by applying the Dubinin Radushkevich (D-R) equation to the CO_2 adsorption data in the relative pressure range $1x10^{-4}$ – $1x10^{-2}$

$$\log V = \log V_o - 2.303K\left(\frac{RT}{\beta}\right)^2\left[\log\frac{P_o}{P}\right]^2 (cm^3/gSTP) \qquad \text{(C.1)}$$

A plot of log V versus log $(P/P_o)^2$ gives straight line with an intercept of log V_o from which V_o, the micropore volume (cm^3/g STP) could be calculated. In this equation, β is a constant which is the ratio of the adsorption potentials. K is also a constant determined by the shape of the pore distribution curve. The micropore volume in the unit of (cm^3/g STP) which refers to the adsorbate state based on the ideal gas behavior at STP was also converted into the unit of (cm^3/g) which is based on the specific volume of the adsorbate in the adsorbed state at 0°C by the following equation

$$V_o(cc/g) = \frac{V_o(cm^3/g - STP)MW_{CO_2}(g/mol)}{(22414\ (cm^3/mol - STP))(\rho_{CO_2}(g/cm^3))} \qquad \text{(C.2)}$$

where ρ is the density of the CO_2 molecule.

Micropore surface area or so called D-R surface area was then evaluated by

$$S_{DR} = \frac{(\sigma nm^2) V_o (cm^3/g - STP)(6.02 \; x10^{23})}{(22414 \quad cm^3)(10^{18} \; nm^2/m^2)} \qquad \text{(C.3)}$$

where σ is the cross sectional area of a CO_2 molecule.

C.2. SAMPLE CALCULATION

Sample Code: AC 6.6
(Water bath Temperature=60°C, Activation Time= 6hours)

Micropore volume (cm^3/g STP) directly obtained from the ASAP 2000M; Micropore Analysis unit which processed the collected CO_2 adsorption data. In the calculations;

Saturation pressure of CO_2 =26142.000 mm Hg at 0°C (Micromeritics ASAP 2000, User Manual, Appendix C, 1993)

Absolute Pressure Range= 28.69383 - 352.1831 mm Hg

Corresponding Relative Pressure Range= $5.9x10^{-4}$- $7.3x10^{-3}$

V_{micro}= 198.198 cm^3/g STP

Corresponding micropore volume in the units of cm^3/g was evaluated by taking the density of CO_2 at 0°C= 1.181 g/cm^3 (Micromeritics ASAP 2000 User Manual, Appendix C, 1993) and replacing into equation C.2:

V_{micro}= 0.575574 cm^3/g

Micropore surface area (D-R surface area) obtained by taking the Cross Sectional Area of CO_2 molecule =0.17 nm^2 (Micromeritics ASAP 2000, User Manual, Appendix C, 1993)

Replacing into equation C.3: S_{D-R}= 905.4 m^2/g

APPENDIX D

ANALYSIS OF HELIUM PYCNOMETER DATA

D.1 DETERMINATION OF TRUE DENSITY

True densities of the samples were determined by helium displacement method. A commercial He Pycnometer apparatus "The Multivolume Pycnometer 1305" manufactured by Micromeritics Co., USA was used to measure true densities of the activated carbons. Figure D.1 shows a schematic representation of the helium pycnometry apparatus.

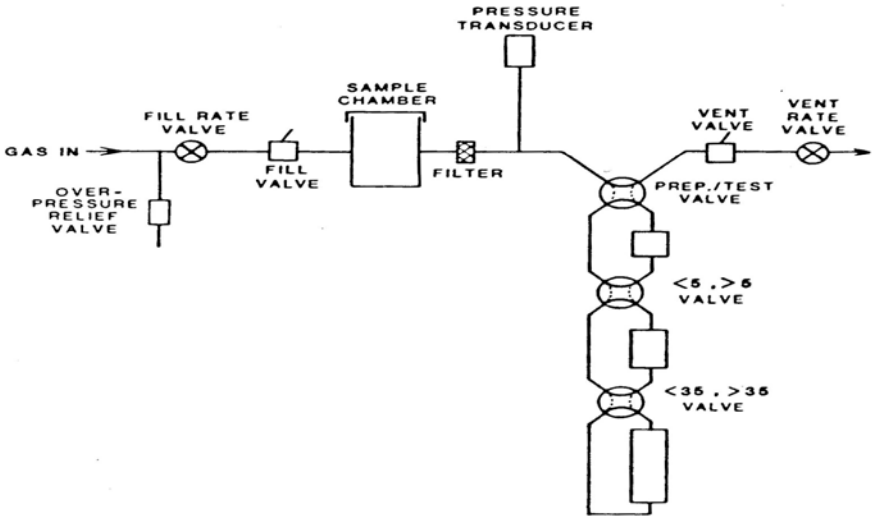

Figure D.1 Schematic Diagram of Helium Pycnometry (Şenel, 1994)

Assume that both V_{CELL} and V_{EXP} are at ambient pressure P_a, are at ambient temperature T_a, and that the valve is then closed. V_{CELL} is then charged

to an elevated pressure P_1. The mass balance equation across the sample cell, V_{CELL} is

$$P_1\left(V_{CELL} - V_{SAMP}\right) = n_C RT_a \qquad \text{(D.1)}$$

where

n_C= the number of moles of gas in the sample cell,

R= the gas constant, and

T_a= the ambient temperature

The mass equation for the expansion volume is

$$P_a V_{EXP} = n_E RT_a \qquad \text{(D.2)}$$

where

n_E= the number of moles of gas in the expansion volume.

When the valve is opened, the pressure will fall to an intermediate value, P_2, and the mass balance equation becomes

$$P_2\left(V_{CELL} - V_{SAMP} + V_{EXP}\right) = n_C RT_a + n_E RT_a \qquad \text{(D.3)}$$

Substituting from equations (D.1) and (D.2) into (D.3)

$$V_{CELL} - V_{SAMP} = \frac{P_a - P_2}{P_2 - P_1} V_{EXP} \qquad \text{(D.4)}$$

If we rearrange this equation,

$$V_{SAMP} = V_{CELL} - \frac{V_{EXP}}{\frac{(P_1 - P_a)}{(P_2 - P_a)} - 1} \quad \text{(D.5)}$$

Since P_1, P_2 and P_a are expressed in equations (D.1) through (D.5) as absolute pressures and equation (D.5) is arranged so that P_a is subtracted from both P_1 and P_2 before use, new P_{1g} and P_{2g} may be redefined as gauge pressures

$P_{1g} = P_1 - P_a$ (D.6)

$P_{2g} = P_2 - P_a$ (D.7)

And equation (D.5) rewritten as

$$V_{SAMP} = V_{CELL} - \frac{V_{EXP}}{\frac{P_{1g}}{P_{2g}} - 1} \quad \text{(D.8)}$$

This equation (D.8) then becomes the working equation for the Multivolume Pycnometer 1305.

D.2. SAMPLE CALCULATION

Sample Code: AC 6.6 (Water bath Temperature=60°C, Activation Time= 6hrs)

V_{CELL}= 7.8388 cm^3

V_{EXP} = 5.9498 cm^3

V_{SAMP}= 0.2607 cm^3

m_{SAMP}= 0.2814 g

$$\rho_{SAMP} = \frac{m_{SAMP}}{V_{SAMP}} = \frac{0.2814}{0.2607} = 1.079 \text{ g/cm}^3$$

APPENDIX E

CHEMICAL COMPOSITIONS OF ACTIVATED CARBONS

Table E.1 Chemical Compositions of Activated Carbons

Sample Code	C (%)	H (%)	N (%)	S (%)	O (%)
Starting Material	50.20	4.78	0.07	16.00	28.48
Carbonized Material	91.53	2.47	0.1	2.62	3.28
Set 3					
Series 1 (2.2 g/hr Steam Flow Rate)					
AC6.1	93.33	0.88	0.46	2.02	3.31
AC6.4	93.64	0.56	0.49	1.87	3.44
AC6.6	93.73	0.51	0.59	1.74	3.43
AC6.8	93.05	0.57	0.40	1.71	4.27
AC6.10	94.34	0.56	0.51	2.15	2.44
Series 2 (8.6 g/hr Steam Flow Rate)					
AC8.1	93.90	0.65	0.59	2.01	2.85
AC8.3	91.80	0.34	0.06	1.72	6.08
AC8.4	94.86	0.70	0.58	2	1.86
AC8.6	92.05	0.72	0.32	2.05	4.86
Series 3 (26.3 g/hr Steam Flow Rate)					
AC9.1	95.16	0.60	0.57	1.79	1.88
AC9.1.5	93.08	0.83	0.46	1.65	3.98
AC9.2	94.11	0.65	0.38	1.97	2.89

APPENDIX F

STEAM FLOWRATE CALULATIONS

In order to calculate the amount of steam sent to the furnace during activation experiments of Set 3, the amount of nitrogen send from the tube is calculated according to the time of the experiment. Assuming that the nitrogen carries saturated vapor to the furnace, the vapor amount is calculated. A sample calculation is given to show the procedure followed.

Sample Code: AC 6.6
(Water bath Temperature=60^{o}C, Activation Time= 6hours)

Flow Rate of Nitrogen = 200 cm^3/min = 12000 cm^3/hr

Temperature = 25 °C

Ambient Pressure = 685 mm Hg

Time of experiment = 6 hrs

Volume of N_2 = Flow Rate of Nitrogen * Time of experiment

= 12000 cm^3/hr * 6 hrs =72000 cm^3 = 72L

Using ideal gas law,

Moles of N_2 = (685/760) * (72) / (0.08206) * (298) = 2.65 moles

Assuming saturation of water vapor: $P_{H2O} = P^*_{H2O}$ = 149.57 mm Hg @ 60^0C

X= Mol Fraction of H_2O vapor = 149.57 mm Hg / P_{atm} = 149.57 / 685 = 0.2184

Moles of H_2O vapor = (X * Moles of N_2) / (1 – X) = 0.74 mol

Mass of H_2O vapor = moles of H_2O vapor * 18g/mol = 13.33 g

APPENDIX G

THERMAL GRAVIMETRIC ANALYSIS (TGA)

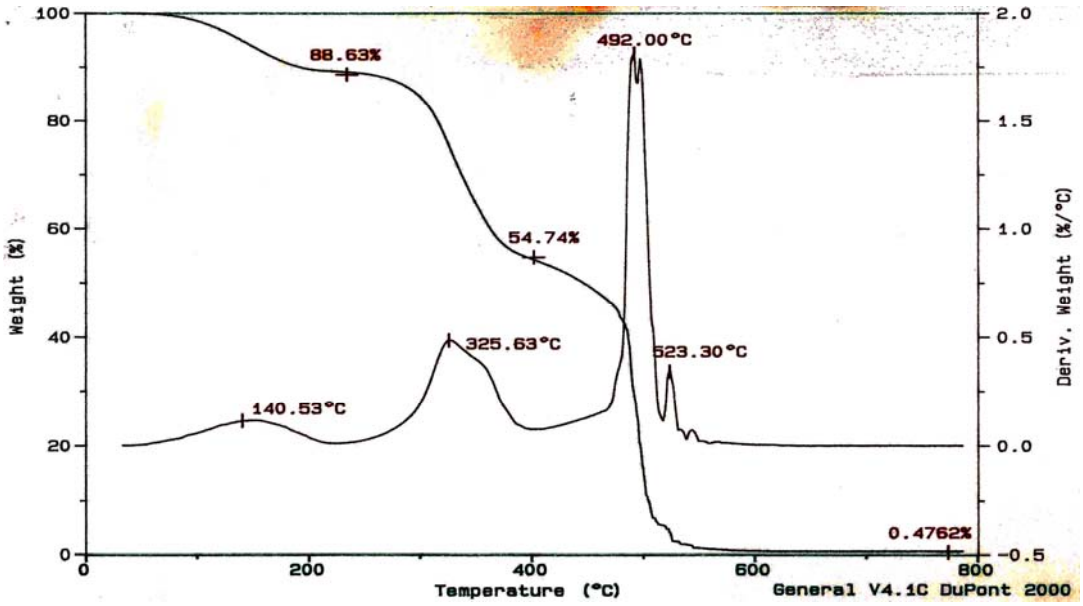

Figure G.1 TGA Result of Starting Material (Lewatit SP112H)

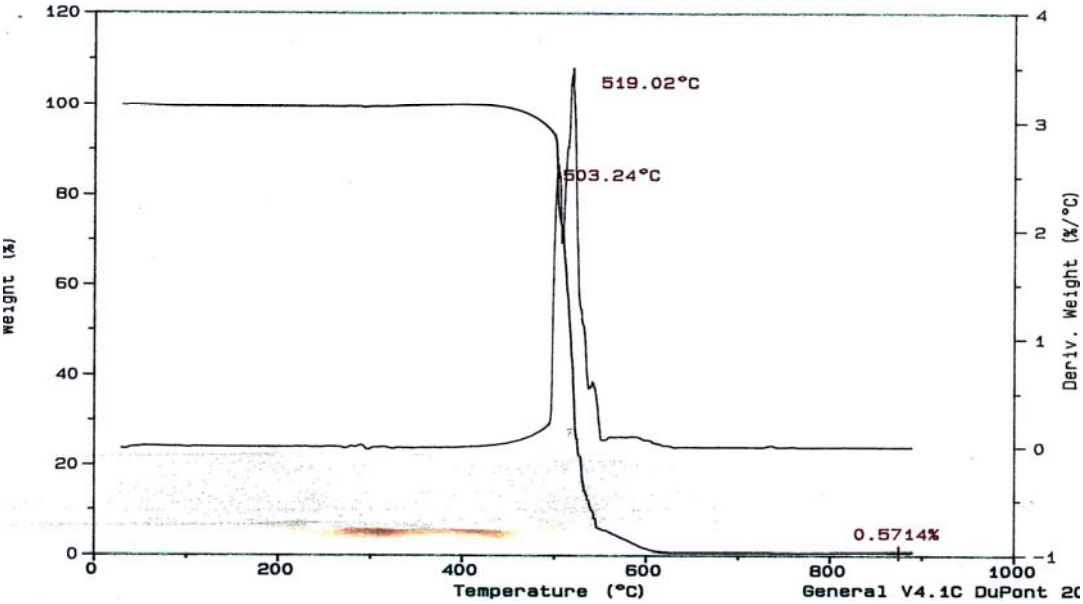

Figure G.2 TGA Result of the Carbonized sample (T=600°C, Time=1hr)

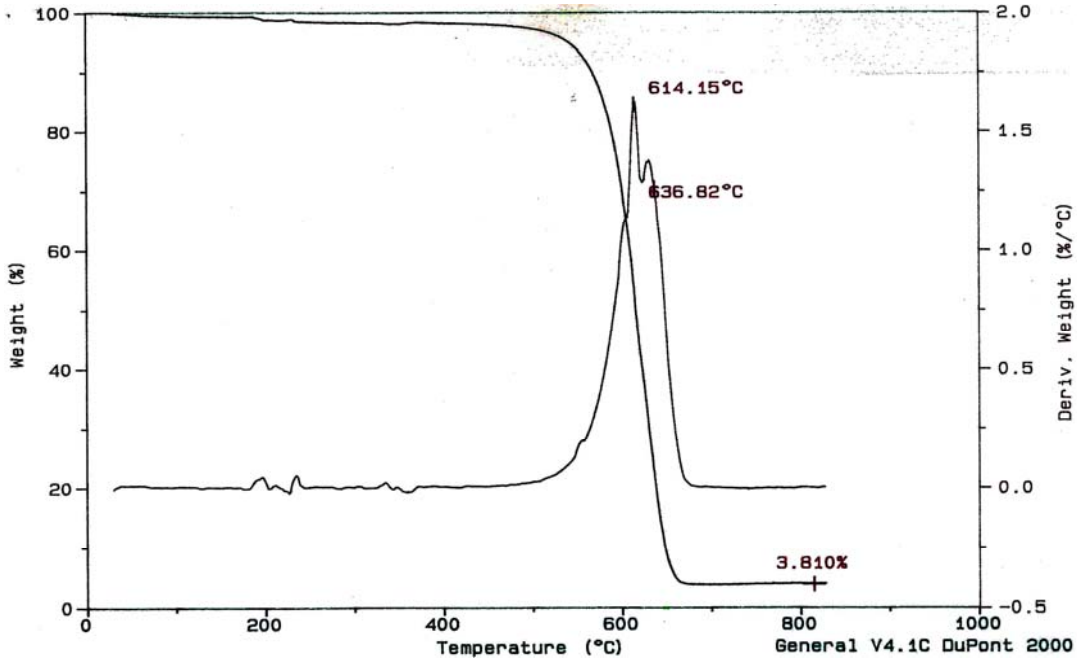

Figure G.3 TGA Result of AC6.6 Sample

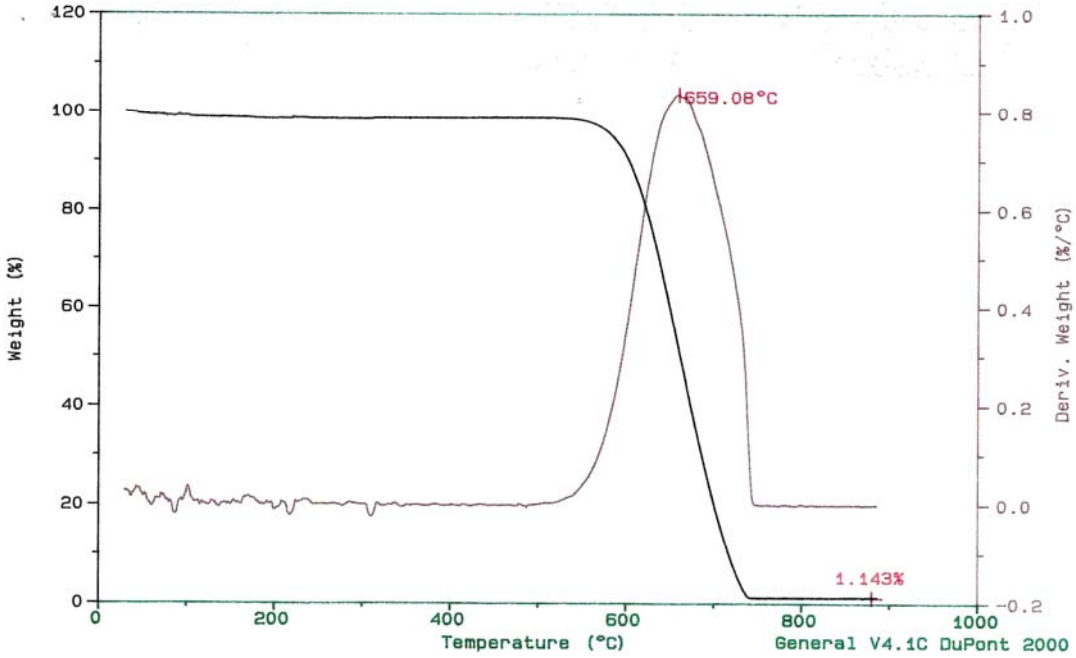

Figure G.4 TGA Result of Commercial Activated Carbon (Kureha)